

Dissertation

QUANTUM CHEMICAL CALCULATIONS ON THE
DIMERIZATION OF RADICAL IONS IN SOLUTION

Kraiwan Punyain

Graz, November 2011

Zur Erlangung des akademischen Grades
des Doktors der Dr.rer.nat. Naturwissenschaften

Vorgelegt bei

O.Univ.-Prof. Dipl.-Chem. Dr. Günter Grampp
Institut für Physikalische und Theoretische Chemie
der Technischen Universität Graz

CONTENTS

| | |
|--|----|
| 1. INTRODUCTION | 1 |
| 2. THEORETICAL BACKGROUND | 11 |
| 2.1 TIME-INDEPENDENT SCHRÖDINGER EQUATION..... | 11 |
| 2.2 BORN-OPPENHEIMER APPROXIMATION | 12 |
| 2.3 BASIS FUNCTIONS..... | 13 |
| 2.4 CLOSED- AND OPEN-SHELL SYSTEM | 14 |
| 2.5 INTRODUCTION TO DENSITY FUNCTIONAL THEORY (DFT)..... | 16 |
| 2.5.1 HYBRID FUNCTIONAL..... | 18 |
| 2.5.2 HYBRID METHOD WITH PERTURBATIVE SECOND-ORDER CORRELATION..... | 19 |
| 2.5.3 TD-DFT and TDA-DFT | 20 |
| 2.6 VAN DER WAALS INTERACTION IN COMPLEX MOLECULES | 24 |
| 2.7 BASIS SET SUPER POSITION ERROR | 25 |
| 2.8 MULTI-CONFIGURATION CALCULATION METHODS..... | 26 |
| 2.8.1 COMPLETE ACTIVE SPACE SELF-CONSISTENT FIELD | 27 |
| 2.8.2 MULTI-REFERENCE MØLLER-PLESSET SECOND-ORDER PERTURBATION (MRMP2)..... | 27 |
| 2.9 COSMO SOLVATION MODEL..... | 29 |
| 3. CALCULATIONAL METHODOLOGY | 31 |

| | | |
|-------|--|-----|
| 3.1 | GEOMETRY OPTIMIZATIONS | 31 |
| 3.2 | ENERGETICS..... | 34 |
| 3.3 | UV/Vis SPECTROSCOPIC CALCULATIONS | 35 |
| 4. | RESULTS AND DISCUSSION | 36 |
| 4.1 | RADICAL ANION DIMERIZATION..... | 36 |
| 4.1.1 | Tetracyanoethylene radical anion in tetrahydrofuran..... | 36 |
| 4.1.2 | 2,3,5,6-Dichlorodicyano-p-benzoquinone radical anion in acetone and dichloromethane | 45 |
| 4.1.3 | TCNQ radical anion in ethanol:methanol mixture (v 4:1)..... | 57 |
| 4.1.4 | Summary of radical anions dimerization | 65 |
| 4.2 | RADICAL CATION DIMERIZATION | 67 |
| 4.2.1 | Paraphenylenediamine radical cation in EtOH/Et ₂ O (vol 2:1) | 67 |
| 4.2.2 | <i>N,N</i> -Dimethyl-p-phenylenediamine radical cation in EtOH/Et ₂ O (vol 2:1)..... | 79 |
| 4.2.3 | 2,3,5,6-Tetramethyl-p-phenylenediamine radical cation in EtOH/Et ₂ O (vol 2:1) | 85 |
| 4.2.4 | <i>N,N,N,N</i> -Tetramethyl-p-phenylenediamine radical cation in EtOH/Et ₂ O (vol 2:1) | 90 |
| 4.2.5 | Summary on substituted PPD's radical cations dimerization | 94 |
| 4.2.6 | 3,3',5,5'-Tetramethylbenzidine radical cation in acetonitrile..... | 96 |
| 4.2.7 | Tetrathiofulvalene radical cation in acetone | 101 |
| 4.2.8 | Summary of radical cations dimerization | 106 |

| | | |
|-----|-------------------------------------|-----|
| 4.3 | EFFECT OF DIELECTRIC CONSTANT | 109 |
| 5. | CONCLUSIONS | 119 |

LIST OF TABLES

| | |
|--|------------|
| <i>Table 3.1: Substances of radical ions in the theoretical investigations.....</i> | <i>32</i> |
| <i>Table 4.1: Calculated relative energies and dimerization energies of [TCNE]₂²⁻2Na⁺ in THF.....</i> | <i>37</i> |
| <i>Table 4.2: Dimerization energies for conformers A1 and A2 of [TCNE]₂²⁻2Na⁺ in THF.....</i> | <i>41</i> |
| <i>Table 4.3: The vertical excitation of the [TCNE]₂²⁻2Na⁺ dimer and TCNE^{•-}Na⁺ monomer.....</i> | <i>45</i> |
| <i>Table 4.4: Relative energies and dimerization energies of [DDQ]₂²⁻2Na⁺ in acetone.....</i> | <i>47</i> |
| <i>Table 4.5: Dimerization energies of [DDQ]₂²⁻2Na⁺ in acetone and dichloromethane.....</i> | <i>51</i> |
| <i>Table 4.6: Relative energies and dimerization energies of [DDQ]₂²⁻2Na⁺ in dichloromethane.....</i> | <i>54</i> |
| <i>Table 4.7: Dimerization enthalpies of TCNQ radical anion.....</i> | <i>59</i> |
| <i>Table 4.8: The dimerization energies of [TCNQ]₂²⁻2Li⁺.....</i> | <i>63</i> |
| <i>Table 4.9: The dimerization energies of [PPD]₂²⁺2Br⁻.....</i> | <i>70</i> |
| <i>Table 4.10: Transition energies and oscillator strengths of all three PPD molecules.....</i> | <i>76</i> |
| <i>Table 4.11: The dimerization energies of [N,N-DMPPD]₂²⁺2Cl⁻.....</i> | <i>82</i> |
| <i>Table 4.12: The dimerization energies of [2,3,5,6-TMPPD]₂²⁺2Cl⁻.....</i> | <i>87</i> |
| <i>Table 4.13: The dimerization energies of [N,N,N',N'-TMPPD]₂²⁺2Cl⁻.....</i> | <i>92</i> |
| <i>Table 4.14: The dimerization energies of [TMB]₂²⁺2Cl⁻.....</i> | <i>99</i> |
| <i>Table 4.15: The dimerization energies of [TTF]₂²⁺2Cl⁻.....</i> | <i>104</i> |
| <i>Table 4.16: List of experimental dielectric constants for solvents.....</i> | <i>109</i> |
| <i>Table 4.17: The dimerization energies of PPD's radical cations for various dielectric constants.....</i> | <i>116</i> |
| <i>Table 4.18: The dimerization energies of radical ions at room temperature and at dimerization temperature.....</i> | <i>117</i> |
| <i>Table 5.1: The dimerization energies for different calculation methods relative to experiment.....</i> | <i>121</i> |

LIST OF FIGURES

| | |
|---|----|
| <i>Figure 1.1: Molecular orbital diagram of dimerization of $[TCNE]^{\bullet-}.Na^+$</i> | 6 |
| <i>Figure 2.1: Restricted and unrestricted Hartree-Fock</i> | 15 |
| <i>Figure 2.2: Solvent accessible surface (SAS) scheme</i> | 29 |
| <i>Figure 3.1: Molecular structure of interested molecules</i> | 34 |
| <i>Figure 4.1: Structure of the five possible conformers of $[TCNE]_2^{2-}2Na^+$ in THF</i> | 37 |
| <i>Figure 4.2: Geometry of the most stable conformer of $[TCNE]_2^{2-}2Na^+$ in THF</i> | 38 |
| <i>Figure 4.3: Potential energy curve of $[TCNE]_2^{2-}2Na^+$ and without counter-ion</i> | 40 |
| <i>Figure 4.4: The calculated vertical excitations of the $[TCNE]_2^{2-}2Na^+$ dimer and monomer</i> | 44 |
| <i>Figure 4.5: Structure of the eight possible conformers of $[DDQ]_2^{2-}2Na^+$ in acetone</i> | 46 |
| <i>Figure 4.6: Geometry of the most stable conformers of $[DDQ]_2^{2-}2Na^+$</i> | 49 |
| <i>Figure 4.7: Molecular orbitals of $[DDQ]_2^{2-}2Na^+$</i> | 52 |
| <i>Figure 4.8: The calculated vertical excitations of the $[DDQ]_2^{2-}2Na^+$ dimer and monomer</i> | 56 |
| <i>Figure 4.9: Relative EPR intensity of TCNQ radical anion undergoing dimerization</i> | 58 |
| <i>Figure 4.10: Fraction of the TCNQ radical anion monomer as a function of temperature</i> | 58 |
| <i>Figure 4.11: The logarithm dimerization equilibrium constant of TCNQ radical anion as a function of temperature</i> | 59 |
| <i>Figure 4.12: The optimized geometry of $TCNQ^{\bullet-}Li^+$ monomer</i> | 60 |
| <i>Figure 4.13: Four optimized geometries of $[TCNQ]_2^{2-}2Li^+$</i> | 61 |
| <i>Figure 4.14: The HOMO orbitals by DFT and CASSCF methods of the most stable $[TCNQ]_2^{2-}2Li^+$</i> | 62 |
| <i>Figure 4.15: The calculated vertical excitations of the $[TCNQ]_2^{2-}2Li^+$ dimer and monomer</i> | 64 |
| <i>Figure 4.16: The optimized structural parameters of $[PPD]^{\bullet+}$ monomer</i> | 67 |
| <i>Figure 4.17: The optimized geometries of $[PPD]_2^{2+}2Br^-$ dimers</i> | 68 |
| <i>Figure 4.18: The molecular orbitals of the most stable $[PPD]_2^{2+}2Br^-$ dimer</i> | 71 |
| <i>Figure 4.19: The molecular orbitals of $PPD^{\bullet+}Br^-$ monomer</i> | 75 |
| <i>Figure 4.20: The calculated vertical excitations of the $[PPD]_2^{2+}2Br^-$ dimer and monomer with explicit solvent ethanol</i> | 77 |

| | |
|---|-----|
| Figure 4.21: The calculated vertical excitations of the $[PPD]_2^{2+} 2Br^-$ dimer and monomer with explicit solvent water..... | 78 |
| Figure 4.22: The optimized geometries of $[N,N-DMPPD]_2^{2+}$ dimer..... | 79 |
| Figure 4.23: The molecular orbitals of $[N,N-DMPPD]_2^{2+} 2Br^-$ | 81 |
| Figure 4.24: The calculated vertical excitations of $[N,N-DMPPD]_2^{2+} 2Br^-$ dimer and monomer..... | 84 |
| Figure 4.25: The optimized geometries of $[2,3,5,6-TMPPD]_2^{2+}$ | 85 |
| Figure 4.26: The molecular orbitals of $[2,3,5,6-TMPPD]_2^{2+} 2Br^-$ | 86 |
| Figure 4.27: The calculated vertical excitations of $[2,3,5,6-TMPPD]_2^{2+} 2Br^-$ dimer and monomer..... | 89 |
| Figure 4.28: The calculated vertical excitations of $[2,3,5,6-TMPPD]_2^{2+} 2Br^-$ dimer and monomer with explicit solvent ethanol..... | 89 |
| Figure 4.29: The optimized geometries of $N,N,N',N'-TMPPD^{\bullet+} Cl^-$ monomer and $[N,N,N',N'-TMPPD]_2^{2+} 2Cl^-$ dimer..... | 90 |
| Figure 4.30: The HOMO orbitals of $[N,N,N',N'-TMPPD]_2^{2+} 2Cl^-$ | 91 |
| Figure 4.31: The calculated vertical excitations of $[N,N,N',N'-TMPPD]_2^{2+} 2Cl^-$ dimer and monomer.. | 93 |
| Figure 4.32: The optimized structural parameters of $TMB^{\bullet+} Cl^-$ monomer and $[TMB]_2^{2+} 2Cl^-$ dimers... | 97 |
| Figure 4.33: The HOMO and LUMO orbitals of $[TMB]_2^{2+} 2Cl^-$ | 98 |
| Figure 4.34: The calculated vertical excitations of the $[TMB]_2^{2+} 2Cl^-$ dimer and monomer..... | 100 |
| Figure 4.35: The optimized geometry of $TTF^{\bullet+} Cl^-$ monomer..... | 102 |
| Figure 4.36: The optimized geometries of $[TTF]_2^{2+} 2Cl^-$ | 102 |
| Figure 4.37: The HOMO orbitals of $[TTF]_2^{2+} 2Cl^-$ | 103 |
| Figure 4.38: The calculated vertical excitations of $[TTF]_2^{2+} 2Cl^-$ dimer and monomer..... | 105 |
| Figure 4.39: The plot of dielectric constants of solvents against temperature..... | 111 |
| Figure 4.40: Dimerization energies of radical cations in various dielectric constants..... | 113 |
| Figure 4.41: Dimerization energies of radical ions as a function of various dielectric constants..... | 114 |

LIST OF ABBREVIATIONS

| | |
|------------------|--|
| Å | Angstrom |
| ° | Degree |
| cm ⁻¹ | Reciprocal centimeter |
| DFT | Density Functional Theory |
| ρ | Electron density |
| E | Energy |
| T_{ni} | Kinetic energy of non interacting electron |
| V_{ne} | The nuclear-electron interaction |
| V_{ee} | The classical electron-electron repulsion |
| E_{XC} | Exchange-correlation energy |
| χ | The orbital |
| h_i^{KS} | The Kohn-Sham one electron operator |
| Z | The atomic number |
| v_{xc} | The exchange-correlation potential |
| $\nabla\rho$ | The gradient of electron density |
| PES | Potential energy surface |
| kcal/mol | Kilocalorie per mole |
| kJ/mol | Kilojoule per mol |
| LDA | Local density approximation |
| GGA | Generalized gradient approximation |
| TCNE | Tetracyanoethylene |
| DDQ | 2,3-Dichloro-5,6-dicyano-p-benzoquinone |
| TCNQ | Tetracyano-p-quinodimethane |
| PPD | p-phenalenediamine |
| N,N-DMPPD | N,N-dimethyl-p-phenalenediamine |
| 2,3,5,6-TMPPD | 2,3,5,6-tetramethyl- p-phenalenediamine |
| N,N,N',N'-TMPPD | N,N,N',N'- tetramethyl- p-phenalenediamine |
| TMB | Tetramethylbenzidine |
| TTF | Tetrathiofulvalene |

ACKNOWLEDGEMENT

I would like to acknowledge people who gave the opportunity and stayed beside me during all of my study.

First, I would like to make a special thank my supervisor, O.Univ.-Prof.Dr.Günter Grampp, who gave me the chance to study Ph.D in Austria with a very good guidance during all of my PhD-Study. I am very proud to deeply thank Ass.-Prof.Dr.Anne-Marie Kelterer, my co-supervisor, who was taking care of me and giving a good suggestion about theoretical chemistry. I would like to thank Dr. Kenneth Rasmussen, who was teaching and helping me with the temperature-dependent EPR measurement and also making a good environment to study in the institute.

I would also like to thank Mr.Eisenkölbl for the help about computer service which was necessary for the theoretical work. I would like to thank Mr. Mario Lang for the helping of cluster service. I wish to thank my friends, Nalinpat Porrawatpreyakorn, Kanthida Kusonmano, Umalee Namdaung, Truong Nguyen Xuan, Beinhardt family and Gigi Zwitterig-Legenstein, who are my best friends in every time and helping me get through the difficult times.

I would like to thank Österreichische Austauschdienst (ÖAD) for providing a Technology grant scholarship to study PhD in Austria. I would like to thank Austrian Academic Exchange Service program Wissenschaftlich-Technische Zusammenarbeit Austria-Slovakia (WTZ SK11/2009) and Research and Development Agency of Slovak Republic for providing a grant to do research in the topic of Semiempirical MD study of pi-conjugated System. I would like to thank Assoc.Prof.doc.Ing.Dr.Vladimir Lukes for a good suggestion in WTZ SK11/2009 project. I would like to thank Naresuan University, Thailand, for financial support from 1thOctober 2011 to 31thDecember 2011.

I would like to thank Institut für Physikalische und Theoretische Chemie, Graz University of Technology for providing computational facilities and laboratory facilities.

Honestly, a big special thank for my family and my girlfriend (Wiruanglong Naksuan) for standing beside me in every time with love and understanding the way of my life. Finally, I would like to give a special thank for Asst.Prof.Dr.Ythana Tantirungrotechai, my master supervisor at Mahidol University, Thailand, who gave me an opportunity to study and doing research in computational chemistry and gives a good suggestion to follow the way of science.

ABSTRACT

Ionic organic radicals form dimers in solution, observed experimentally as diamagnetic species by temperature-dependent EPR and low temperature UV/Vis spectroscopy. Dimerization of radical anions of tetracyanoethylene, 2,3-dichloro-5,6-dicyano-p-benzoquinone, tetracyano-p-quinodimethane and of radical cations of p-phenylenediamine, *N,N*-dimethyl-p-phenylenediamine, 2,3,5,6-tetramethyl-p-phenylenediamine, *N,N,N',N'*-tetramethyl-p-phenylenediamine, 3,3',5,5'-tetramethylbenzidine, tetrathiofulvalene in solution was investigated theoretically according to geometry, energetics and UV/Vis spectroscopy. Density Functional Theory including dispersion correction describes stable dimers after geometry optimization with conductor-like screening model of solvation and inclusion of the counter-ion. Energy corrections were done on double-hybrid density functional theory with perturbative second-order correlation (B2PLYP-D) including basis set superposition error (BSSE), and multireference Møller-Plesset second-order perturbation theory method MRMP2 based on complete active space method CASSCF(2,2) single point calculation, respectively. All π -dimers exhibit long multicenter π -bonds, which are longer than a normal covalent bond but shorter than the sum of van der Waals radii, with strongly interacting orbitals. Dispersion interaction and electrostatic attraction from counter-ion play an important role to stabilize the radical ion dimers in solution. Dispersion-corrected double hybrid functional B2PLYP-D and CASSCF(2,2) can describe the interaction energetics properly.

Vertical excitations were computed with Tamm-Dancoff approximation for time-dependent Density Functional Theory (TDA-DFT) at the B3LYP level with the cc-pVTZ basis set. When including ethanol solvent molecules explicitly, for p-phenylenediamine, a strong interaction of the counter-ion and the solvent ethanol with the monomeric species is observed, whereas in the dimers the strong interaction of both radical cations is the dominating factor for the additional peak in UV/Vis spectra. The dielectric constants of the solvents are increasing when the temperature decreased and influences the calculated dimerization energy significantly by 6-20 kJ/mol to higher values.

Keywords: dimerization energy, vertical transition, dispersion-corrected density functional method, B2PLYP-D, CASSCF, COSMO solvation model, dielectric constant.

ZUSAMMENFASSUNG

Organische Radikationen können Dimere in Lösung bilden, was experimentell durch temperaturabhängige ESR-Spektren und in UV/Vis-Spektren bei tiefen Temperaturen beobachtet wurde. Die Dimerisierung der Radikalanionen von Tetracyanoethylen, 2,3-Dichlor-5,6-dicyano-p-Benzochinon, Tetracyano-p-chinondimethan und der Radikalkationen von p-Phenylendiamin, N,N-Dimethyl-p-phenylendiamin, 2,3,5,6-Tetramethyl-p-phenylendiamin, N,N,N',N'-Tetramethyl-p-phenylendiamin, 3,3',5,5'-Tetramethylbenzidin, Tetrathiofulvalen in Lösung wurde in dieser Arbeit theoretisch im Hinblick auf Geometrie, Energetik und UV/Vis-Absorptionen untersucht.

Mit der Dichtefunktionaltheorie, einschließlich Dispersionskorrektur, erhält man stabile Dimere nach Geometrieoptimierung mit dem Conductor-like-Screening-Modell zur Beschreibung des Lösungsmittels und unter Einbeziehung der Gegenionen. Energie-Korrekturen wurden mittels Doppel-Hybrid-Dichtefunktionaltheorie mit Störungstheorie zweiter Ordnung (B2PLYP-D) und nachfolgender Korrektur des Basissatz-Superposition-Errors (BSSE) sowie mit Multireferenz Møller-Plesset Störungstheorie zweiter Ordnung (MRMP2) basierend auf dem "complete active space" CASSCF (2,2) durchgeführt. Alle π -Dimere weisen lange Multizentren- π -Bindungen auf, die länger sind als normale kovalente Bindung, aber kürzer als die Summe der van-der-Waals-Radien. Die Orbitale zeigen starke Wechselwirkungen. Dispersionswechselwirkungen und elektrostatische Anziehung mit den Gegenionen spielen eine wichtige Rolle für die Stabilisierung der Radikationen in Lösung. BSSE-B2PLYP-D- und CASSCF (2,2) Methoden beschreiben die Dimerisierungsenergie in der richtigen Größenordnung.

Vertikale Anregungen wurden mittels der Tamm-Dancoff-Näherung für zeitabhängige Dichtefunktionaltheorie (TDA-DFT) auf B3LYP-Niveau mit dem cc-pVTZ-Basissatz und Ethanol als Lösungsmittelmolekülen berechnet. Eine starke Wechselwirkung der Gegenionen und des Lösungsmittels Ethanol mit den Monomeren wurde für p-Phenylendiamin beobachtet, während die starken Wechselwirkungen der beiden Radikalkationen der dominierende Faktor für die Bildung der Dimere und der Grund für die zusätzlichen Absorption im UV/Vis-Spektrum ist.

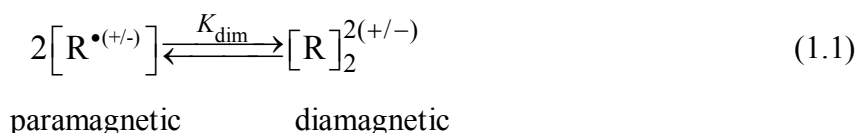
Die Dielektrizitätskonstante von Lösungsmitteln steigt bei sinkender Temperatur, was eine Änderung der berechneten Dimerisierungsenergie von 6-20 kJ/mol verursacht .

Keywords: Dimerisierungsenergie, vertikaler Übergang, Dispersions-korrigierte Dichtefunktionaltheorie, B2PLYP-D, CASSCF, COSMO Lösungsmittel-Modell, Dielektrizitätskonstante

1. INTRODUCTION

Dimerization of organic radical ions in solution is one of the most important reactions in organic radical chemistry. From current knowledge, it seems that nearly all radical ions, cations and anions and also neutral radicals can dimerize in solution^[1, 2]. Interestingly, free ionic organic radicals which bear the same charges can dimerize to supramolecular complexes exhibiting long multicenter C-C bonds that are longer than normal covalent bond, but shorter than the sum of the van der Waals radii. Such dimers show a change in property from paramagnetic to diamagnetic. The dimerization processes of ionic organic radical ions in solution can be experimentally detected by temperature-dependent EPR-spectroscopy and UV/Vis spectroscopy. The enthalpies of dimerization (ΔH_{dim}) and the dimerization constants (K_{dim}) of many ionic organic radicals in solution have been determined by their measurements^[1-13]. It is interesting to tackle the problem, why ionic radicals bearing the same charge form dimers in solution as well as in the solid state.

As proposed by R. Chang^[1], the dimeric diamagnetic species is in equilibrium with the monomeric paramagnetic species as shown in equation (1.1).



In the next paragraphs it is described, how the dimerization enthalpy and the dimerization constant can be evaluated from temperature-dependent EPR experiment. The experimental measurements of dimerization processes by temperature-dependent EPR spectroscopy are evaluated via the EPR intensity as a function of temperature. The dimerization constant (K_{dim}) is the equilibrium between paramagnetic (monomer) and diamagnetic (dimer) species^[1, 2].

$$K_{\text{dim}} = \frac{[(R^{2(+/-)})_2]}{[R^{\bullet(+/-)}]} \quad (1.2)$$

under equilibrium condition, the produced dimer concentration is:

$$\left[(R^{2(+/-)})_2 \right] = \frac{1}{2} c_0 - \frac{1}{2} \left[R^{*(+/-)} \right]_{eq,T} \quad (1.3)$$

where the concentration of radical ion is defined as

$$\left[R^{*(+/-)} \right] = \alpha c_0 \quad (1.4)$$

with:

α = the fraction of paramagnetic monomer $R^{*(+/-)}$

c_0 = the stoichiometric concentration of ionic radical $R^{*(+/-)}$

Then the dimer concentration can be extracted substituting equation (1.4) to equation (1.3) results in

$$\left[(R^{2(+/-)})_2 \right] = (1 - \alpha) \frac{c_0}{2} \quad (1.5)$$

So, the dimerization constant (K_{dim}) after putting equations (1.4) and (1.5) into equation (1.2) is

$$K_{dim} = \frac{1 - \alpha}{2c_0\alpha^2} \quad (1.6)$$

The enthalpy of dimerization, ΔH_{dim} can be extract from the van't Hoff equation of the dimerization constant.

$$K_{dim} = \frac{1 - \alpha}{2c_0\alpha^2} = K_0 \exp\left(-\frac{\Delta H_{dim}}{RT}\right) \quad (1.7)$$

To get the values of the fraction of paramagnetic monomer (α), the area under the EPR absorption signal getting from the double integral of first derivative EPR signal is proportional to the ionic radical concentration following the Curie-Weiss law (equation 1.8).

$$\left[R^{*(+/-)} \right] = A \sim \frac{C}{(T - \theta)} \quad (1.8)$$

where

A = the area under the EPR absorption signal

T = the absolute temperature

θ = the Curie temperature

C = specific Curie constant

An experimental example is given in chapter 4 for TCNQ^{•-} including the graphs for explanation.

A second experimental method to detect the dimerization process is temperature-dependent UV/Vis spectroscopy. New absorption peaks appear in the visible region if the dimerization occurs. The indicated dimer peaks present in the region of 500 nm to 800 nm and the intensity of the indicated dimer peak is a function of the temperature with increasing intensity when temperature is decreased. The thermodynamic parameter of ionic radical dimerization in solution can be extracted from the UV/Vis measurements. According to equation (1.6), the equilibrium dimerization constant (K_{dim}) can be observed^[14].

The fraction of the stoichiometric concentration of existing paramagnetic monomer (α) comes from the calculation of apparent extinction coefficient (ε), which can be calculated from the optical density and the stoichiometric concentration (α). It related to the true extinction coefficient of dimer and monomer.

$$\varepsilon = \alpha\varepsilon^M + (1 - \alpha)\frac{1}{2}\varepsilon^D \quad (1.9)$$

Where

ε = the apparent extinction coefficient for dimerization

ε^M = the extinction coefficient of monomer

ε^D = the extinction coefficient of dimer

The value of the extinction coefficient of monomer (ε^M) and dimer (ε^D) were determined by an extrapolation procedure because there is not pure monomer or pure dimer in the solution. The extrapolation procedure was done by using the extinction coefficient at λ_{max} of dimer and monomer peaks and calculated by substituting α in equation (1.9) into equation (1.6) and yielding equations (1.10) and (1.11).

For the monomer peak (subscript 1) we get

$$\left[2K_{\text{dim}} / (\varepsilon_1^M - \frac{1}{2}\varepsilon_1^D) \right] \left(\varepsilon_1 - \frac{1}{2}\varepsilon_1^D \right)^2 c_0 = \varepsilon_1^M - \varepsilon_1 \quad (1.10)$$

For the dimer peak (subscript 2) we get

$$\left[\left(\frac{1}{2}\varepsilon_2^D - \varepsilon_2^M \right) / 2K_{\text{dim}} \right]^{1/2} \left[(\varepsilon_2 - \varepsilon_2^M) / c_0 \right]^{1/2} = \frac{1}{2}\varepsilon_2^D - \varepsilon_2 \quad (1.11)$$

where

K_{dim} = the dimerization constant

ε_1 = the apparent extinction coefficient for dimerization at monomer peak

ε_2 = the apparent extinction coefficient for dimerization at dimer peak

When plotting $\left[\left(\varepsilon_1 - \frac{1}{2} \varepsilon_1^D \right)^2 c_0 \right]$ against ε_1 for the monomer peak and $\left[(\varepsilon_2 - \varepsilon_2^M) / c_0 \right]^{1/2}$ against ε_2 for the dimer peak, the value ε_1^M and ε_2^D for monomer and dimer were determined by the intercepts, and also the value of K obtained from the slope.

The equilibrium dimerization constant (K_{dim}) in solution at each temperature was calculated from the fraction of the stoichiometric concentration of existing monomer (α) which was obtained from the measured extinction coefficient follow the equation (1.6). The enthalpy of dimerization (ΔH_{dim}) was observed by plotting the equilibrium dimerization constant (K_{dim}) against the reciprocal temperature for every measured temperature. From the slope of the plot, the enthalpy of dimerization (ΔH_{dim}) can be calculated by van't Hoff equation as showed in equation (1.7)

Resonance Raman spectroscopy is also a technique that can obtain the characteristic feature of the dimer^[9, 10]. The resonance Raman measurement used the information from temperature-dependent UV/Vis spectroscopy that the dimer at low temperature exhibits the absorption band of dimer. The Raman spectrum is measured by exciting the radiation frequencies in the range of the absorption band of the monomer and dimer to the sample at low temperature that the dimer occurred. The resonance Raman spectrum, of dimer, exhibits new resonance Raman peaks that correspond to an intradimer vibration at low frequencies which is different from the spectrum that was excited by the radiation frequencies of monomer absorption peaks.

X-ray crystallography is another technique to characterize dimer in crystal structure^[3-6, 15, 16]. The X-ray data show the intradimer distances of e.g. π -TCNE dimers with various counter-ions of 2.83-3.09 Å describing the existence of unusual multicenter long π -bond^[15, 16] which is shorter than the sum of van der Waals of two π -carbon (3.4 Å). X-ray crystallography provides the important information on structural parameters of dimers in supra molecular complexes to understand why dimers are stable. It reveals the position of counter-ions and the arrangement of monomer fragments in dimers because in some dimers the counter-ions are located in different position with possible

lateral rotation of monomer fragment with respect to another fragment in dimer geometry^[4, 5].

Many experimentalists have investigated radical ion dimerization. Kochi and co-worker synthesized and characterized ionic organic dimers by X-ray crystallography^[3-6]. They used temperature-dependent UV/VIS spectroscopy and electron paramagnetic resonance spectroscopy (EPR) to identify the dimeric character and properties of several ionic organic radicals after dimerization in solution^[3-6]. It is well known that the dimers exhibit unusual long multicenter bonds with π - π -interaction of the monomeric units. From the X-ray crystallographic data, the structures of tetracyanoethylene, 2,3-dichloro-5,6-dicyano-*p*-benzoquinone radical anion dimers with tetra-butylammonium (Bu_4N^+) counter ions and chloranil anion dimer with tetrapropylammonium counter ions show an interplanar distance of $2.9 \pm 0.1 \text{ \AA}$ which is longer than a normal covalent C-C bond^[3]. However this interplanar distance is significantly shorter than the sum of the van der Waals radii of the two fragments. According to Fig. 1.1, the interaction between the singly occupied molecular orbital (SOMO) containing the radical electron of radical ion monomer units of tetracyanoethylene radical anion with sodium counter-ion generate the bonding orbital, which is the highest occupied molecular orbital (HOMO) of the organic π -dimer. The most important experimental finding works are discussed in the next paragraphs including work from the group of Kochi^[3] and work from our institute^[2].

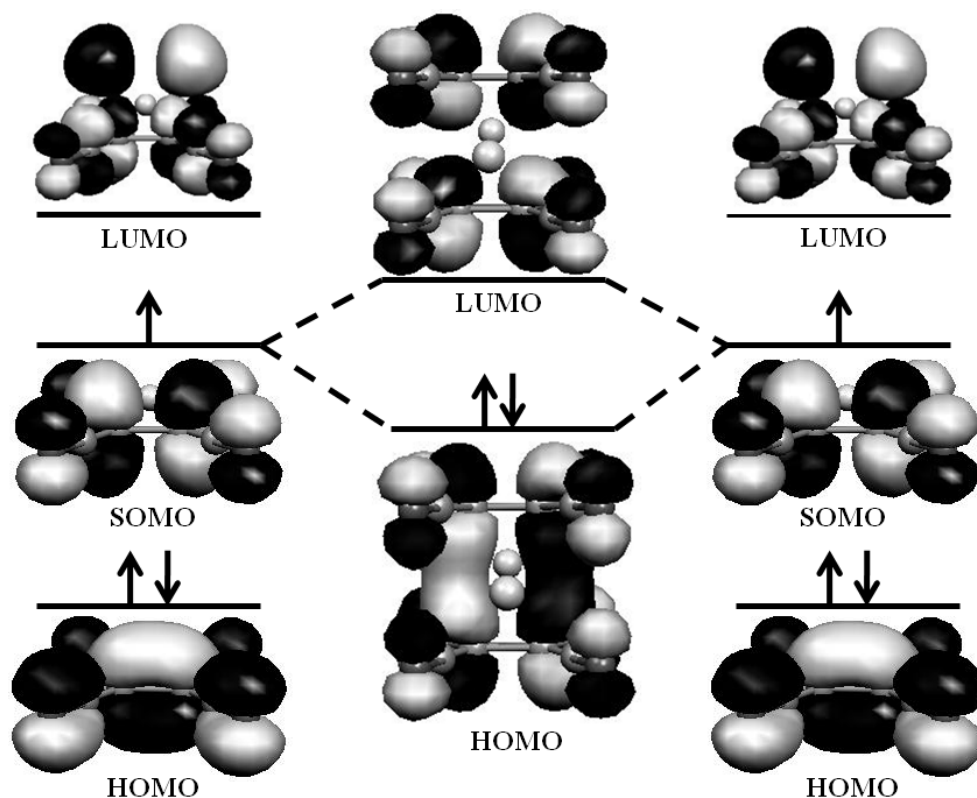


Figure 1.1: Molecular orbital diagram of dimerization of $[\text{TCNE}]^{\bullet-} \cdot \text{Na}^+$.

Radical cations from Wurster's salt and their substituted species, like unsubstituted and substituted *p*-phenylenediamine radical cations are another class of interesting radical ions which can form dimers in solution. The electronic absorption spectra of *p*-phenylenediamine ($\text{PPD}^{\bullet+}$), *N,N*-dimethyl-*p*-phenylenediamine ($\text{N,N-DMPPD}^{\bullet+}$) and 2,3,5,6-tetramethyl-*p*-phenylenediamine ($2,3,5,6\text{-TMPPD}^{\bullet+}$) radical cations using bromide as counter-ions have been investigated at low temperature in ethanol solution experimentally^[8]. At low radical concentration between 0.1-1 mM, UV/Vis spectra show new absorption bands which are assigned as dimer peak by Kimura *et. al*^[8] and Yokoyama *et. al*^[9]. UV/Vis spectra and Raman spectra measurements showed the same features in methanol (no dimer peak at room temperature, dimerization at low temperature), but in water, the dimer peak was already present at room temperature for $\text{PPD}^{\bullet+}$ ^[10]. Grampp *et. al.* measured dimerization enthalpies of $[\text{PPD}]_2^{2+}$, $[\text{N,N-DMPPD}]_2^{2+}$ and $[2,3,5,6\text{-TMPPD}]_2^{2+}$ dication dimers using the bromide salt for $\text{PPD}^{\bullet+}$ and perchlorate (ClO_4^-) salt for $\text{N,N-DMPPD}^{\bullet+}$ and $2,3,5,6\text{-TMPPD}^{\bullet+}$ in volume mixing solvent ethanol/ethylether (EtOH/Et₂O v/v 2:1) with radical concentration of

0.05 mM by temperature-dependent EPR-spectroscopy indicating a dimerization at -90°C ^[7].

From our knowledge, the organic radical ion dimerization processes mostly occurs at low temperature in the range of $180\text{-}200\text{ K}$ ^[2] but it is found that some ionic organic radicals can dimerize at higher temperature above 0°C ^[11, 12]. H.Awano and H. Ohigashi published the UV/Vis absorption spectra of of 3,3',5,5'-tetramethylbenzidine radical cation ($\text{TMB}^{\bullet+}$) with perchlorate counter-ion in acetonitrile measured in the temperature range from 15°C to 60°C showing the absorption band of dimer at 660 nm ^[11, 12]. This dimer peak at 660 nm is temperature-dependent with its highest intensity at 15°C , decreasing when the temperature increases and it disappears at 60°C . E.E.Ernstbrunner *et.al* discussed the dimerization of *p*-phenylenediamine radical cation ($\text{PPD}^{\bullet+}$) with bromide counter-ion in aqueous solution measured by UV/Vis spectroscopy^[10]. It was found that dimerization occurred at room temperature (293 K) showing the dimeric peak at 600 nm . When changing solvent to methanol, dimerization did not occur at room temperature.

The results in Ernstbrunner work indicate that the dielectric constant maybe play an important role in the dimerization process since the dielectric constant of water is much higher than methanol. The fact that dimerization in other solvents mainly occurs at low temperature, when the dielectric constant is increased, supports this assumption^[10]. This interpretation is one topic of this work.

In the next paragraphs an introduction to known theoretical findings is given. In recent years, several research groups have investigated theoretically the dimerization of organic radical ions such as tetracyanoethylene $^{\bullet-}$, tetracyano-*p*-quinodimethane $^{\bullet-}$, 2,3-dichloro-5,6-dicyano-*p*-benzoquinone $^{\bullet-}$, tetrachloro-*p*-benzoquinone $^{\bullet-}$, tetracyanopyrazine $^{\bullet-}$, tetracyano-*p*-benzoquinone $^{\bullet-}$, tetrathiofulvalene $^{\bullet+}$, oligothiophene $^{\bullet+}$ and terthiophene $^{\bullet+}$ ^[15-31]. They compared calculated structural parameters and thermodynamic properties with the experimental values. For example, single and multideterminant theoretical methods have been performed to investigate the intradimer distance, the character of interaction and the dimerization energy.

First in the present work, the results on the two most popular molecules ($\text{TCNE}^{\bullet-}$ and $\text{PPD}^{\bullet+}$) are discussed to get insight into the state of the art before starting my work. Dimers of radical anions of TCNE were mostly published. Novoa's group has studied the dimerization process of TCNE radical anion in a number of publications^[15-17, 22-29].

They used Density Functional Theory on the Mn and Cu crystal structures of the monomers and dimers^[17]. Novoa also investigated open-shell and closed-shell singlet and triplet states of the $[\text{TCNE}]_2^{2-}$ dimer including the solvent dichloromethane using the B3LYP functional^[24]. In these studies, it was found that Density Functional Theory (B3LYP), Møller-Plesset second order perturbation theory (MP2) and multi determinant complete active space method using an active space of two electrons in two orbitals (CASSCF(2,2)) destabilize the pure $[\text{TCNE}]_2^{2-}$ dimer^[18, 24, 27]. CASSCF calculations on the dimer of $[\text{TCNE}]_2^{2-}$ led to high positive dimerization energy (+68 kJ/mol^[21]) relative to the experiment (-33.4 kJ/mol^[1]). Inclusion of explicit solvent molecules in the calculations resulted in a locally stable minimum at short dimer distance^[24]. This was not confirmed by CASSCF(2,2) calculations, but confirmed when dispersion was included via the multireference MCQDPT method. Dispersion effects were described to stabilize the dimer and compute negative dimerization energies (-101 kJ/mol with MCQDPT^[24], -117 kJ/mol with MRMBPT2^[27] methods, respectively). The counter-ion was included by Head-Gordon using the multireference and perturbation methods (MRMP2 and MP2, respectively)^[20, 21] for $[\text{TCNE}]_2^{2-}$ also stabilizing the dimer (-72.4 kJ/mol).

The results on $[\text{TCNE}]_2^{2-}$ dimer show the importance of the counter-ion and that open-shell calculations result in different minima. Strong interaction of the monomer units has been suggested by these studies in agreement with the small interplanar distance found in X-ray studies characterized as 2-electron/4-center bond for $[\text{TCNE}]_2^{2-}$. The inclusion of multireference method to describe the multireference character of radical anion was necessary to describe the dimer with explicit solvent properly. Multireference method with second order perturbation (MRMP2) calculations including the counter-ion^[20] resulted in dimerization energies (-52.3 kJ/mol)^[20] close to the experimental energies (-33.4 kJ/mol)^[1]. Concluding the studies on $[\text{TCNE}]_2^{2-}$ dimer, it was found that dispersion interaction may play a role as well as the inclusion of counter-ions, and that the multireference character of the radical ion dimers should be taken into account.

T. Kamisuki and C. Hirose performed theoretical studies on $[\text{PPD}]_2^{2+}$ dimer to localize the possible stable geometries and to calculate vibrational frequencies in the monomer and dimers^[32]. MP2/6-31G* and B3LYP/6-31G* methods were taken in their work. They reveal meta-stable minima on potential energy surface plots varying the

intradimer distance, where the most stable geometry shows an inter-radical distance of 3.2 Å.

This thesis is focused on the theoretical study of the dimerization process of the organic radical ions in both, radical anions of tetracyanoethylene ($\text{TCNE}^{\bullet-}$), 2,3-dichloro-5,6-dicyano-p-benzoquinone ($\text{DDQ}^{\bullet-}$), tetracyano-p-quinodimethane ($\text{TCNQ}^{\bullet-}$) and radical cations of paraphenylenediamine ($\text{PPD}^{\bullet+}$), *N,N*-dimethyl-PPD ($\text{N,N-DMPPD}^{\bullet+}$), 2,3,5,6-tetramethyl-PPD ($\text{2,3,5,6-TMPPD}^{\bullet+}$), *N,N,N',N'*-tetramethyl-PPD ($\text{N,N,N',N'-TMPPD}^{\bullet+}$), 3,3',5,5'-tetramethylbenzidine ($\text{TMB}^{\bullet+}$), tetrathiofulvalene ($\text{TTF}^{\bullet+}$) in solution. For tetracyano-p-quinodimethane radical anion ($\text{TCNQ}^{\bullet-}$) dimerization, also are presented temperature-dependent EPR measurement to have a reference for the dielectric constant discussion. The counter-ions have been included in this study. Based on the knowledge of the strongly interacting species in the dimerization process, the Density Functional Method with inclusion of dispersion correction was chosen for the first time, to my best of knowledge, B3LYP-D for optimization and B2PLYP-D for energy correction containing correlation in the perturbation for such radical dimerization. The solvent was modeled by the conductor-like screening model (COSMO) for the experimental relevant solvents. The dielectric constant and refractive index of mixing solvents were taken from available experimental data^[33-47] and the dependence of the energetics from dielectric constant was investigated for the first time. Multideterminant methods like complete active space (CASSCF) and multireference method including Møller-Plesset second order perturbation correction (MRMP2) serve as benchmark and for testing the necessity of multideterminant method and quality of multireference methods.

The UV absorption spectra for the investigated compounds can trace the different monomeric and dimeric species in the dimerization process. Vertical excitation energies of the most stable conformers have been calculated at TDA-DFT level of theory within the COSMO model of solvation and compared to experimental data^[1, 3, 8-14, 48] for dimerization of radical ions of $\text{TCNE}^{\bullet-}$, $\text{DDQ}^{\bullet-}$, $\text{TCNQ}^{\bullet-}$, $\text{PPD}^{\bullet+}$, *N,N*-DMPPD^{•+}, 2,3,5,6-TMPPD^{•+}, *N,N,N',N'*-TMPPD^{•+}, TMB^{•+}, TTF^{•+}. Additionally, ethanol solvent molecules have been added explicitly to the monomer and dimer geometries of $\text{PPD}^{\bullet+}$, $[\text{PPD}]_2^{2+}$, *N,N*-DMPPD^{•+}, $[\text{N,N-DMPPD}]_2^{2+}$, 2,3,5,6-TMPPD^{•+}, $[\text{2,3,5,6-TMPPD}]_2^{2+}$, as well as water molecules to the $\text{PPD}^{\bullet+}$ and $[\text{PPD}]_2^{2+}$, for

detailed discussion of the UV/Vis spectra in solution to see the effect of explicit solvent to the computed UV/Vis spectra.

The aim of this work was to get a complete picture of dimerization in solution including the effect of dielectric constant, temperature, theoretical method and to describe and understand the dimerization process. Further, I want to provide the appropriate calculational methodology for the investigation of radical ions dimerization in solution by computational chemistry. Last, I explain the UV/Vis spectra of dimers and monomers, why each absorption peak occurred and the effect of substituting groups and solvents to the absorption spectra. Chapter 2 contains a brief summary of theoretical methods used. Chapter 3 describes the computational methods. Chapter 4 presents all data discussion of results. Chapter 5 gives a conclusion of the work. Part of the work (Chapter 4.2) is published in

Authors: Kraiwan Punyain, Anne-Marie Kelterer*, Günter Grampp

Title: Theoretical studies on the dimerization of substituted paraphenylenediamine radical cations

Journal: Spectrochimica Acta Part A

Doi: 10.1016/j.saa.2011.08.048

2. THEORETICAL BACKGROUND

Erwin Schrödinger invented Schrödinger equation in 1926 which is most useful for the application of quantum chemistry and solid state physics. Schrödinger equation can be solved analytically for the one electron system such as hydrogen or helium atom but for many electrons system the Schrödinger equation cannot be solved analytically. Many approximations had been developed for the calculation to solve the Schrödinger equation. In this chapter, we give a brief summary of theoretical methods which were used in these calculations.

2.1 TIME-INDEPENDENT SCHRÖDINGER EQUATION

The time-independent Schrödinger equation is shown in equation (2.1).

$$\hat{H}\Psi = E\Psi \quad (2.1)$$

where

\hat{H} = Hamiltonian operator for the system

Ψ = the total wave function

E = the total energy of the system

The total energy of the system is defined by the Hamiltonian operator which is the sum of kinetic energy and potential energy^[49].

The Hamiltonian for N electrons and M nuclei is defined in equation 2^[49].

$$\hat{H} = -\sum_{i=1}^N \frac{1}{2} \nabla_i^2 - \sum_{A=1}^M \frac{1}{2M_A} \nabla_A^2 - \sum_{i=1}^N \sum_{A=1}^M \frac{Z_A}{r_{iA}} + \sum_{i=1}^N \sum_{j>1}^N \frac{1}{r_{ij}} + \sum_{A=1}^M \sum_{B>A}^M \frac{Z_A Z_B}{R_{AB}} \quad (2.2)$$

where

M_A = the mass of nucleus A

Z_A = the atomic number of nucleus A

Z_B = the atomic number of nucleus B

r_{iA} = the distance between electron i and nucleus A

r_{ij} = the distance between electron i and j

R_{AB} = the distance between nucleus A and nucleus B

2.2 BORN-OPPENHEIMER APPROXIMATION

The nucleus consists of proton and neutron, it is much heavier than electron by around 1860 times^[50]. Thus the movement of the nucleus is very slowly when compared to the movement of the electrons. One approximation that considers the electrons are moving around the fixed nuclei is the Born-Oppenheimer approximation^[49]. In this approximation, the kinetic energy of the nuclei can be neglected and the repulsion between the nuclei can be treated to be constant in the Hamiltonian operator. The new Hamiltonian following Born-Oppenheimer approximation with the motion of N electrons in the field of M nuclei is called the electronic Hamiltonian (shown in equation (2.3)).

$$\hat{H}_{elec} = -\sum_{i=1}^N \frac{1}{2} \nabla_i^2 - \sum_{i=1}^N \sum_{A=1}^M \frac{Z_A}{r_{iA}} + \sum_{i=1}^N \sum_{j>1}^N \frac{1}{r_{ij}} \quad (2.3)$$

The Schrödinger equation of the electrons is shown in equation (2.4).

$$\hat{H}_{elec} \Phi_{elec} = E_{elec} \Phi_{elec} \quad (2.4)$$

where the electronic wave function describes the motion of electrons and depends on the electron and nuclear coordinate.

$$\Phi_{elec} = \Phi_{elec}(r_i, R_A) \quad (2.5)$$

where the electronic energy depends only on nuclear coordinate.

$$E_{elec} = E_{elec}(R_A) \quad (2.6)$$

When substituting the electronic energy into the total Hamiltonian in equation (2.2) this is generating a new total Hamiltonian form.

$$\hat{H} = -\sum_{A=1}^M \frac{1}{2M_A} \nabla_A^2 + E_{elec} + \sum_{A=1}^M \sum_{B>A}^M \frac{Z_A Z_B}{R_{AB}} \quad (2.7)$$

2.3 BASIS FUNCTIONS

There are two kinds of spin of electrons which are spin up, $\alpha(\omega)$, and spin down, $\beta(\omega)$, respectively. The two spin functions are orthonormal. An electron is described by three spatial coordinates, \mathbf{r} , and one spin coordinate, ω , and denote four coordinate as \mathbf{x} .

$$\mathbf{x} = \{\mathbf{r}, \omega\} \quad (2.8)$$

Since electrons are fermions. There is no two electrons have the same number of all four quantum number (n, l, m_l, m_s) called Pauli exclusion principle. The electrons wave function must be antisymmetric with respect to the interchange of the coordinate \mathbf{x} (space and spin) of any two electrons^[49].

$$\Phi(\mathbf{x}_1, \dots, \mathbf{x}_i, \dots, \mathbf{x}_j, \dots, \mathbf{x}_N) = -\Phi(\mathbf{x}_1, \dots, \mathbf{x}_j, \dots, \mathbf{x}_i, \dots, \mathbf{x}_N) \quad (2.9)$$

The wave function of an electron is defined as an orbital and described in both spatial distribution and spin which is represented in spin orbital, $\chi(\mathbf{x})$. Each spatial orbital, $\psi(r)$, can form two different spin orbitals corresponding to spin up and spin down.

$$\chi(\mathbf{x}) = \begin{cases} \psi(r)\alpha(\omega) \\ \text{or} \\ \psi(r)\beta(\omega) \end{cases} \quad (2.10)$$

where $\chi(\mathbf{x})$ = the spin orbital

$\psi(r)$ = the spatial orbital

$\alpha(\omega)$ = spin up

$\beta(\omega)$ = spin down

The wave function of many electrons in molecule is represented as molecular orbitals and written as Slater determinant. The molecular orbitals of N -electron occupy in N spin orbitals is written as follow.

$$\Psi(\mathbf{x}_1, \mathbf{x}_2, \dots, \mathbf{x}_N) = (N!)^{-1/2} \begin{pmatrix} \chi_1(\mathbf{x}_1) & \chi_2(\mathbf{x}_1) \cdots & \chi_N(\mathbf{x}_1) \\ \chi_1(\mathbf{x}_2) & \chi_2(\mathbf{x}_2) \cdots & \chi_N(\mathbf{x}_2) \\ \vdots & \vdots & \vdots \\ \chi_1(\mathbf{x}_N) & \chi_2(\mathbf{x}_N) \cdots & \chi_N(\mathbf{x}_N) \end{pmatrix} \quad (2.11)$$

where $(N!)^{-1/2}$ is a normalization factor.

The many electrons wave function can be written in a short hand notation which shows only the diagonal elements of the Slater determinant.

$$\Psi(\mathbf{x}_1, \mathbf{x}_2, \dots, \mathbf{x}_N) = |\chi_1(\mathbf{x}_1)\chi_2(\mathbf{x}_2) \cdots \chi_N(\mathbf{x}_N)\rangle \quad (2.12)$$

When labels the electron in order to $\mathbf{x}_1, \mathbf{x}_2, \dots, \mathbf{x}_N$, the many electrons wave function can be written further shortened to equation (2.13) which satisfy the antisymmetric wave function.

$$\Psi(\mathbf{x}_1, \mathbf{x}_2, \dots, \mathbf{x}_N) = |\chi_1 \chi_2 \cdots \chi_N\rangle \quad (2.13)$$

2.4 CLOSED- AND OPEN-SHELL SYSTEM

CLOSED-SHELL: RESTRICTED HARTREE-FOCK (RHF)

The molecular system has an even number of the total electrons (N) and the spatial orbitals contain two electrons, one spin up (α) and one spin down (β) in the same spatial orbitals^[49] (shown in **Figure 2.1**).

Giving a set of K orthonormal spatial orbitals $\{\psi_i | i = 1, 2, \dots, K\}$ and the set of $2K$ spin orbitals $\{\chi_i | i = 1, 2, \dots, 2K\}$ is formed by multiply α or β spin functions to each spatial orbital. The restricted spin orbitals have the form of

$$\begin{aligned} \chi_{2i-1}(\mathbf{x}) &= \psi_i(\mathbf{r})\alpha(\omega) \\ \chi_{2i}(\mathbf{x}) &= \psi_i(\mathbf{r})\beta(\omega) \end{aligned} \quad (2.14)$$

The determinants are formed from the spin orbitals which is called restricted determinants. Thus the ground state wave function of the interested system is called “Restricted Hartree-Fock wave function” which can be written as

$$|\Psi_{\text{RHF}}\rangle = |\chi_1 \chi_2 \cdots \chi_{N-1} \chi_N\rangle = |\psi_1 \bar{\psi}_1 \cdots \psi_a \bar{\psi}_a \cdots \psi_{N/2} \bar{\psi}_{N/2}\rangle \quad (2.15)$$

Each of the occupied spatial molecular orbitals is doubly occupied of spin up (α) and spin down (β) electrons. The number of the occupied spatial orbitals in restricted Hartree-Fock is equal to the number of the total electrons divided by two ($N/2$).

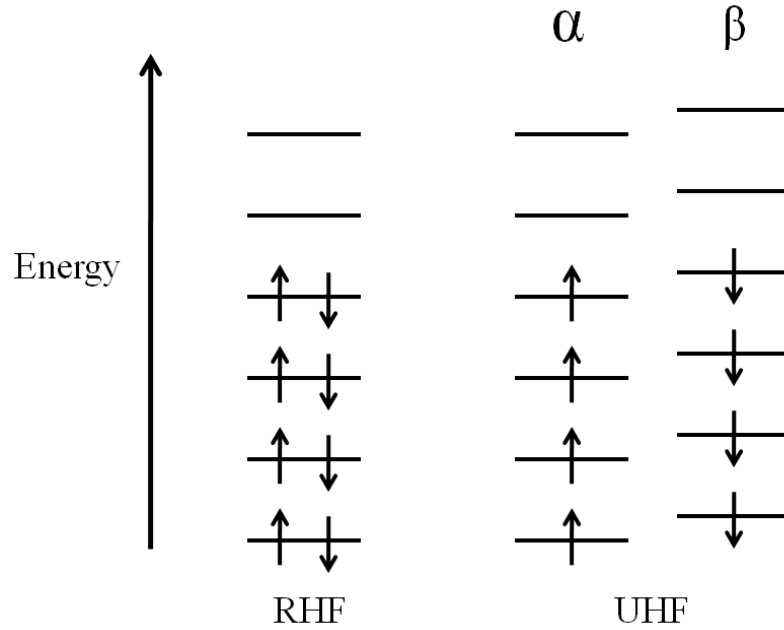


Figure 2.1: *Restricted and unrestricted Hartree-Fock.*

OPEN-SHELL: UNRESTRICTED HARTREE-FOCK (UHF)

Unrestricted Hartree-Fock is different from Restricted Hartree-Fock that the unrestricted determinants are formed from unrestricted spin orbitals which have different spatial orbitals for different spin^[49].

Giving a set of K orthonormal spatial orbital of $\{\psi_i^\alpha\}$ for spin up (α) and a different set of K orthonormal spatial orbitals of $\{\psi_i^\beta\}$ for spin down (β) but these two sets are not orthogonal.

$$\langle \psi_i^\alpha | \psi_j^\beta \rangle = S_{ij}^{\alpha\beta} \quad (2.16)$$

where $S_{ij}^{\alpha\beta}$ is an overlap matrix.

Then the $2K$ unrestricted spin orbitals are formed which is an orthonormal set although the α and β spatial orbitals are not orthogonal.

$$\begin{aligned} \chi_{2i-1}(\mathbf{x}) &= \psi_i^\alpha(\mathbf{r})\alpha(\omega) \\ \chi_{2i}(\mathbf{x}) &= \psi_i^\beta(\mathbf{r})\beta(\omega) \end{aligned} \quad (2.17)$$

The energies of two spatial orbitals where alpha (α) and beta (β) spin occupied are different and influenced spin-spin correlation.

Assume that in the molecular system have N electrons spin up (α) and N electrons spin down (β), the unrestricted Hartree-Fock wave function can be written as

$$|\Psi_{\text{UHF}}\rangle = |\psi_1^\alpha \bar{\psi}_1^\beta \psi_2^\alpha \bar{\psi}_2^\beta \cdots \psi_N^\alpha \bar{\psi}_N^\beta\rangle \quad (2.18)$$

2.5 INTRODUCTION TO DENSITY FUNCTIONAL THEORY

(DFT)

Density Functional Theory (DFT) is a calculational method of the electronic structure that is most widely used. In DFT, the ground state electronic energy is a functional of the electron density^[51] (ρ) which is proofed by Hohenberg and Kohn^[52]. The electron density (ρ) is the square of the wave function and a functional means a function of function. When integrated overall space of electron density (ρ), the total number of electrons (N) is obtained^[50].

$$N = \int \rho(r) dr \quad (2.19)$$

The energy functional was divided into five specific components as presented in equation (2.20)^[50].

$$E[\rho(r)] = T_{ni}[\rho(r)] + V_{ne}[\rho(r)] + V_{ee}[\rho(r)] + \Delta T[\rho(r)] + \Delta V_{ee}[\rho(r)] \quad (2.20)$$

where

$E[\rho(r)]$ = the total energy of all specific energy parts

$T_{ni}[\rho(r)]$ = the kinetic energy of non-interacting electron

$V_{ne}[\rho(r)]$ = the nuclear-electron interaction energy

$V_{ee}[\rho(r)]$ = the classical electron-electron repulsion energy

$\Delta T[\rho(r)]$ = the correction to the kinetic energy

$\Delta V_{ee}[\rho(r)]$ = all non-classical correction to the electron-electron repulsion energy

When inserting the electron density as shown in equation (2.21)

$$\rho = \sum_{i=1}^N \langle \chi_i | \chi_i \rangle \quad (2.21)$$

where χ_i is the orbital used to minimize the total energy in equation (2.22).

Thus the total electronic energy of all specific energy parts can be written as

$$\begin{aligned} E[\rho(r)] = & \sum_i^N \left(\langle \chi_i | -\frac{1}{2} \nabla_i^2 | \chi_i \rangle - \langle \chi_i | \sum_k^{\text{nuclei}} \frac{Z_k}{|r_i - r_k|} | \chi_i \rangle \right) \\ & + \sum_i^N \langle \chi_i | \frac{1}{2} \int \frac{\rho(r')}{|r_i - r'|} | \chi_i \rangle + E_{XC}[\rho(r)] \end{aligned} \quad (22)$$

The E_{XC} term is called the exchange-correlation energy which is the summation of the correction to the kinetic energy deriving from the interacting nature of the electrons

and all non-classical corrections to the electron-electron repulsion energy (ΔV_{ee}) that are difficult and unknown the exact formula.

In 1965, Kohn and Sham constructed the Hamiltonian operator for a non-interacting electron which is a sum of one-electron operators^[53]. In the calculation, one has to find the orbital χ to minimize the energy following Kohn-Sham equation.

$$h_i^{KS} \chi_i = \varepsilon_i \chi_i \quad (2.23)$$

Where h_i^{KS} is the Kohn-Sham one-electron operator

$$h_i^{KS} = -\frac{1}{2} \nabla_i^2 - \sum_k^{nuclei} \frac{Z_k}{|r_i - r_k|} + \int \frac{\rho(r')}{|r_i - r'|} dr' + V_{XC} \quad (2.24)$$

and

$$V_{XC} = \frac{\delta E_{XC}}{\delta \rho} \quad (2.25)$$

where V_{XC} is a so-called functional derivative.

The Kohn-Sham equation for non-interacting system that the density is the same as the real system is defined in equation (2.26).

$$\sum_{i=1}^N h_i^{KS} | \chi_1 \chi_2 \chi_3 \dots \chi_N \rangle = \sum_{i=1}^N \varepsilon_i | \chi_1 \chi_2 \chi_3 \dots \chi_N \rangle \quad (2.26)$$

The exchange-correlation energy is the summation of the correction of kinetic energy (ΔT) and the correction of the electron-electron repulsion (ΔV_{ee}) and depend on the electron density (ρ).

$$E_{XC}[\rho(r)] = \int \rho(r) \varepsilon_{XC}[\rho(r)] dr \quad (2.27)$$

where ε_{XC} = the energy density

$$E_{XC}[\rho(r)] = E_X[\rho(r)] + E_C[\rho(r)] \quad (2.28)$$

Some of the exchange-correlation functionals using in our calculations will be presented following.

2.5.1 HYBRID FUNCTIONAL

The connection between the non-interacting and the real system (full interacting) is called Adiabatic Connection Method (ACM) which is also called hybrid method^[50]. It is the convert of the non-interacting system to the interacting system. The exchange-correlation energy is computed following the equation (2.29).

$$E_{XC} = \int_0^1 \langle \psi(\lambda) | V_{XC}(\lambda) | \psi(\lambda) \rangle d\lambda \quad (2.29)$$

λ is a factor between 0 (non-interacting) to 1 (full interacting) explaining the range of interaction. When λ equal to zero, the electrons are non-interacting and it has only pure exchange energy with no dynamical correlation energy. This exchange energy is exact for non-interacting systems because the Slater determinant of the Kohn-Sham orbitals is an exact wave function which is equal to the conventional Hartree-Fock exchange energy. The exchange-correlation energy of adiabatic connection method is described as:

$$E_{XC} = E_X^{HF} + z(E_{XC}^{DFT} - E_X^{HF}) \quad (2.30)$$

But the parameter z is unknown and treated as empirical constant that will be optimized for the functional. If we define a is equal to $1-z$, we get the exchange-correlation energy equation as:

$$E_{XC} = (1-a)E_{XC}^{DFT} + aE_X^{HF} \quad (2.31)$$

B3PW91 functional was first developed by Becke^[54]. Three empirical parameters (a , b and c) were added and expressed in equation (2.32):

$$E_{XC}^{B3PW91} = (1-a)E_X^{LSDA} + aE_X^{HF} + b\Delta E_X^B + E_C^{LSDA} + c\Delta E_C^{PW91} \quad (2.32)$$

where in the term $(1-a)E_X^{LSDA}$ and E_C^{LSDA} is the average of the exact exchange energy at $\lambda=0$ and the LSDA exchange-correlation energy at $\lambda=1$ (half-and-half method which z

value in equation 31 equal to 0.5), E_X^{HF} is the exact exchange energy, ΔE_X^B is Becke's 1988 gradient correction for exchange and ΔE_C^{PW91} is the gradient correction for correlation of Perdew and Wang. The values of three parameters are $a = 0.20$, $b = 0.72$ and $c = 0.81$, respectively.

B3LYP is a functional of adiabatic connection method (Hybrid method) modified from B3PW91 functional by Stephens^[55] to use LYP instead of PW91 for the correlation energy which is the most popular and widely used nowadays. The form of the exchange-correlation energy of B3LYP functional defined in equation (2.33):

$$E_{XC}^{B3LYP} = (1 - a)E_X^{LSDA} + aE_X^{HF} + b\Delta E_X^B + (1 - c)E_C^{LSDA} + cE_C^{LYP} \quad (2.33)$$

where the parameters a , b and c are the same as in B3PW91 functional. So B3LYP functional contains 20% of the exact Hartree-Fock exchange energy.

2.5.2 HYBRID METHOD WITH PERTURBATIVE SECOND-ORDER CORRELATION

Perturbation was combined to the Kohn-Sham Density Functional Theory (KS-DFT) to generate a new exchange-correlation functional (shown in equation (2.27)) constructed by Grimme^[56].

$$E_{XC} = (1 - a_X)E_X^{GGA} + a_X E_X^{HF} + bE_C^{GGA} + cE_C^{PT2} \quad (2.33)$$

and

$$E_C^{PT2} = \frac{1}{4} \sum_{ia} \sum_{jb} \frac{[\langle ia | jb \rangle - \langle ib | ja \rangle]^2}{\varepsilon_i + \varepsilon_j - \varepsilon_a - \varepsilon_b} \quad (2.34)$$

where

E_X^{GGA} is the GGA exchange energy

E_C^{GGA} is the GGA correlation energy

E_C^{PT2} is the second-order Møller-Plesset-type expression for the correlation energy

a_x is the Hartree-Fock exchange mixing parameter

b is the contribution of GGA

c is the contribution to perturbative correlation

The calculational method performs a usual self-consistent hybrid Kohn-Sham DFT followed by a standard Møller-Plesset second-order perturbation (MP2) procedure.

The new functional is called B2-PLYP which is an interpolation approach between pure GGA-Density Functional Theory with Møller-Plesset second-order perturbation (MP2)^[56]. It is a combination between B88 and LYP in the GGA part which is also a part of the B3LYP hybrid functional which allows some assessment of the effect of the second-order perturbation. The values of three minimum parameter^[56] (a_x , b and c) in B2-PLYP functional as shown in equation 33 are $a_x = 0.53$, $b = 1 - c = 0.73$ and $c = 0.27$. So B2PLYP functional contains 53% of the exact Hartree-Fock exchange energy.

2.5.3 TD-DFT and TDA-DFT

The time-dependent Schrödinger equation for the wave function theory^[49] is

$$i\hbar \frac{\partial}{\partial t} \Psi = \hat{H} \Psi \quad (2.35)$$

where

Ψ = the wave function

$i\hbar \frac{\partial}{\partial t}$ = the energy operator

\hat{H} = the Hamiltonian operator

The three dimension single particle time-dependent Schrödinger equation can be written as

$$i\hbar \frac{\partial}{\partial t} \Psi(r,t) = \hat{H} \Psi = \left(-\frac{\hbar^2}{2m} \nabla^2 + V(r) \right) \Psi(r,t) \quad (2.36)$$

where

$\Psi(r,t)$ = the wave function for the single particle at position r time t

$$\hat{H} = -\frac{\hbar^2}{2m} \nabla^2 + V(r)$$

$-\frac{\hbar^2}{2m}\nabla^2$ = the kinetic energy operator

∇^2 = the Laplace operator: $\frac{\partial^2}{\partial x^2} + \frac{\partial^2}{\partial y^2} + \frac{\partial^2}{\partial z^2}$ for three dimension

$V(r)$ = the time-independent potential energy at position r

Equation (2.36) can be written in the form of atomic unit express as

$$i\frac{\partial}{\partial t}\Psi(r,t) = \hat{H}\Psi = \left(-\frac{\nabla^2}{2} + V(r)\right)\Psi(r,t) \quad (2.37)$$

TIME-DEPENDENT DENSITY FUNCTIONAL THEORY (TD-DFT)

It is interesting to apply density functional theory (DFT) to the electronic excitation because it used less computational time than multi-configuration calculations. Time-dependent density functional theory (TD-DFT) in adiabatic approximation was published^[57-59] and is useful for molecular excitation calculations in quantum chemistry.

The time-dependent Kohn-Sham equation in atomic unit describes the non-interacting system as follows:

$$i\frac{\partial}{\partial t}\varphi_i(r,t) = \left(-\frac{\nabla^2}{2} + v_{KS}(r,t)\right)\varphi_i(r,t) \quad (2.38)$$

The Hamiltonian operator consists of the kinetic operator and potential^[59]. The time-dependent Kohn-Sham equation choose the non-interacting system to form the density becomes identical to the density of the interacting system. The time-dependent potential $v_{KS}(r,t)$ depends on density, $\rho(r,t)$, and time, t . The potential, $v_e(r,t)$, is the summation of static potential, $v_{stat}(r)$, and time-dependent external potential, $v_i(r)f(t)$. The density, $\rho(r,t)$, depends on the summation of square of spin orbitals. The time-dependent exchange-correlation functional, $A_{XC}[\rho]$, is the analogue of, $E_{XC}[\rho]$, in the static case which is a functional of the density as a function of space and time.

$$v_{KS}(r,t) = v_e(r,t) + \int d^3r' \frac{\rho(r',t)}{|r-r'|} + \frac{\delta A_{XC}[\rho]}{\delta \rho(r,t)} \quad (2.39)$$

where

$$v_e(r, t) = v_{stat}(r) + v_t(r) f(t) \quad (2.40)$$

$$\rho(r, t) = \sum_{i=1}^N |\varphi_i(r, t)|^2 \quad (2.41)$$

$$\delta A_{XC}[\rho] = \int dt E_{XC}[\rho] \Big|_{\rho=\rho(r,t)} \quad (2.42)$$

In the electronic excitation process (the time-dependent response of the interacting system), the situation of the molecule is initially in ground state and the time dependent part of potential $v_e(r, t)$ is adiabatically switched on. The first-order density response $\rho^{(1)}$ is described by the linear response kernel of the interacting system $\chi(t, t', r, r')$ or alternatively described by the linear response kernel of the non-interacting (Kohn-Sham) system $\chi_{KS}(t, t', r, r')$. In this case the response is the linear response kernel of the non-interacting (Kohn-Sham) system because it is easy to calculate.

$$\rho^{(1)}(r, t) = \int d^3 r' dt' \chi_{KS}(t, t', r, r') \left[v_t(r') f(t') + \int d^3 r'' \frac{\rho^{(1)}(r'', t')}{|r' - r''|} + \int d^3 r'' \frac{\delta^2 E_{XC}}{\delta \rho(r') \delta \rho(r'')} \rho^{(1)}(r'', t') \right] \quad (2.43)$$

When we use the Fourier transform, $f(\omega) = \int e^{i\omega t} f(t) dt$,

the equation (2.43) becomes

$$\rho^{(1)}(r, \omega) = \int d^3 r' \chi_{KS}(\omega, r, r') \left[v_t(r') f(\omega) + \int d^3 r'' \frac{\rho^{(1)}(r'', \omega)}{|r' - r''|} + \int d^3 r'' \frac{\delta^2 E_{XC}}{\delta \rho(r') \delta \rho(r'')} \rho^{(1)}(r'', \omega) \right] \quad (2.44)$$

Then we use the parametrization with the ground state Kohn-Sham orbital $\phi_{k\sigma}(r)$ to find a self consistent first-order response $\rho^{(1)}(r, \omega)$.

$$\rho^{(1)}(r, \omega) = \sum_{i,a,\sigma} [P_{ia\sigma}(\omega) \phi_{a\sigma}^*(r) \phi_{i\sigma}(r) + P_{ai\sigma}(\omega) \phi_{a\sigma}(r) \phi_{i\sigma}^*(r)] \quad (2.45)$$

Where

i, j = the indices for occupied orbitals

a, b = the indices for virtual orbitals

k, l, m, n = the indices for general orbitals

σ = the spin variable α or β

The linear response kernel of the non-interacting (Kohn-Sham), $\chi_{KS,\sigma\sigma'}(\omega, r, r')$, is expressed as

$$\chi_{KS,\sigma\sigma'}(\omega, r, r') = \delta_{\sigma\sigma'} \sum_{ia} \left(\frac{\phi_{i\sigma}^*(r) \phi_{a\sigma}(r) \phi_{i\sigma}(r') \phi_{a\sigma}^*(r')}{\omega - (\varepsilon_{a\sigma} - \varepsilon_{i\sigma})} - \frac{\phi_{i\sigma}(r) \phi_{a\sigma}^*(r) \phi_{i\sigma}^*(r') \phi_{a\sigma}(r')}{\omega + (\varepsilon_{a\sigma} - \varepsilon_{i\sigma})} \right) \quad (2.46)$$

and

$$(v_t)_{ia\sigma} = \int d^3r \phi_{i\sigma}^*(r) v_t(r) \phi_{a\sigma}(r) \quad (2.47)$$

Then the two density matrix equation for occupied-virtual $P_{ia\sigma}(\omega)$ and virtual-occupied $P_{ai\sigma}(\omega)$ are obtained.

$$\left[\delta_{\sigma\tau} \delta_{ij} \delta_{ab} (\varepsilon_{a\sigma} - \varepsilon_{i\sigma} + \omega) + K_{ia\sigma, jbt\tau} \right] P_{jbt\tau} + K_{ia\sigma, bj\tau} P_{bj\tau} = -(v_t)_{ia\sigma} \quad (2.48)$$

$$\left[\delta_{\sigma\tau} \delta_{ij} \delta_{ab} (\varepsilon_{a\sigma} - \varepsilon_{i\sigma} - \omega) + K_{ai\sigma, bj\tau} \right] P_{bj\tau} + K_{ai\sigma, jbt\tau} P_{jbt\tau} = -(v_t)_{ai\sigma} \quad (2.49)$$

where the matrix K is

$$K_{kl\sigma, mn\tau} = \int d^3r d^3r' \phi_{k\sigma}^*(r) \phi_{l\sigma}(r) \left(\frac{1}{|r-r'|} + \frac{\delta^2 E_{XC}}{\delta\rho_\sigma(r) \delta\rho_\tau(r')} \right) \phi_{n\tau}^*(r') \phi_{m\tau}(r') \quad (2.50)$$

Then used the notation

$$X_{ia\sigma} = P_{ia\sigma}(\omega)$$

$$Y_{ai\sigma} = P_{ai\sigma}(\omega)$$

$$V_{ia\sigma} = (v_t)_{ia\sigma}$$

$$V_{ai\sigma}^* = (v_t)_{ai\sigma}$$

The matrix equation for $P_{ia\sigma}(\omega)$ and $P_{ai\sigma}(\omega)$ can be written in the in the form of

$$\left[\begin{pmatrix} L & M \\ M^* & L^* \end{pmatrix} - \omega \begin{pmatrix} -1 & 0 \\ 0 & 1 \end{pmatrix} \right] \begin{pmatrix} X \\ Y \end{pmatrix} = -f(\omega) \begin{pmatrix} V \\ V^* \end{pmatrix} \quad (2.51)$$

with

$$L_{ia\sigma, jbt\tau} = \delta_{\sigma\tau} \delta_{ij} \delta_{ab} (\varepsilon_{a\sigma} - \varepsilon_{i\sigma}) + K_{ia\sigma, jbt\tau} \quad (2.52)$$

$$M_{ia\sigma, bj\tau} = K_{ia\sigma, bj\tau} \quad (2.53)$$

Due to the matrix on the left hand side in equation (2.51) has zero eigenvalue because the excitation energies in response theory are characterized as the poles of the response functions. So we obtain a non-Hermitian eigenvalue equation.

$$\begin{pmatrix} L & M \\ M^* & L^* \end{pmatrix} \begin{pmatrix} X \\ Y \end{pmatrix} = \omega \begin{pmatrix} -1 & 0 \\ 0 & 1 \end{pmatrix} \begin{pmatrix} X \\ Y \end{pmatrix} \quad (2.54)$$

Solve the equation (2.52) and (2.53) in the equation 54 to obtain the TD-DFT excitation energies ω .

TIME-DEPENDENT DENSITY FUNCTIONAL THEORY WITH TAMM-DANCOFF APPROXIMATION (TDA-DFT)

The Tamm-Dancoff approximation time-dependent density functional theory^[60] (TDA-DFT) is different from TD-DFT that considering only the virtual-occupied density matrix elements $P_{ai\sigma}(\omega)$ and neglecting the occupied-virtual density matrix elements $P_{ia\sigma}(\omega)$. Then we obtained only equation (2.49) for the virtual-occupied density matrix equation. A Hermitian eigenvalue equation is one-half dimension of TD-DFT and obtained the TDA-DFT excitation energy, ω .

$$LY = \omega Y \quad (2.55)$$

Consequence for energies and oscillator strengths.

2.6 VAN DER WAALS INTERACTION IN COMPLEX MOLECULES

Long-range dispersion interactions are factors that play an important role in complex molecules especially for molecular weak interaction between atoms and molecules. It is in equilibrium with electrostatic and exchange-repulsion interactions^[61, 62]. Density Functional Theory (DFT) is the most widely used in molecular structure calculation that include electron correlation effects. The dispersion correction to the total energy of density functional theory can be written as^[61, 62]:

$$E_{DFT-D} = E_{DFT} + E_{disp} \quad (2.56)$$

where

E_{DFT} = the total DFT energy

E_{disp} = the empirical dispersion

The dispersion energy can be corrected after Grimme, who used a parameter Lenard-Jones potential for 2-center interactions.

$$E_{disp} = -S_6 \sum_{i=1}^{N_{at}-1} \sum_{j=i+1}^{N_{at}} \frac{C_6^{ij}}{R_{ij}^6} f_{dmp}(R_{ij}) \quad (2.57)$$

N_{at} = the number of atoms in the system

C_6^{ij} = the dispersion coefficient for atom pair ij

S_6 = a global scaling factor

R_{ij} = the distance between atom i and j

$f_{dmp}(R_{ij})$ = a damping function to avoid near-singularities for small R

$$f_{dmp}(R_{ij}) = \frac{1}{1 + e^{-\alpha(R/R_0 - 1)}}$$

R_0 = sum of atomic van der Waals radii

A simple average form of the dispersion coefficient for atom pair ij is described as:

$$C_6^{ij} = 2 \frac{C_6^i C_6^j}{C_6^i + C_6^j} \quad (2.58)$$

2.7 BASIS SET SUPER POSITION ERROR

For a dimer, the interaction energy can be obtained by subtracting the energy of the separate monomers, A and B, from the total energy of the dimer^[63].

$$\Delta E_{int} = E_{(dimer)} - E_{(monomer A)} - E_{(monomer B)}$$

In the weak molecular interaction calculation, the correction of the basis set superposition error (BSSE) is necessary for the interaction energy. Boys and Bernadi published the BSSE formula^[64] to calculate the interaction energy of the monomer A and B in dimer AB.

$$\Delta E = E_{AB}^{AB}(AB) - E_A^A(A) - E_B^B(B) - \left[E_A^{AB}(AB) - E_A^{AB}(A) + E_B^{AB}(AB) - E_B^{AB}(B) \right] \quad (2.59)$$

and

$$BSSE = \left[E_A^{AB}(AB) - E_A^{AB}(A) + E_B^{AB}(AB) - E_B^{AB}(B) \right] \quad (2.60)$$

Where

$E_{AB}^{AB}(AB)$ = the total energy of dimer AB

$E_A^A(A)$ = the total energy of monomer A

$E_B^B(B)$ = the total energy of monomer B

$E_A^{AB}(AB)$ = the total energy of fragment A in dimer AB

$E_B^{AB}(AB)$ = the total energy of fragment B in dimer AB

$E_A^{AB}(A)$ = the total energy of isolated fragment A in dimer AB

$E_B^{AB}(B)$ = the total energy of isolated fragment B in dimer AB

2.8 MULTI-CONFIGURATION CALCULATION METHODS

Multi-configuration self-consistent field is a post Hartree-Fock method that uses the wave function constructed by more than one electron configuration (not only one ground state Slater determinant but includes excited state determinants). The multi-configuration wave function^[49] is written as:

$$|\Phi\rangle_0 = c_0 |\psi_0\rangle + \sum_{ar} c_a^r |\psi_a^r\rangle + \sum_{\substack{a<b \\ r<s}} c_{ab}^{rs} |\psi_{ab}^{rs}\rangle + \sum_{\substack{a<b<c \\ r<s<t}} c_{abc}^{rst} |\psi_{abc}^{rst}\rangle + \dots \quad (2.61)$$

where

$|\Phi\rangle_0$ = the exact many-electron wave function

$|\psi_0\rangle$ = the restricted closed-shell Hartree-Fock determinant

$|\psi_a^r\rangle$ = the singly excited determinant

$|\psi_{ab}^{rs}\rangle$ = the doubly excited determinant

$|\psi_{abc}^{rst}\rangle$ = the triply excited determinant

The excited determinants are different from the ground state determinant, for example, the single excited determinant, $|\psi_a^r\rangle$, the spin orbital χ_a is replaced by the spin orbital χ_r . The restrictions on the summation indices ($a < b < c$ and $r < s < t$, etc) insure that a given excited determinant is included in the sum only once.

Two methods (CASSCF and MRMP2) of multi-configuration calculations will be presented in this chapter.

2.8.1 COMPLETE ACTIVE SPACE SELF-CONSISTENT FIELD (CASSCF)

The necessary condition in CASSCF calculation is that it has a limited number of active electrons (m) and a limited number of active molecular orbitals (n) which contain occupied and virtual molecular orbitals^[63]. The electrons in CASSCF calculation are divided into two sets, the first set of electrons is the inactive electrons which are doubly occupied in the inactive molecular orbitals space, the second set of electrons is the active electrons occupied in the active molecular orbitals space and can be excited to the higher active virtual molecular orbitals space. The coefficients of the atomic orbitals in the molecular orbitals are optimized. In CASSCF calculations, dynamic correlation is included. Selecting the right active electrons and active space (m, n) is very important in CASSCF calculations. There is no fixed rule for selecting the active electrons and active space (m, n) but it needs some tricks depending on the molecular problem.

2.8.2 MULTI-REFERENCE MØLLER-PLESSET SECOND-ORDER PERTURBATION (MRMP2)

Multi-reference Møller-Plesset second-order perturbation (MRMP2) was constructed by K. Hirao^[65-67]. The multi-reference technique with many-body second-order perturbation theory is presented in the MRMP2 calculation. A theory of MRMP2 is described as follow.

The starting point of MRMP2 is the energy of the MCSCF wave function can be described as

$$E = 2 \sum_i f_i h_{ii} + \sum_{ij} (a_{ij} J_{ij} - b_{ij} K_{ij}) \quad (2.62)$$

and

$$2f_i = D_i^i \quad (2.63)$$

Where

D_i^i = diagonal elements of the one-electron density matrix

a_{ij}, b_{ij} = the energy coefficient

J_{ij} = the Coulomb integrals

K_{ij} = the exchange integrals

The general variational condition is given as

$$\sum_i \langle \delta\varphi_i | F_i^{MCSCF} | \varphi_i \rangle = 0 \quad (2.64)$$

Where

F_i^{MCSCF} = the general Fock operator

$$F_i^{MCSCF} = f_i h + \sum_j (a_{ij} J_j - b_{ij} K_j) \quad (2.65)$$

The zero-order Hamiltonian H_0 of one-electron operator is necessary for many-body perturbation. But one-electron operator for multi-reference given in equation (2.62) has no physical meaning. So one-electron operator for MCSCF wave function defined as

$$F = h + \sum_j f_j (2J_j - K_j) \quad (2.66)$$

The natural orbitals (λ_i) were used to remove the arbitrary of the density weighting and give the one-electron operator as

$$\hat{F} = \sum_v |\lambda_v\rangle \langle \lambda_v | F | \lambda_v\rangle \langle \lambda_v | \quad (2.67)$$

The zero-order Hamiltonian (H_0) written as

$$H_0 = \sum_I |\Phi_I\rangle \langle \Phi_I | \sum_i \hat{F}(i) | \Phi_I\rangle \langle \Phi_I | \quad (2.68)$$

The zero-order Hamiltonian operated with eigen function Φ_i result in the eigen value W_I .

$$H_0 \Phi_I = W_I \Phi_I \quad (2.69)$$

The eigen value of MCSCF wave function Φ_0 is

$$W_0 = 2 \sum_i f_i \langle \lambda_i | F | \lambda_i \rangle \quad (2.70)$$

The effective charge response to dielectric screening is located at δ^{SC} outside the center of solvent molecule. The minimum distance between solvent molecule and atom A of solute AB is R_A^* is equal to $R_A - \delta^{SC}$ which δ^{SC} will be in the range of 0.5 Å to R^{solv} .

When the distribution of the electric charge (q) is known, the charge on surface segments (q^*) is possible to calculate in COSMO model.

$$q = f(\varepsilon)q^* \quad (2.72)$$

where $f(\varepsilon)$ is the ε -dependent correction factor

$$f(\varepsilon) = \frac{(\varepsilon - 1)}{(\varepsilon + \frac{1}{2})} \quad (2.73)$$

3. CALCULATIONAL METHODOLOGY

Methodology utilized to calculate dimerization process in this work is divided into three parts as following:

- 3.1 Geometry optimizations
- 3.2 Energy corrections
- 3.3 UV/Vis spectroscopic calculations

3.1 GEOMETRY OPTIMIZATIONS

All possible starting geometries were created by using information from X-ray crystallographic data^[3-6, 15, 16, 69, 70] and the theoretical results^[17, 18, 20, 21, 25, 27, 28, 32, 71-73].

Counter-ions were added to radical monomer and dimer according to the charge distribution close to the negatively charged atom of the molecules for anion radical dimerization and positively charged atom for cation radical dimerization. Broken symmetry of orbitals using unrestricted Kohn-Sham (UKS) wave function in an open-shell calculation has been performed with Density Functional method for all monomer and dimer geometries. Becke's 3-parameter Lee Yang Parr functional^[74] including Grimme's dispersion correction^[61, 62] (B3LYP-D) was used for optimizations with the Dunning correlation consistent polarized double- ζ valence basis set (cc-pVDZ)^[75].

Solvent effect was included by the Conductor-like Screening Model COSMO^[33]. The dielectric constant and refractive index of binary mixture solvent used in the COSMO model of solvation were taken from published experimental values^[33-47]. Frequency calculations were performed to the optimized geometries to verify the local minimum of the radical monomers and dimers of molecules. The most probable dimer conformers were identified according to Boltzmann distribution of the electronic energy after checking the frequencies for the minimum character of the geometries. Only the most probable conformations were further investigated.

All substances, counter-ions and solvents in dimerization processes which are studied in this work are shown in **Table 3.1**. The geometry optimization procedure is shown in **Scheme 3.1**.

Table 3.1: Substances, counter-ions and solvents of the theoretical investigation of ionic radical dimerization.

| Substance | Counter-ion | Solvent |
|---|---|------------------------------|
| Radical anions: | | |
| Tetracyanoethylene (TCNE ^{•-}) | Na ⁺ | Tetrahydrofuran |
| 2,3-Dichloro-5,6-dicyano-p-benzoquinone (DDQ ^{•-}) | Na ⁺ | Acetone |
| 2,3-Dichloro-5,6-dicyano-p-benzoquinone (DDQ ^{•-}) | Na ⁺ | Dichloromethane |
| Tetracyano-p-quinodimethane (TCNQ ^{•-}) | Li ⁺ , Na ⁺ , K ⁺ , NBu ₄ ⁺ | EtOH/MeOH (4:1) |
| Radical cations: | | |
| Paraphenylenediamine (PPD ^{•+}) | Br ⁻ | EtOH/Et ₂ O (2:1) |
| <i>N,N</i> -Dimethyl-PPD (<i>N,N</i> -DMPPD ^{•+}) | Cl ⁻ , Br ⁻ | EtOH/Et ₂ O (2:1) |
| 2,3,5,6-Tetramethyl-PPD (2,3,5,6-TMPPD ^{•+}) | Cl ⁻ , Br ⁻ | EtOH/Et ₂ O (2:1) |
| <i>N,N,N',N'</i> -Tetramethyl-PPD (<i>N,N,N',N'</i> -TMPPD ^{•+}) | Cl ⁻ | EtOH/Et ₂ O (2:1) |
| Tetrathiofulvalene (TTF ^{•+}) | Cl ⁻ | Acetone |
| 3,3',5,5'-Tetramethylbenzidine (TMB ^{•+}) | Cl ⁻ | Acetonitrile |

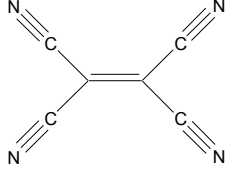
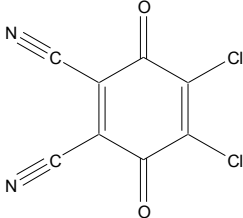
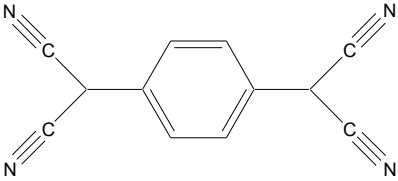
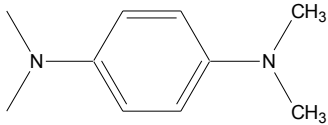
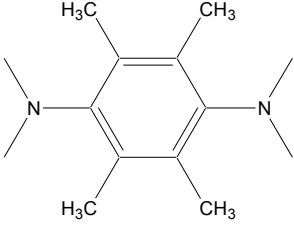
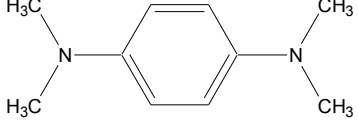
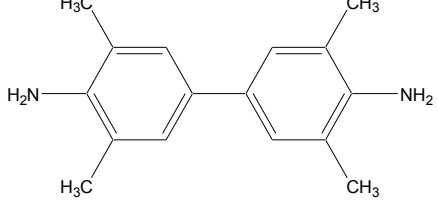
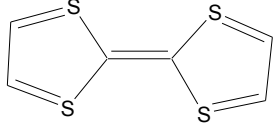
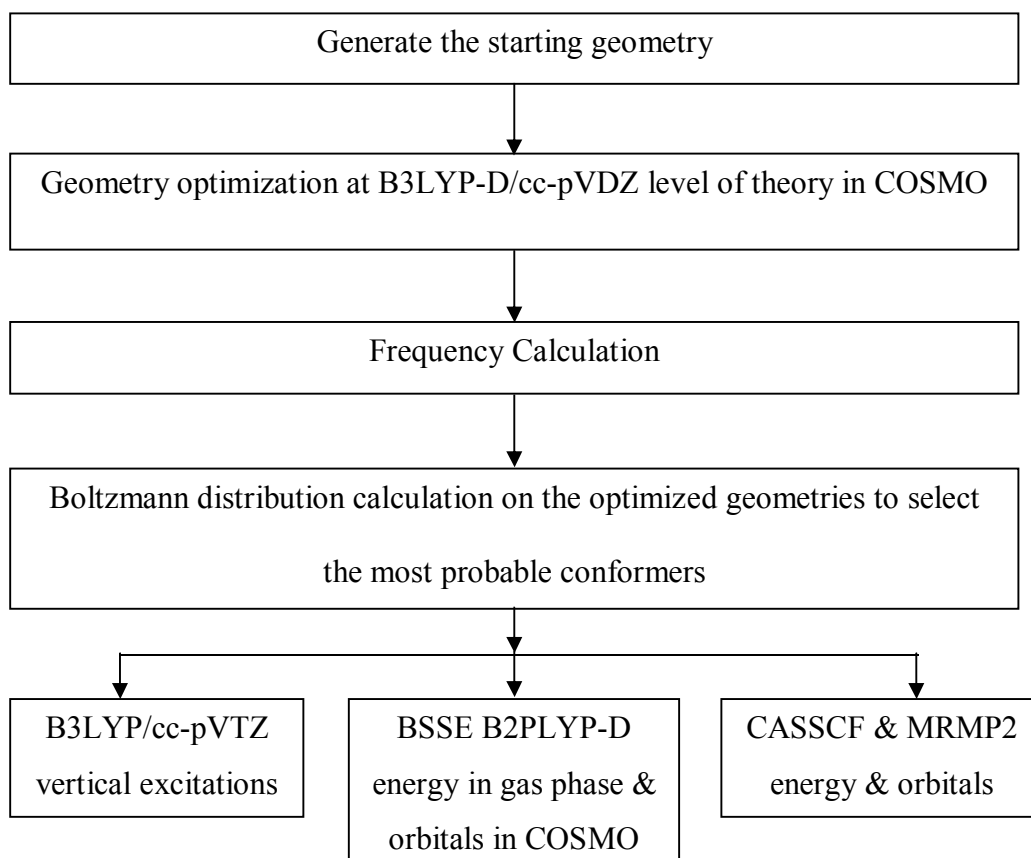
| Structure | Abbreviation |
|---|-----------------|
|  | TCNE |
|  | DDQ |
|  | TCNQ |
|  | PPD |
|  | N,N'-DMPPD |
|  | 2,3,5,6-TMPPD |
|  | N,N,N',N'-TMPPD |
|  | TMB |
|  | TTF |

Figure 3.1: *Molecular structure of interested molecules which was studied in this work.*

Scheme 3.1



3.2 ENERGETICS

Energy calculations include basis set super position error (BSSE) with the counterpoise correction method after Boys-Bernardi^[64]. At DFT level the Second Order Perturbative Corrected Double hybrid functional^[56] was used with inclusion of van der Waals correction^[61, 62] (B2PLYP-D) with the Dunning correlation consistent polarized triple- ζ valence basis set (cc-pVTZ)^[75]. To prove whether the single determinant ansatz can be used and to account for the electron correlation, single point calculations were made with a multireference method using second order perturbation (MRMP2) on a complete active space method. The active spaces include two electrons in two orbitals (CASSCF(2,2)) for dimers and three electrons in three orbitals

CASSCF(3,3) for monomers. Test of larger CAS space for molecules were also performed.

The energy of dimerization was calculated according to:

$$E_{\text{dimerization}} = E_{\text{dimer}} - 2 \cdot E_{\text{monomer}} \quad (3.1)$$

The BSSE corrected DFT energies as well as the CASSCF and MRMP2 energies were used to calculate the dimerization energy from electronic energy in gas phase and compared with the enthalpy of dimerization from temperature-dependent EPR^[2, 7], UV/Vis experimental data and available theoretical information [ref].

3.3 UV/VIS SPECTROSCOPIC CALCULATIONS

The vertical excitation calculations were performed with time-dependent Density Functional Theory in the Tamm-Dancoff approximation (TDA-DFT) at the B3LYP level with the Dunning correlation consistent polarized triple- ζ valence basis set (cc-pVTZ). For the optimized geometries of the most probable conformers of dimers and monomers 40 excitations were computed by following convolution of spectra using the program *ORCA_ASA*^[76] after Gaussian broadening of 1200 cm^{-1} for dimer and 900 cm^{-1} for monomer as taken from experimental data spectra^[3]. For DFT and TD-DFT calculations, the solvent effect was taken into account by the Conductor-like Screening Model COSMO^[33]. Explicit solvent molecules were taken into account in some molecules in the optimization process to see the influence of solvents to the UV/Vis spectra of dimers and monomers and to compare the calculated spectra with the available experimental UV/Vis spectra^[1, 3, 8-11, 13, 14, 48].

All calculations were performed with the program package ORCA^[77]. The molecular geometries were drawn with the program ChemDraw, *XYZ viewer*^[78] and *MOLEKEL*^[79], and the molecular orbitals with *MOLEKEL*^[79].

4. RESULTS AND DISCUSSION

4.1 RADICAL ANION DIMERIZATION

In our theoretical investigations for dimerization three radical anions were included. Those radicals are tetracyanoethylene, 2,3-dichloro-5,6-dicyano-*p*-benzoquinone and tetracyano-*p*-quinodimethane radical anions (TCNE^{•-}, DDQ^{•-} and TCNQ^{•-}), respectively.

4.1.1 Tetracyanoethylene radical anion in tetrahydrofuran

The dimerization of the tetracyanoethylene radical anion (TCNE^{•-}) has been measured experimentally in 2-methyltetrahydrofuran with sodium metal as reducing agent^[1]. In our study, tetrahydrofuran (THF) was chosen as the solvent and sodium cations, Na⁺, serve as counter-ions. Five stable conformers of the [TCNE]₂²⁻2Na⁺ dimer have been found (see **Figure 4.1**) representing different possible conformations of the [TCNE]₂²⁻2Na⁺ dimer with the counter-ions at different position. Relative energies, geometry parameters and the energy of dimerization are depicted in **Table 4.1**.

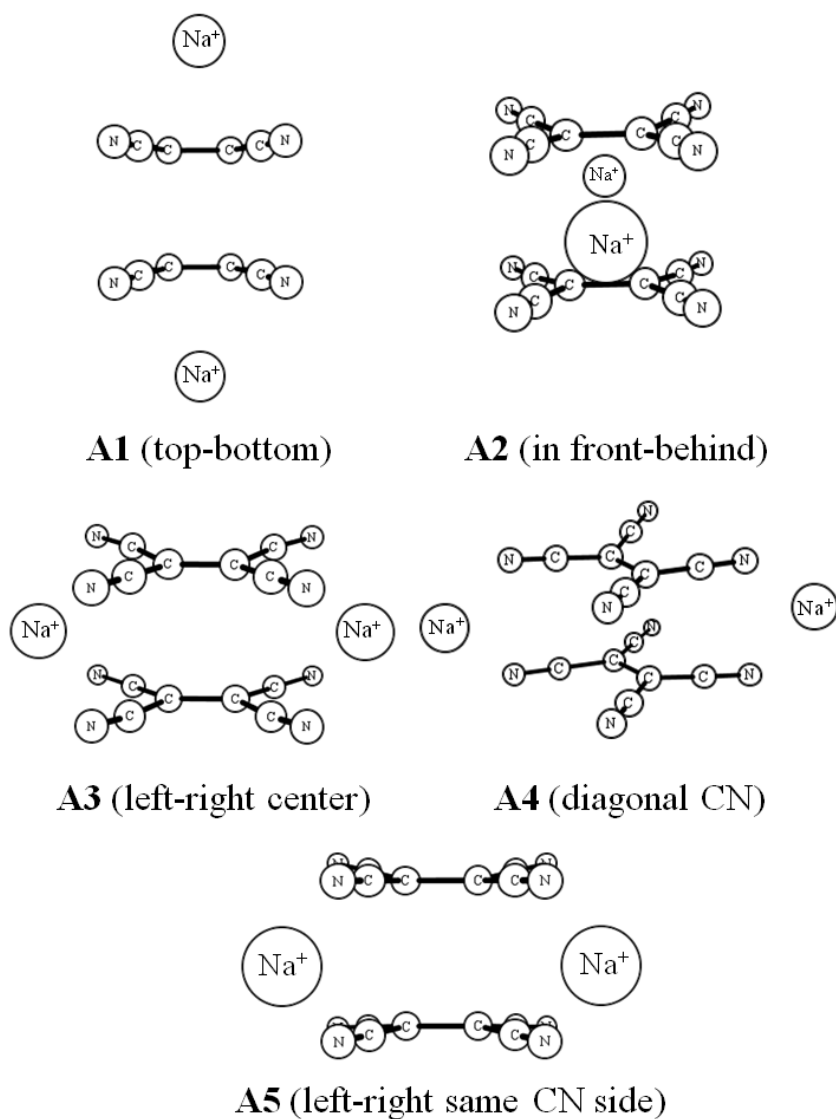


Figure 4.1: Structure of the five possible conformers (A1- A5) of $[TCNE]_2^{2-}2Na^+$ in THF.

Table 4.1: Calculated relative energies ΔE and dimerization energies ΔG of $[TCNE]_2^{2-}2Na^+$ in THF using B3LYP-D/cc-pVDZ method. The intradimer distance (d) is the distance of the two monomer C=C bonds. Energies are given in kJ/mol.

| Geometry | d(Å) | Relative energy | | Dimerization energy | | EPR ^[1] |
|-----------|------|-----------------|-------------------------|---------------------|------------|--------------------|
| | | E_{el+ZPE} | ΔG_{free}^{298} | ΔE | ΔG | ΔH |
| A1 | 2.76 | 181.42 | 176.37 | -35.93 | 36.39 | |
| A2 | 2.93 | 0.00 | 0.00 | -119.59 | -42.24 | |
| A3 | 2.97 | 99.81 | 93.50 | -76.62 | -7.13 | -33.4 |
| A4 | 2.89 | 26.52 | 20.49 | -88.03 | -21.77 | |
| A5 | 2.89 | 39.30 | 34.87 | -75.85 | -7.41 | |

Geometries

Conformer **A1** shows a perfect π -stacking with a intradimer distance of 2.76 Å and with the counter-ions at top and bottom position of the stacked C=C bonds. This conformation was also found by Head-Gordon^[20] and described in detail. In our study, **A1** has a relative high free energy (176 kJ/mol) and was therefore only included in the further study for comparison with^[20]. The B3LYP-D free energy of dimerization is calculated as destabilizing the dimer (+36.4 kJ/mol) when including temperature effects in free energy ΔG .

Conformer **A2** is the global minimum in our study. The structural parameters of **A2** are shown in **Figure 4.2**. It is also perfectly π -stacked with the sodium counter-ions in the intradimer plane and therefore has a somewhat larger monomer to monomer distance of 2.93 Å. It corresponds well to the X-ray crystallographic data of $[\text{TCNE}]_2^{2-}$ dimer with two $(\text{Bu}_4\text{N})^+$ counter ions ($d = 2.87 \text{ \AA}$)^[3]. The C=C bond length is roughly 1.44 Å. The cyano groups bend away from the center of dimer by approximately 2.5° for both fragments. The sodium counter-ions sit in front and behind the plane of the interacting C=C bonds, around 2.62 Å away from nitrogen and located in the center of the four cyano groups. The bond angles of C-C-N deviate from 180° by approximately 8° because of the interaction of the nitrogen atoms with the sodium counter-ions.

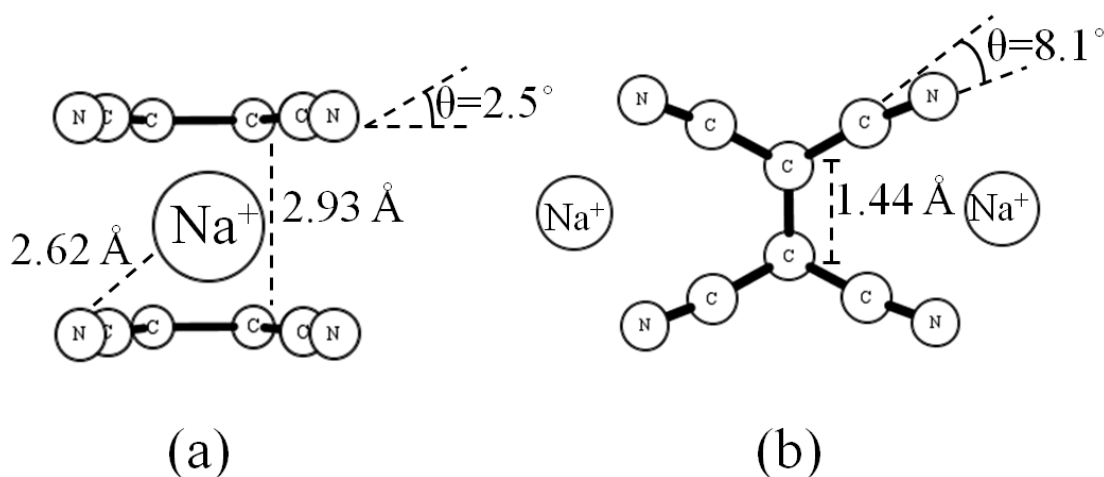


Figure 4.2: Geometry of the most stable conformer **A2** of $[\text{TCNE}]_2^{2-} 2\text{Na}^+$ in THF calculated at B3LYP-D/cc-pVDZ level of theory (a) side view (b) top view.

Energetics

Dimer conformer **A1** shows the Gibb's free energy of dimerization of 36.39 kJ/mol, which is not stable at room temperature. Conformer **A2** has the lowest dimerization energy (-42.24 kJ/mol using B3LYP-D Gibb's free energy), which is in agreement with experimental dimerization energies (ranging from -24 kJ/mol^[2] to -37.66 kJ/mol^[3]) confirming a spontaneous dimerization in the solvent THF.

All the other three conformers (**A3**, **A4**, **A5**) show the counter-ions almost located between the CN groups and deviate from the clear π -stacked orientation of the interacting C=C bonds. They have relative high free energies (93.5 kJ/mol for **A3**, 20.5 kJ/mol for **A4**, 34.9 kJ/mol for **A5**) and therefore play no role THF. Additionally, their free energy of dimerization would confirm less stability of the dimer compared to **A2**.

Orbital description

To describe the dimerization process, a closer look to the interacting molecular orbitals of conformer **A2** has been taken. The highest occupied molecular orbital (HOMO) of **A2** is located in the center of both C=C bonds of both fragments. It can be described as π -interaction between the two monomer fragments, resulting from the two, strongly interacting electrons of the singly occupied molecular orbital (SOMO) of each open-shell anionic radical monomer combined to generate a positive linear combination to give the bonding (HOMO) orbital of the dimer molecule. The anti-bonding (LUMO) orbital is the negative linear combination of the two SOMO orbitals. The two-electrons in the HOMO orbital are delocalized on four carbon atoms and this confirms the two-electrons/ four-center π -bond^[15]. The molecular orbitals of monomer and dimer **A2** are shown in Chapter 1, **Figure 1.1**.

To describe the energetics of the dimerization procedure in more detail, the potential energy surface (PES) of $[\text{TCNE}]_2^{2-}2\text{Na}^+$ dimer in THF for different intradimer C-C separation has been investigated with the B3LYP-D method including dispersion and without dispersion energy correction (B3LYP).

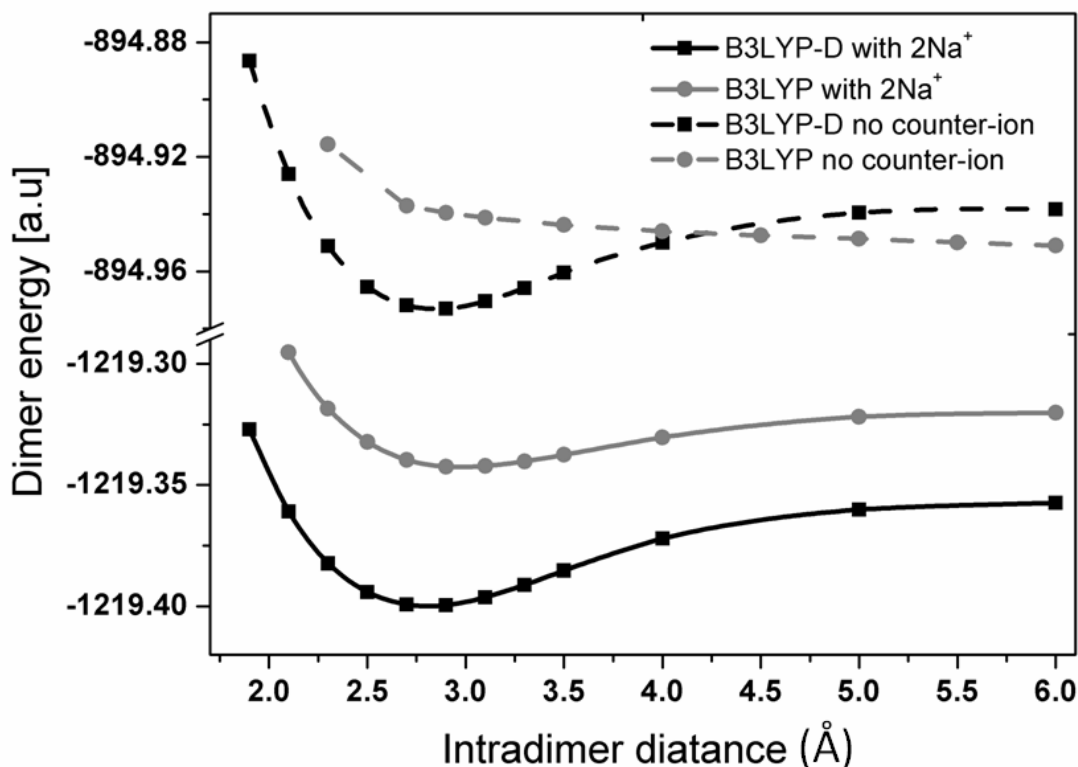


Figure 4.3: Potential energy curve as a function of intradimer distance of conformation **A1** and without counter-ion with (■) and without (●) dispersion, B3LYP-D and B3LYP, respectively.

Figure 4.3 indicates that dispersion plays an important role, in order to stabilize the dimers as described also by Sancho-Gracia^[80].

Dimerization energies for **A1** and **A2** have been also calculated using other methods: double and triple-zeta basis sets, single determinant methods with and without dispersion, a double hybrid functional including short-range correction for the interaction and including BSSE correction as well as multideterminant methods accounting for correlation by the CASSCF and MRMP2 method, as shown in **Table 4.2**.

Table 4.2: Dimerization energies (ΔE , in kJ/mol) for conformers **A1** and **A2** of $[\text{TCNE}]_2^{2-}2\text{Na}^+$ in THF using B3LYP-D/cc-pVDZ geometries and different methods of calculation.

| | A1 | A2 | EPR ^[1] |
|-----------------------|------------|------------|--------------------|
| | ΔE | ΔE | ΔH |
| B3LYP-D/cc-pVTZ | -33.82 | -214.94 | |
| B2PLYP-D/cc-pVDZ | -63.35 | -252.27 | |
| B2PLYP-D/cc-pVTZ | -64.02 | -232.07 | |
| BSSE B3LYP-D/cc-pVDZ | 173.87 | 80.62 | -33.4 |
| BSSE B3LYP-D/cc-pVTZ | 177.46 | 80.92 | |
| BSSE B2PLYP-D/cc-pVDZ | 61.52 | -54.52 | |
| BSSE B2PLYP-D/cc-pVTZ | 56.81 | -61.54 | |
| CASSCF(6,4)/DZ | 49.66 | -86.52 | |
| MRMP2/CAS(6,4) | -120.54 | -216.68 | |
| CASSCF(2,2)/DZ | 64.03 | -73.83 | |
| CASSCF(2,2)/TZ | 48.97 | -55.72 | |
| MRMP2/CAS(2,2) (DZ) | -144.29 | -397.25 | |
| MRMP2/CAS(2,2) (TZ) | -89.32 | -224.57 | |

The dimer **A2** is with all methods strongly stabilized as compared to dimer **A1**. CASSCF calculation with counter-ions shows **A2** to be more stable than **A1** by approximately the same amount for both CAS spaces (304.2 and 302.6 kJ/mol (CAS(2,2) and CAS(6,4), respectively). But after perturbation correction of the energies (MRMP2) there is a difference in the relative energy in the both CAS spaces (322.4 and 165.6 kJ/mol for CAS(2,2) and CAS(6,4), respectively). The energy of dimerization shows the same trend: the CASSCF dimerization energies of **A2** do not differ much for the two CAS spaces (see Table 2) while in the following MRMP2 calculation, the smaller CAS space (2,2) (i) shows a large overestimation of the dimerization energy over the larger CAS space (6,4) (ii). The strong overestimation of the dimerization energy might be due to the unsymmetrical CAS spaces for the monomer and dimer. The monomer CAS space (3,3) includes the minimum orbitals (HOMO, SOMO and LUMO) in both cases (i) and (ii), but for a proper linear combination of the two monomers a (6,6) CAS space with the right orbitals in the dimer showing the same p_z character as in the monomer would be necessary. This was not possible

because orbitals exhibiting the linear combination of the monomer LUMO orbitals could not be located in lower orbital energy region. It should be noted, that the LUMO orbitals of the monomer and dimer have been chosen carefully according to the pz plane of the C=C bonds in TCNE plane, and they had to be rotated to generate the shown CAS space. The investigated CASSCF orbitals are shown in **Figure 1.1**. In both CASSCF calculations (i) and (ii) the contribution from excited state determinant stayed more or less the same (13 % versus 15 % depending on the small or larger number of orbitals used). This overstabilization might be a result of using equation 3.1 with different CASSCF wavefunctions for monomer and dimer on which the multireference method is based. Similar quality results have been produced for $[\text{TCNE}]_2^{2-}$ by Novoas group^[24] using MCQDPT/CASSCF(2,2) method (-101 kJ/mol vs. -36.8 kJ/mol in experiment). The CASSCF space in Novoas work (private communication) included the HOMO, SOMO, LUMO and LUMO+1 orbitals for the monomer (in a CAS(3,4)), and the HOMO and LUMO orbitals for the dimer in a CAS(2,2). Selection of active electrons and active orbitals in CASSCF calculation is very sensitive in these calculations when using monomer and dimer energy for calculation of dimerization energies. Head-Gordon had therefore evaluated the dimerization energy of $[\text{TCNE}]_2^{2-}2\text{K}^+$ by the potential curve of dimerization^[20]. He also received some overstabilization with multireference method MRMP2/PP(1), but not as much (-72.4 kJ/mol without BSSE, -52.3 kJ/mol with BSSE).

Therefore we decided to neglect this contribution from multideterminant character and use short-range corrected DFT functional B2PLYP-D with the inclusion of some perturbation character on the computation of the dimerization energies in the other calculations.

On going from double to triple zeta basis set a small effect was found. As can be seen from BSSE corrections, the standard hybrid B3LYP-D functional destabilizes the dimer **A1**, so that it should not occur in solution. Double hybrid functional B2PLYP-D including a short range correction and some correlation via the perturbation, computes again an unstable dimer **A1** (+56.81 kJ/mol) and a stabilized dimer **A2** (-61.54 kJ/mol). The BSSE corrected dimerization energy of **A2** with the B2PLYP-D compares well with the reported results in the literature^[20] and is in the same order as the experimental dimerization enthalpy (-33.4 kJ/mol)^[1]. Therefore BSSE corrected dimerization energy with B2PLYP-D/cc-pVTZ method has been chosen for the further

molecules, respectively. The calculated dimerization energy from dimers CASSCF(2,2) and monomers CASSCF(3,3) are 48.97 and -55.72 kJ/mol for **A1** and **A2**, respectively, which again is in the same order of magnitude of experimental dimerization enthalpy. In the further molecules CASSCF(2,2) for dimers and CASSCF(3,3) for monomers will be used.

Calculation of the potential energy curve for $[\text{TCNE}]_2^{2-}$ dimer with inclusion of counter-ions is not simple, because the counter-ions move between the monomeric species when increasing the monomer distance. This leads to overstabilization at distances of 5-8 Å, and problems in the convergence at very high distances occurred. Test calculations on $[\text{TCNE}]_2^{2-}$ with sodium counter-ions with B3LYP-D method shows the same potential energy curve behaviour as in Head-Gordons work^[20] and resulted for the top-bottom conformation **A1** of counter-ion a dimerization energies of -35.93 kJ/mol (BSSE uncorrected B3LYP-D/cc-pVDZ) and of -56.81 kJ/mol (BSSE corrected B2PLYP-D/cc-pVTZ), respectively.

Vertical excitation

For a more specific interpretation of the relation between geometry and electronic structure in the dimerization process, a comparison of the experimental UV spectra (Kochi^[3] and Simons^[18]) to the calculated vertical transitions of both, the monomeric and the dimer **A2** species is performed. Experimentally, the monomer of TCNE radical anion shows a strong absorption at 428 nm (2.90 eV), while for the dimeric species two peaks could be located in Me-THF at 530 nm (2.34 eV) and 370 nm (3.35 eV).

The TDA-DFT calculations at B3LYP/cc-pVTZ level of theory were done with the most stable conformer **A2** and monomer (shown in **Fig. 4.4** and **Table 4.3**). They show that the first peak for the dimer could be assigned to the HOMO → LUMO transition ($\pi \rightarrow \pi^*$) in agreement with^[18], while the second peak stems from the HOMO-1 → LUMO transition ($\pi \rightarrow \pi^*$). The absorption of the monomer consists mainly in the HOMO beta orbital under SOMO orbital to the LUMO beta orbital upper than SOMO orbital, HOMO → LUMO, $\pi \rightarrow \pi^*$ transition. Although the experimental 0.56 eV (102 nm) shift is not obtained in the B3LYP/cc-pVTZ calculations, the monomer unit also shows a larger calculated energy (3.24 eV) than the dimer HOMO → LUMO energy (3.13 eV, 396 nm). It is well known that B3LYP underestimates vertical transition energies with charge transfer character, therefore the calculated

spectra are blue-shifted relative to the experimental ones, especially when using small basis set. However the calculated UV spectrum using DFT method and THF in a COSMO model of solvation including Na^+ as counterions confirms the red-shift of the first transition in the dimerization process as detected in the experimental spectrum of $[\text{TCNE}]_2^{2-}$ dimer and $\text{TCNE}^{\bullet-}$ monomer using Na^+ as counter ion in 2-methyltetrahydrofuran^[81].

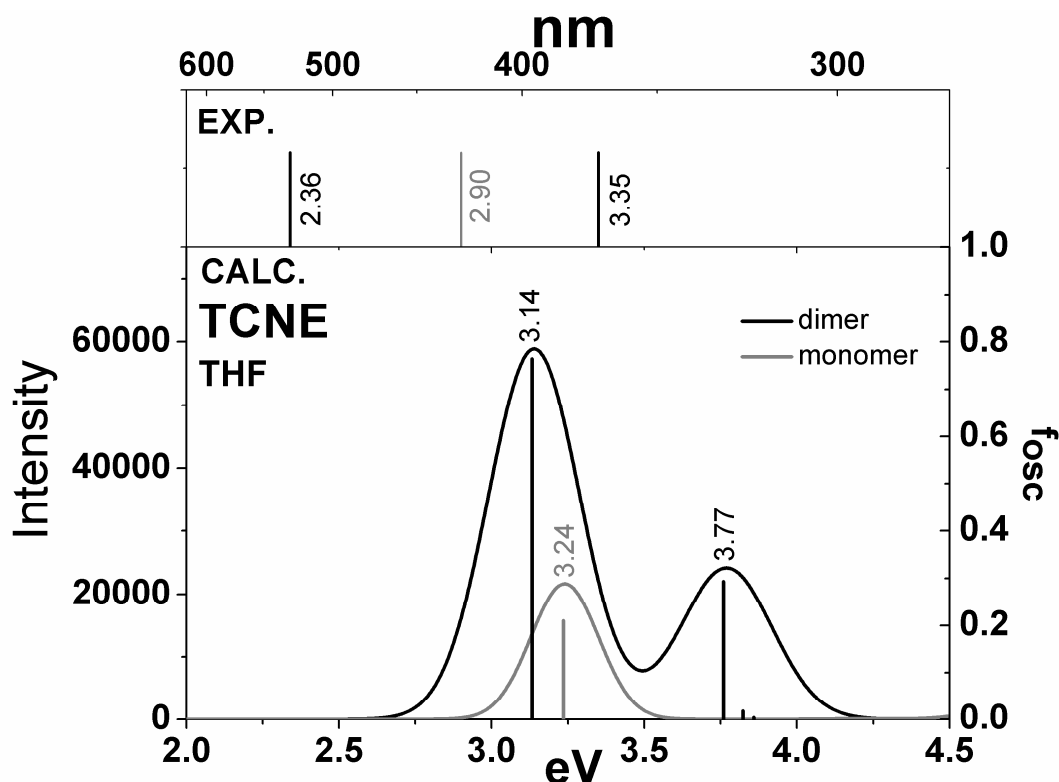


Figure 4.4: The TDA-B3LYP calculated vertical excitations (bottom, lines are shown with oscillator strengths) and convoluted UV/Vis spectrum (bottom) of the $[\text{TCNE}]_2^{2-}2\text{Na}^+$ dimer **A2** (black) and $\text{TCNE}^{\bullet-}\text{Na}^+$ monomer (gray) in THF. The energies of experimental peak maxima^[1, 3] are shown as vertical lines (top).

A more detailed discussion on the solvent interacting with monomer and dimer and therefore influencing the spectrum will be given in the PPD radical cation dimerization.

Table 4.3: The vertical excitation of the $[\text{TCNE}]_2^{2-} 2\text{Na}^+$ dimer and $\text{TCNE}^{\bullet-} \text{Na}^+$ monomer.

| TCNE | State | eV | nm | f | Orbital transition |
|---------|-----------------|------|-------|--------|------------------------------|
| Dimer | S ₃ | 3.13 | 395.9 | 0.7643 | HOMO→LUMO |
| | S ₁₀ | 3.76 | 329.8 | 0.2938 | HOMO-1→LUMO |
| | S ₁₂ | 3.82 | 324.3 | 0.0180 | HOMO→LUMO+3 |
| | S ₁₄ | 3.86 | 321.3 | 0.0038 | HOMO→LUMO+4 |
| | S ₂₄ | 4.81 | 258.0 | 0.0012 | HOMO→LUMO+9 |
| Monomer | S ₂ | 3.24 | 383.3 | 0.2106 | HOMO→LUMO |
| | S ₅ | 4.23 | 293.1 | 0.0010 | SOMO→LUMO+3 |
| | S ₇ | 4.67 | 265.7 | 0.0155 | SOMO→LUMO+8 & HOMO-3→LUMO |

4.1.2 2,3,5,6-Dichlorodicyano-p-benzoquinone radical anion in acetone and dichloromethane

Dimerization of 2,3-dichloro-5,6-dicyano-*p*-benzoquinone radical anion ($\text{DDQ}^{\bullet-}$) has been found experimentally in acetone ($\epsilon = 20.7$) and dichloromethane ($\epsilon = 9.08$) using $(\text{Bu}_4\text{N})^+\text{I}^-$ and sodium as reducing agents, respectively^[2, 3]. In our calculations we used $\text{DDQ}^{\bullet-}$ radical anions with sodium cation as counter-ions with COSMO model of solvation. According to our results from TCNE radical anion dimerization, we neglected the few percent of multireference character in the system and used only UHF wave function at the B3LYP-D/cc-pVDZ level of theory with dispersion correction for the geometries optimization and Boltzmann weighing of the geometries. Finally, B2PLYP-D functional was used including the BSSE correction for the dimerization energies and for comparison with the experimental results.

4.1.2.1 Acetone

Investigation of potential energy surface resulted in eight possible $[\text{DDQ}]_2^{2-} 2\text{Na}^+$ dimer conformers **B1-B8** in acetone, which are shown in **Figure 4.5**. The relative energies, intradimer distance and the dimerization free energies are presented in **Table 4.4**.

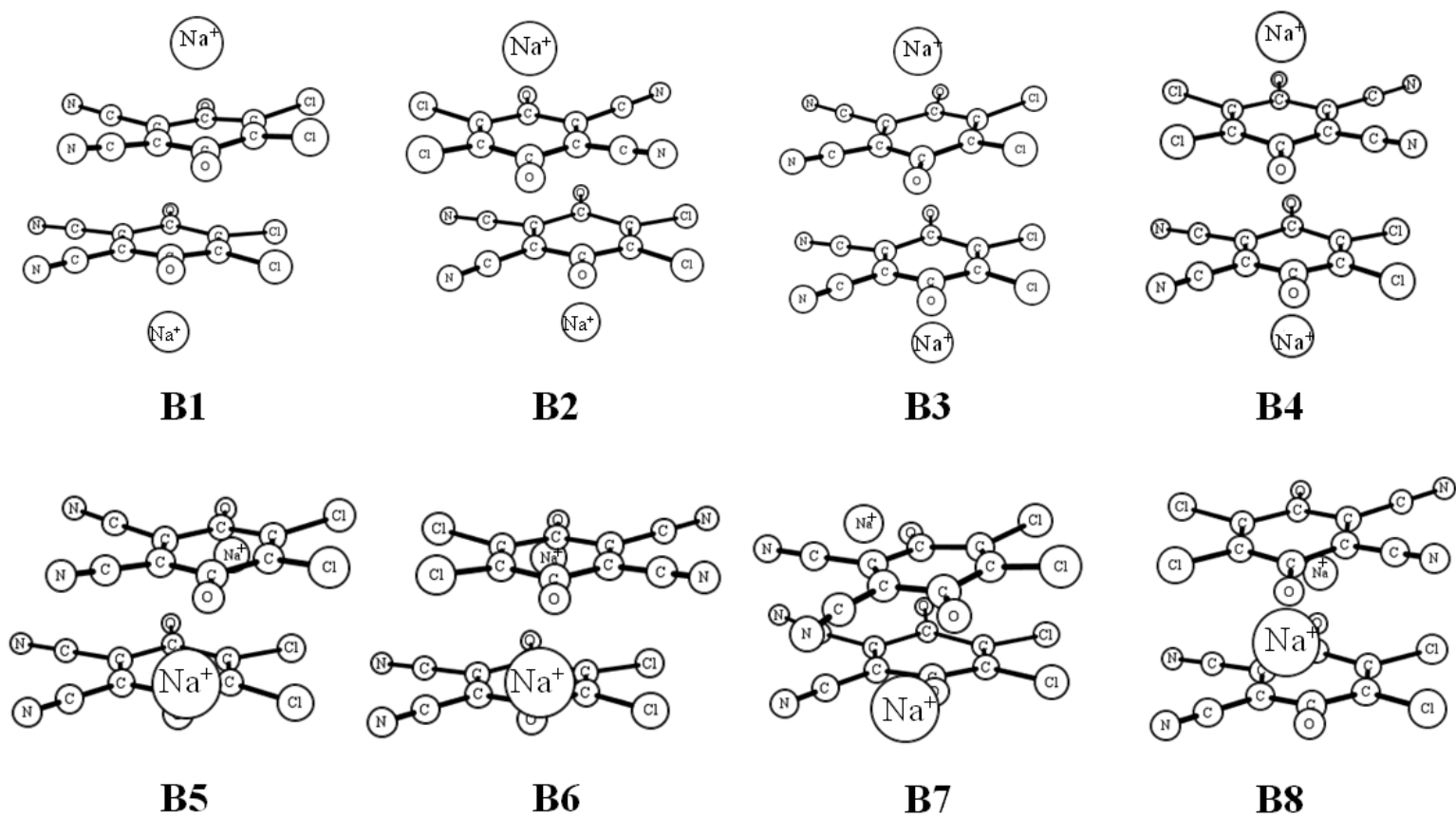


Figure 4.5: Structure of the eight possible conformers (B1- B8) of $[DDQ]_2^{2-} 2Na^+$ in acetone.

Table 4.4: Calculated relative energies ΔE and dimerization energies ΔG of $[\text{DDQ}]_2^{2-}2\text{Na}^+$ in acetone using B3LYP-D/cc-pVDZ method. The intradimer distance (d) is the distance of the two monomer benzene rings. Energies are given in kJ/mol.

| Geometry | d(Å) | Relative energy | | Dimerization energy | | experiment | |
|-----------|------|---------------------|--------------------------------|---------------------|------------|-------------------------------|-------------------------------|
| | | $E_{\text{el+ZPE}}$ | $\Delta G_{\text{free}}^{298}$ | ΔE | ΔG | $\Delta H_{\text{exp}}^{[2]}$ | $\Delta H_{\text{exp}}^{[3]}$ |
| B1 | 3.04 | 208.03 | 201.34 | -41.7 | 30.3 | | |
| B2 | 2.94 | 199.19 | 197.89 | -50.67 | 26.85 | | |
| B3 | 2.73 | 188.86 | 177.72 | -61.15 | 6.68 | | |
| B4 | 2.74 | 186.38 | 179.43 | -62.83 | 8.39 | -15.2 | -29.7 |
| B5 | 3.07 | 0.00 | 0.39 | -115.49 | -35.13 | | |
| B6 | 3.09 | 13.21 | 20.02 | -100.97 | -15.51 | | |
| B7 | 2.79 | 1.43 | 0.00 | -114.74 | -35.53 | | |
| B8 | 2.79 | 10.18 | 12.87 | -104.57 | -22.65 | | |

Conformation **B7** is the global minimum and shows the lowest dimerization free energy (-35.53 kJ/mol) together with conformer **B5** (-35.13 kJ/mol), which has a relative Gibbs free energy of only 0.39 kJ/mol. Both conformers will therefore be present in acetone solution to around the same amount (54 % for **B7** and 46 % for **B5**, respectively). Both conformers are π -stacked with the chlorine atoms at one side and the cyano groups at the other side of the long molecular axis (in a cis-orientation of Cl and CN) showing a stronger interaction of the two monomers at **B7** ($d = 2.79 \text{ \AA}$) relative to **B5** ($d = 3.07 \text{ \AA}$) (see **Fig. 4.6**). In **B7** the two monomer units are shifted via the long O=C-C=O axis towards each other by 1.89 \AA with a small rotation of the two monomers by approximately 9.7° leading to a perfect interaction of positive and negative charges in of the C=O groups with a smaller overlap and therefore a smaller repulsion of the functional groups. The sodium counter-ions are sitting in the intradimer plane between the oxygen atom and the cyano group resulting in a somewhat unsymmetric geometry. The lateral rotation of one monomer relative to another was also found experimentally occurring in tetracyanopyrazine anion dimer salt and measured by X-ray crystallographic analysis^[5]. **B5** shows a small offset of 0.89 \AA of the two long O=C-C=O axis parallel to each other, and the somewhat larger intradimer distance is a consequence of the stronger repelling C=O groups with the same charges closer together. The charges at the C=O group are well separated. Oxygen atoms have a negative charge of around -0.3 a.u., while the connecting carbon atoms have a positive charge of +0.18-0.23 a.u. Interestingly, the benzene ring has a small negative charge on one side of the O=C-C=O axis and a small positive charge on the other side in both conformers resulting from the charges of the functional groups Cl and CN. The sodium counter-ions have their position in the intradimer plane close to the oxygen atoms.

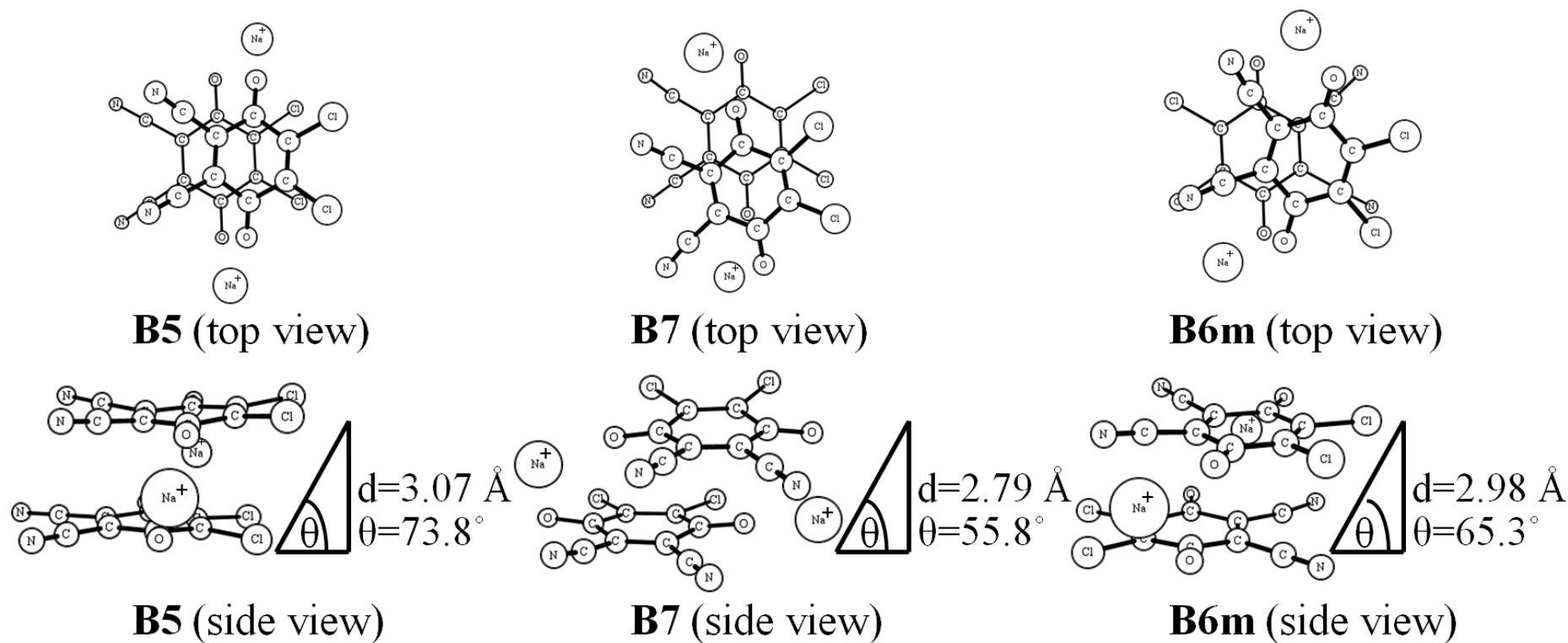


Figure 4.6: Geometry of the most stable conformers of $[DDQ]_2^{2-} 2Na^+$ (**B5** and **B7** in acetone, **B6m** in dichloromethane) calculated at B3LYP-D/cc-pVDZ level of theory (a) side view, (b) top view.

Conformers **B6** and **B8** are the trans conformations of **B5** and **B7**, having the sodium counterions again in the intradimer plane, but with much higher relative Gibbs free energies (20.0 and 12.9 kJ/mol for **B6** and **B8**, respectively). The energy of dimerization is still stabilizing these two conformers, but for experiment they will not play a role in the solvent acetone.

Conformers **B1-B4** have the sodium counterions in top-bottom orientation relative to the π -stacked monomers, with the Cl and CN groups in different cis- and trans orientations and they show very high relative Gibbs free energies and destabilizing positive energies of dimerization, as shown in **Table 4.4**, therefore **B1-B4** will not be present in solution.

The BSSE corrected B2PLYP-D/cc-pVTZ dimerization energies of both **B7** and **B5** are -10.37 kJ/mol and -15.30 kJ/mol, respectively (see **Table 4.5**), and they corresponds well with the EPR and UV-Vis experimental data (-15.2 kJ/mol^[2] and -29.7 kJ/mol^[3]). CASSCF method fails to reproduce dimerization of DDQ radical anion in acetone.

Table 4.5: Dimerization energies (ΔE , in kJ/mol) for conformers **B5**, **B7**, and **B6m** of $[\text{DDQ}]_2^{2-}2\text{Na}^+$ in acetone and dichloromethane using B3LYP-D/cc-pVDZ geometries.

| Solvents | Geometry | B2PLYP-D/ | BSSE B2PLYP-D/ | CASSCF ^a / | experiment | |
|-----------------|------------|------------|----------------|-----------------------|-------------------------------|-------------------------------|
| | | cc-pVTZ | cc-pVTZ | cc-pVTZ | $\Delta H_{\text{exp}}^{[2]}$ | $\Delta H_{\text{exp}}^{[3]}$ |
| | | ΔE | ΔE | ΔE | | |
| Acetone | B5 | -212.35 | -15.3 | 46.51 | -15.20 (EPR) | -29.7 (EPR) |
| | B7 | -238.25 | -10.37 | 41.95 | | |
| Dichloromethane | B6m | -272.09 | -46.88 | 53.75 | -24.00 (EPR) | -37.7 (EPR) |
| | | | | | | -31.8 (UV-Vis) |

^a CASSCF(3,3)/CASSC(2,2) data are given.

From these results, it can be concluded that there are two conformers of $[\text{DDQ}]_2^{2-}2\text{Na}^+$ dimers occurring during dimerization process in acetone. These two conformers have also been found in the solid state salt of $[\text{DDQ}]_2^{2-}$ dimer with Na^+ and K^+ as counter ions^[4].

To describe the different interactions on the dimerized species **B5** and **B7**, the electrostatic interaction including the molecular orbitals as well as the charge distribution on the atoms involved in the strong interaction of the monomeric units is discussed in the following as well as the effect to the absorption process, which has been investigated experimentally by Kochi^[4], too.

The CASSCF and DFT give the same result for the molecular orbitals (HOMO and LUMO) of **B5** and **B7** are presented in **Figure 4.7**.

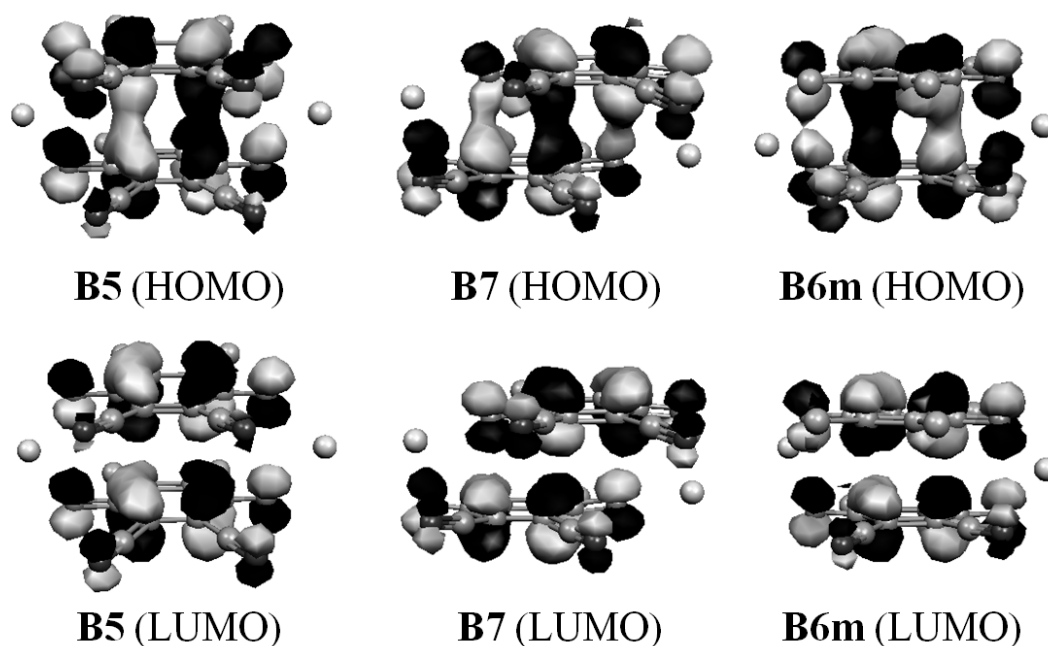


Figure 4.7: Molecular orbitals of $[\text{DDQ}]_2^{2-}2\text{Na}^+$ conformers **B5** and **B7** in acetone and **B6m** in dichloromethane with contour isovalue 0.03.

In conformer **B5**, the highest occupied molecular orbital (HOMO) contains the two electrons stemming from the singly occupied molecular orbital (SOMO) of each anionic radical monomer fragment delocalized over the twelve carbon atoms in the benzene ring and it exhibits a π -bond interaction of these two fragments over the benzene ring as recommended in^[4]. These π -bond is interpreted to be a two-electron/twelve-center ($2e^-/12c$) bond^[4].

The appearance of the HOMO orbital in **B7** is different, because the two electrons coming from SOMO of each anionic radical monomer fragment building the HOMO are delocalized over the carbon atoms in the benzene ring and one oxygen atom in each fragment. However it still exhibits a π -bond between these two fragments. In this case, these π -bond is suggested to be a two-electron/fourteen-center ($2e^-/14c$) bond^[4].

4.1.2.2 Dichloromethane

The calculations in dichloromethane (DCM) result also in eight stable conformations (**B1m-B8m**) similar to the ones in acetone with slightly larger lateral rotation of the monomer units within the COSMO model of solvation, but with only one clear global minimum in DCM. Conformer **B6m** is stabilized much over the other three conformers (**B5m**, **B7m**, **B8m**) with the counter-ion Na^+ in the intradimer plane at the long O=C-C=O axis having similar relative Gibbs free energies in DCM of 14.55 - 23.41 kJ/mol (see **Table 4.6**). Conformer **B6m** also yields the lowest free dimerization energy (-71.42 kJ/mol) while the higher energy conformers are less stabilized (-48.02 to -56.87 kJ/mol). The geometries of **B1m-B8m** are only slightly different to **B1-B8** geometries according to lateral rotation with similar geometry parameters and therefore only the global minimum **B6m** is shown in **Fig. 4.6** and **Fig. 4.7**.

Table 4.6: Calculated relative energies ΔE and dimerization energies ΔG for conformers **B1m-B8m** of $[\text{DDQ}]_2^{2-} 2\text{Na}^+$ in dichloromethane using B3LYP-D/cc-pVDZ method. The intradimer distance (d) is the distance of the two monomer benzene rings. Energies are in kJ/mol.

| Geometry | d(Å) | Relative energy | | Dimerization energy | | experiment | |
|------------|------|---------------------|-------------------------|---------------------|------------|-------------------------------|-------------------------------|
| | | $E_{\text{el+ZPE}}$ | ΔG_{rel} | ΔE | ΔG | $\Delta H_{\text{exp}}^{[2]}$ | $\Delta H_{\text{exp}}^{[3]}$ |
| B1m | 2.9 | 247.81 | 248.84 | -42.93 | 34.88 | | |
| B2m | 2.82 | 236.43 | 236.38 | -52.94 | 22.43 | | |
| B3m | 2.73 | 228.09 | 219.89 | -61.96 | 5.94 | | |
| B4m | 2.73 | 225.09 | 221.44 | -64.61 | 7.48 | -24.0 | -37.7 (EPR) |
| B5m | 3.05 | 11.71 | 14.55 | -137.33 | -56.87 | (EPR) | -31.8 (UV-Vis) |
| B6m | 2.98 | 0.00 | 0.00 | -150.08 | -71.42 | | |
| B7m | 2.79 | 21.48 | 22.71 | -127.37 | -48.71 | | |
| B8m | 2.81 | 21.39 | 23.41 | -127.66 | -48.02 | | |

Conformer **B6m** has a geometry with the Cl and CN groups in trans orientation showing a large lateral rotation of the monomers (approx. 18 degrees) relative to the long axis (see **Figure 4.6**). This leads to a conformation with a intradimer distance of 2.98 Å, in which the functional groups have the lowest repulsive orientation stabilizing **B6m** over the other three conformers. This is also reflected in the charge distribution, which shows again charge separation of the C=O groups, but this time with little unsymmetry. The sodium counter-ions are located on one side and between the oxygen atoms in **B6m**.

BSSE corrected B2PLYP-D/cc-pVTZ method yields a dimerization energy of -46.88 kJ/mol for **B6m** which is in the region of the experimental findings (by EPR experimental data (-24.0 kJ/mol^[2] and -37.7 kJ/mol^[3] by EPR spectroscopy and -31.8 kJ/mol by UV-Vis spectroscopy^[3]) as reported in **Table 4.5**. CASSCF method fails to reproduce dimerization the same as in acetone solvent.

Fig. 4.7 illustrates the HOMO and LUMO orbitals of **B6m**. The electrons form a π -bond over twelve carbon atoms in the benzene ring of the two fragments in the HOMO orbital. It can be suggested that the bonding in the dimer **B6m** is again a two-electron/twelve-center π -bonding ($2e/12c$) bond in dichloromethane as for **B5** in acetone.

Figure 4.8 presents the calculated B3LYP/cc-pVTZ UV-Vis spectra of the DDQ radical anion monomer as well as of the most stable $[\text{DDQ}]_2^{2-} \cdot 2\text{Na}^+$ dimers (**B6m**) in dichloromethane. The excitation energy of the monomer SOMO \rightarrow LUMO transition ($\pi \rightarrow \text{Na}^+$ charge transfer) is shown at 2.60 eV (476 nm), while the first peak of the dimers **B6m** showing the HOMO \rightarrow LUMO transition ($\pi \rightarrow \pi^*$) at 2.36 eV (525 nm). This calculated red-shift of 0.24 eV (49 nm) in the dimerization process compares well with the experimental red-shift of 0.36 eV (122 nm) found by Kochi^[3]. The second peak in the convoluted dimer spectrum was assigned as the HOMO \rightarrow LUMO+1 transition ($\pi \rightarrow \pi^*$) with a vertical transition energy of 2.97 eV (418 nm).

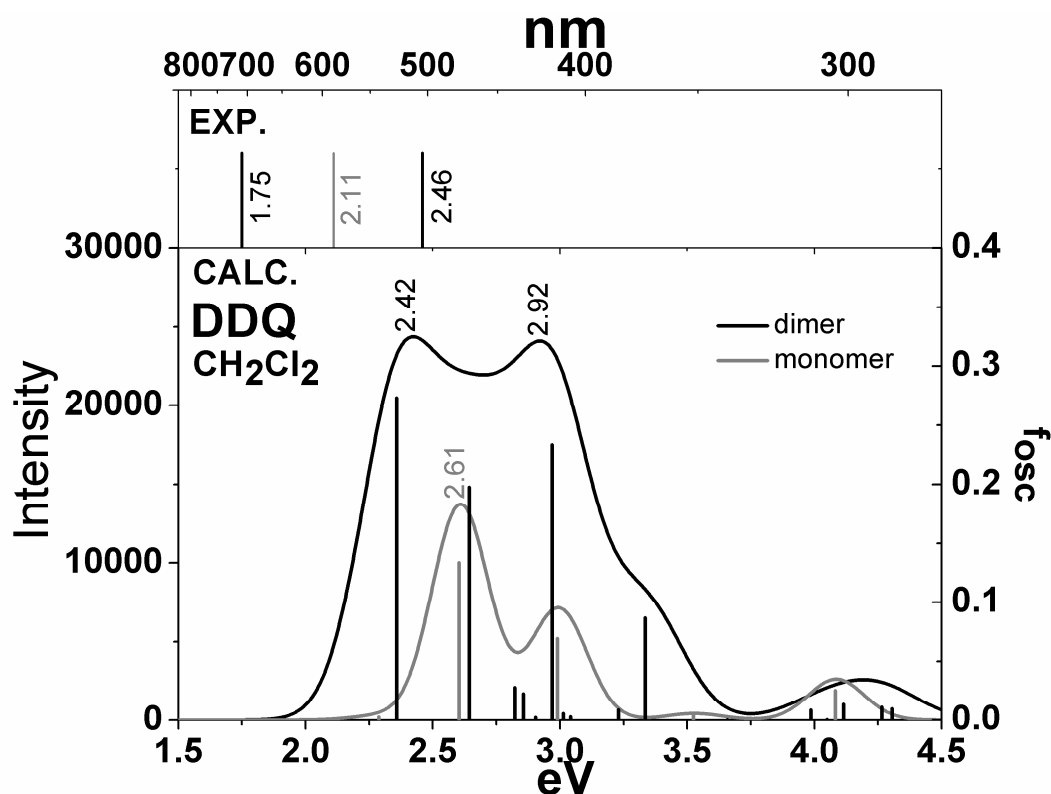


Figure 4.8: The TDA-B3LYP calculated vertical excitations (bottom, lines are shown with oscillator strengths) and convoluted UV/Vis spectrum (bottom) of the $[DDQ]_2^{2-}Na^+$ dimer (black) and $DDQ^{\bullet-}Na^+$ monomer (gray) in dichloromethane. The energies of experimental peak maxima^[1, 3] are shown as vertical lines (top).

Although the vertical transition energies calculated with B3LYP method show a systematic shift relative to the experimental data, the red-shift of the dimer relative to the monomer could be confirmed with an error of ~ 0.1 eV for the pure molecules within the COSMO model of solvent but no explicit solvents.

4.1.3 TCNQ radical anion in ethanol : methanol mixture (vol 4:1)

4.1.3.1 Experiment

In this study temperature-dependent EPR measurements were carried out by Bruker ELEXSYS EPR-spectrometer, E-500, at X-band with 100 kHz field modulation of 5G amplitude. Temperature was controlled with a Bruker variable temperature controller and was stable within 0.2 K. Overmodulated spectra were recorded in the range of temperature from 180-320 K raising up 10 K in each step. The area under overmodulated spectra were received from the double integral with the base line corrections^[2]. Tetracyano-p-quinodimethane radical anion (TCNQ^{•-}) salts with lithium (Li⁺), sodium (Na⁺), potassium (K⁺) and butylammonium (Bu₄N⁺) counter-ions were dissolved in mixture of ethanol and methanol (vol 4:1) with the concentration 0.05 mM. Purified nitrogen was bubbled through the solutions for 15 min to remove oxygen. The normalized EPR-integral of each substance and Curie-Weiss law ($A \sim C/(T-\theta)$) were plotted against temperature (shown in **Fig. 4.9**) for TCNQ radical anion with sodium counter-ion showing the behavior of an EPR-signal in the dimerization process as a function of temperature. The fraction of paramagnetic monomer (α) was plotted versus reciprocal temperature (**Fig. 4.10**). The fraction of paramagnetic monomer decreases from the maximum ($\alpha = 1$), dissociated radical monomer, as a function of temperature. Enthalpy of dimerization can be extracted from the van't Hoff plots of logarithm of dimerization equilibrium constants (K_{dim}) versus the reciprocal temperature (**Fig. 4.11**).

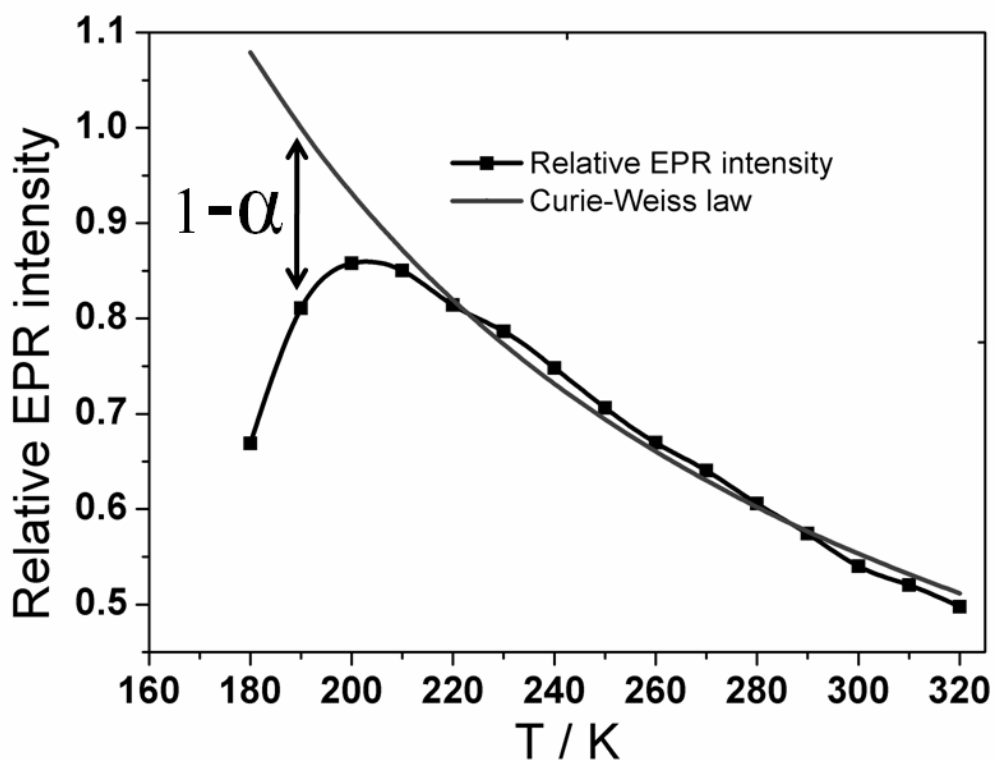


Figure 4.9: Relative EPR intensity of TCNQ radical anion with Na^+ counter-ion undergoing dimerization in EtOH:MeOH vol 4:1.

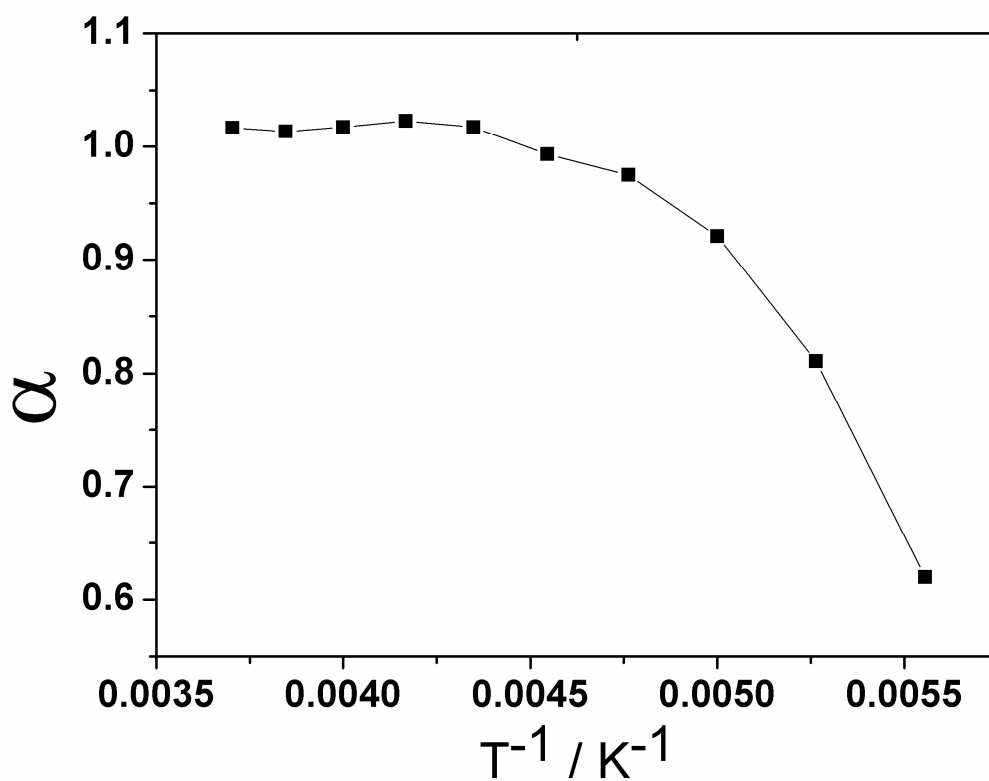


Figure 4.10: Fraction of the TCNQ radical anion monomer with Na^+ counter-ion as a function of temperature in EtOH:MeOH vol 4:1.

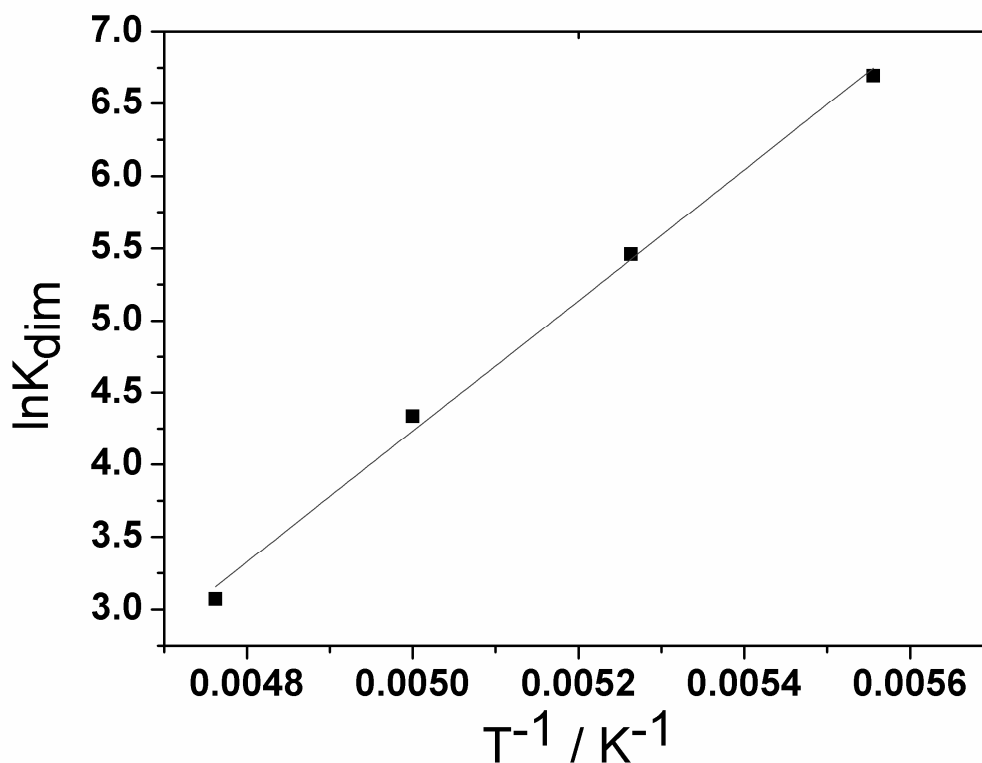


Figure 4.11: The natural logarithm dimerization equilibrium constant K_{dim} of TCNQ radical anion with Na^+ counter-ion as a function of temperature in EtOH:MeOH vol 4:1.

Table 4.7: Dimerization enthalpies (ΔH_{dim}) and dimerization equilibrium constant (K_{dim}) at 300 K and 200 K of TCNQ radical anion with various counter-ions in EtOH:MeOH vol 4:1.

| Substance | ΔH_{dim} (kJ/mol) | K_{dim} (M^{-1}) (300 K) | K_{dim} (M^{-1}) (200 K) |
|---------------------------|---------------------------|--------------------------------|--------------------------------|
| TCNQ \bullet^-Li^+ | -34.2 | 13.15 | 79.26 |
| TCNQ \bullet^-Na^+ | -37.6 | 20.46 | 76.34 |
| TCNQ \bullet^-K^+ | -34.5 | 5.51 | 72.43 |
| TCNQ $\bullet^-(Bu_4N)^+$ | -26.0 | -13.71 | 53.29 |

The data from **Table 4.1.3.1** show that the dimerization enthalpies (ΔH_{dim}) of TCNQ radical anion with various counter-ions (Li^+ , Na^+ , K^+ , $(Bu_4N)^+$) are in the range of -25 kJ/mol to -38 kJ/mol. Dimerization equilibrium constants (K_{dim}) at 200 K are much higher than at 300 K meaning that the dimerization processes occurred at low temperature much more than at high temperature. This was confirmed by temperature-dependent UV/Vis measurement by Boyd and co-worker^[14] where the absorption intensity of dimer peak increased when temperature decreased.

R.H. Boyd and W.D. Phillips studied a dimerization of tetracyanoquinodimethane anion radical with lithium counter-ions ($\text{TCNQ}^{\bullet-}\text{Li}^+$) in acetonitrile by UV/Vis spectroscopy^[14]. They found that there are two absorption peaks of the dimer at 643 nm and 369 nm (1.93 and 3.36 eV). Radical monomer shows two absorption bands at 737 and 408 nm (1.68 and 3.04 eV). The dimer peak at 643 nm (1.93 eV) increased and the monomer peak at 737 nm (1.68 eV) become weaker when temperature was decreasing from 60.1°C to 2.0°C. Data measured in this study correspond well with earlier work -41.0 kJ/mol ^[3].

4.1.3.2 Theoretical investigation

Dimerization of tetracyanoquinodimethane radical anion with lithium counter-ion ($\text{TCNQ}^{\bullet-}\text{Li}^+$) in ethanol and methanol mixture vol 4:1 was chosen for the theoretical investigations. According to the experimental value, the dielectric constant was set to 27.93^[38] and the refractive index was set to 1.354^[37]. The optimized geometry of the $\text{TCNQ}^{\bullet-}\text{Li}^+$ radical monomer at B3LYP-D/cc-pVDZ level of theory is presented in **Fig. 4.12**. Lithium counter-ion is located near nitrogen atom of one cyano group with a distance of approximately 2.01 Å.

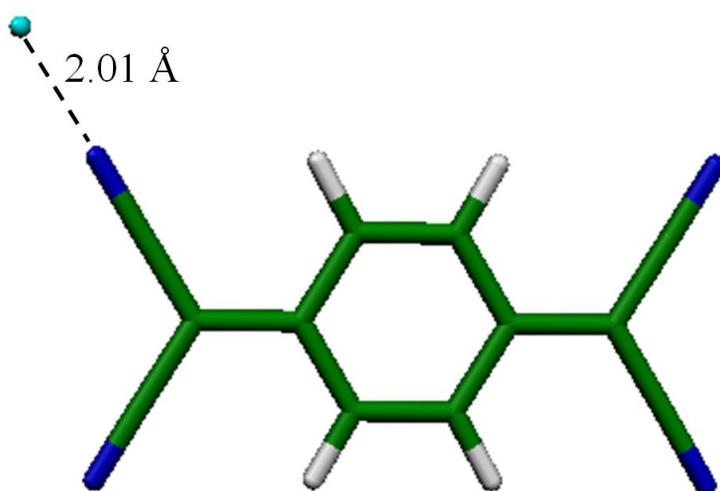


Figure 4.12: The optimized geometry of $\text{TCNQ}^{\bullet-}\text{Li}^+$ monomer at B3LYP-D/cc-pVDZ level of theory.

Four optimized geometries of $[\text{TCNQ}]_2^{2-}2\text{Li}^+$ dimer (**C1-C4**) were found as shown in **Fig. 4.13**. Two fragments of $\text{TCNQ}^{\bullet-}$ monomer arrange themselves in eclipsed and stacked position. Lithium counter-ions are located in cis and trans position relative to the side of dimers. Two fragments shift along the short axis of molecule by around 0.9 Å in dimers **C1** and **C2**. The intradimer distance of all four dimers is around 3.0 ± 0.1 Å (exact values are shown in **Table 4.8**).

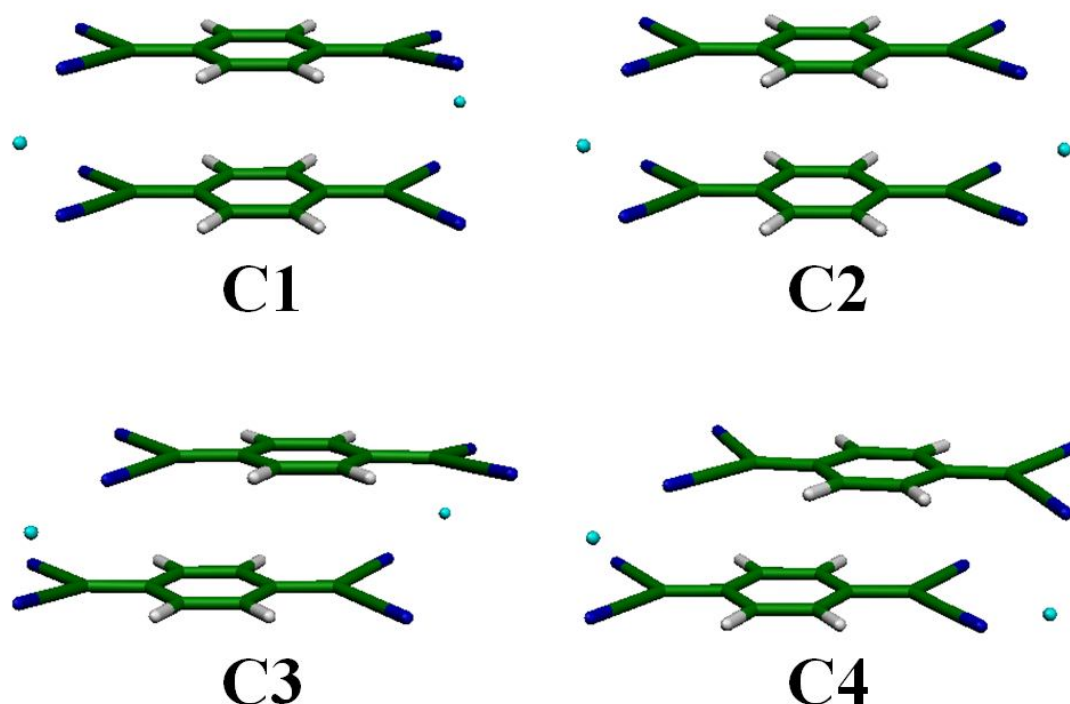


Figure 4.13: Four optimized geometries of $[\text{TCNQ}]_2^{2-}2\text{Li}^+$ dimers (**C1 - C4**) computed at B3LYP-D/cc-pVDZ level of theory.

Dimer **C1** is the most stable conformer of $[\text{TCNQ}]_2^{2-}2\text{Li}^+$ dimers with 93.98 % in Boltzmann distribution. For the most stable conformer dimer **C1**, the intradimer separation between the two monomer fragments is 3.06 Å and lithium counter-ions are located in the trans position of dimer with a distance of 2.07 Å from the nearest nitrogen atom of cyano group. **Figure 4.14** shows the HOMO orbital of dimer **C1** computed by DFT and CASSCF methods. The HOMO orbital computed by DFT method shows a 2 electron/ 4 center π -bonding mainly interacting over the amino nitrogens while CASSCF give a 2 electron/ 16 center π -bond including also the interaction of the two benzene rings.

BSSE calculations in gas phase at B2PLYP-D/cc-pVTZ yield a dimerization energy of -164.77 kJ/mol for conformer **C1** which has much overstabilization compared to the experimental enthalpy from temperature-dependent EPR measurement (-34.22 kJ/mol). CASSCF yields a dimerization energy of -54.99 kJ/mol for the most stable conformer **C1** which is an overstabilization of -20 kJ/mol relative to the experiment.

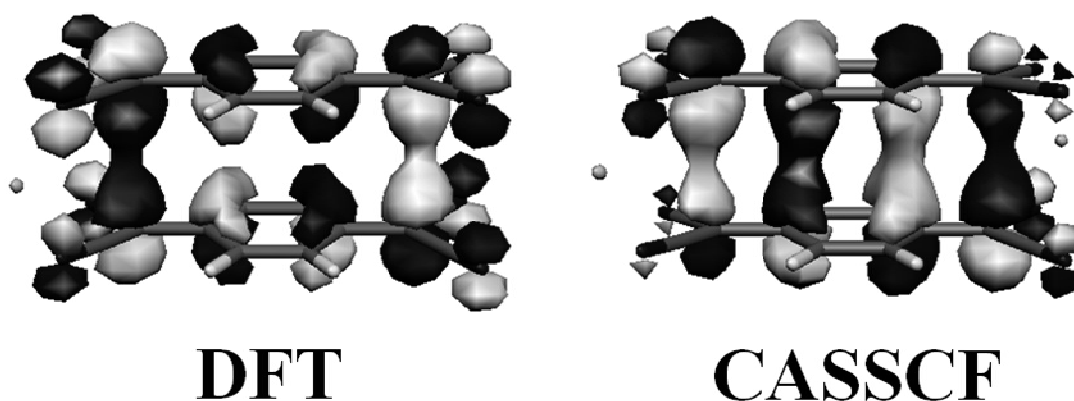


Figure 4.14: The HOMO orbitals computed by DFT and CASSCF methods of the most stable conformer $[\text{TCNQ}]_2^{2-} 2\text{Li}^+$ dimer (**C1**).

One reason for too low calculated dimerization energies might be missing description of explicit interaction of amino group with solvent. The solvents ethanol and methanol show strong H-bonding possibility and will therefore change the charge distribution and energetics, especially in the monomer. This will lead to a different energetics as discussed for PPD radical cation dimerization in Chapter 4.2.

Table 4.8: The intradimer distances, relative energies, Boltzmann distribution and dimerization energies of the most stable conformers of $[\text{TCNQ}]_2^{2-}2\text{Li}^+$ dimers.

| TCNQ | dimer geometry | | B2PLYP-D cc-pVTZ | | E _{dim} [kJ/mol] | | ΔH _{dim} [kJ/mol] | |
|-----------|----------------------------|---|------------------------------|--------------------------------------|------------------------------|------------------------------|--------------------------------|--------|
| | ring geometry r (pi-pi) | lithium geometry ^a r(Li..N(CN)) | E _{rel} [kJ/mol] | N _i / N ₀ % | UB3LYP-D cc-pVDZ | BSSE UB2PLYP-D cc-pVTZ | CASSCF ^b cc-pVTZ | exp. |
| C1 | eclipsed 3.06 Å | tran 2.07 Å | 0.00 | 93.98 | -129.88 | -164.77 | -54.99 | |
| C2 | eclipsed 3.07 Å | cis 2.07 Å | 7.30 | 4.94 | -128.81 | -158.30 | -50.55 | -34.22 |
| C3 | staggered 3.06 Å | trans 2.07 Å | 11.65 | 0.85 | -117.28 | -152.23 | -80.51 | |
| C4 | staggered 2.98 Å | cis 2.06 Å | 14.92 | 0.23 | -115.62 | -147.95 | -65.82 | |

^a distances are given to the closest nitrogen atom.

^b CASSCF(3,3)/CASSCF(2,2) data are given.

UV/Vis spectrum of the most stable $[\text{TCNQ}]_2^{2-}2\text{Li}^+$ dimer and $\text{TCNQ}^{\bullet-}\text{Li}^+$ monomer was computed by TDA-DFT method at B3LYP/cc-pVTZ level of theory in ethanol and methanol mixture (vol 4:1) and compared to the experimental UV/Vis spectra in acetonitrile^[14]. The convoluted UV/Vis spectrum in **Fig. 4.15** shows the agreement between the calculated spectra and the experimental absorption spectra. The first convoluted peak of dimer at 534 nm (2.32 eV) is the combination between two excitations, first from HOMO-3 \rightarrow LUMO ($\pi\rightarrow\pi^*$ transition) at 568 nm (2.34 eV) and second from HOMO-1 \rightarrow LUMO ($\pi\rightarrow\pi^*$ transition) at 507 nm (2.44 eV). The second dimer peak comes from the transition of HOMO \rightarrow LUMO+2 ($\pi\rightarrow\text{Li}_{xy}$) at 294 nm (4.21 eV). The first monomer peak shows the transition from beta orbitals HOMO \rightarrow LUMO ($\pi\rightarrow\pi^*$ transition) at 619 nm (2.00 eV) while the second peak comes from SOMO \rightarrow LUMO+1 ($\pi\rightarrow\text{Li}_{xy}$ transition) at 330 nm (3.76 eV). The computed spectra show again a hypsochromic shift from the experiment by around 0.4 eV but still reproduced blue shift of the dimer relative to monomer peaks as in the experimental data.

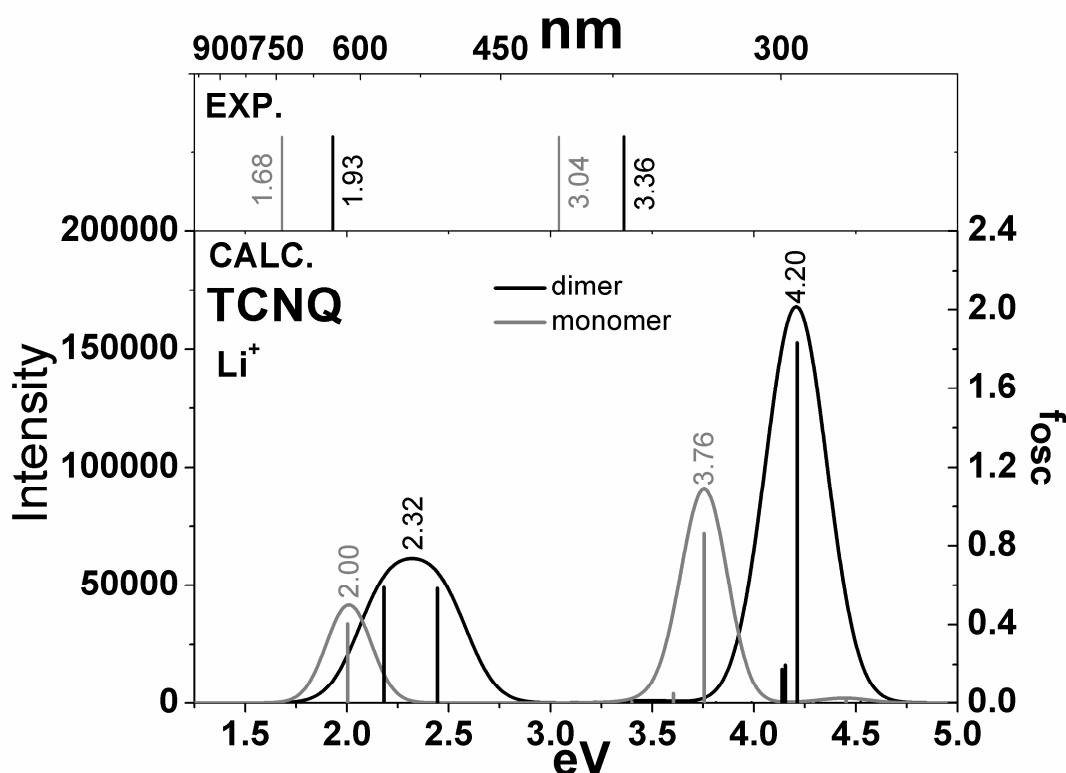


Figure 4.15: The TDA-B3LYP calculated vertical excitations (bottom, lines are shown with oscillator strengths) and convoluted UV/Vis spectrum (bottom) of the $[\text{TCNQ}]_2^{2-}2\text{Li}^+$ dimer (black) and $\text{TCNQ}^{\bullet-}\text{Li}^+$ monomer (gray). The energies of experimental peak maxima are shown as vertical lines (top).

4.1.4 Summary of radical anions dimerization

Theoretical investigation of three radical anions (TCNE \bullet^- , DDQ \bullet^- , TCNQ \bullet^-) were performed for dimerization in solution. Both EPR experiment and theoretical calculations were performed to TCNQ radical anion. In the theoretical investigation part, Density Functional Theory at B3LYP-D/cc-pVDZ level of theory was chosen for geometry optimization. Counter-ions play an important role to stabilize dimers. It was found that dispersion correction stabilized dimers and yields structural parameters of the optimized dimer geometries corresponding well with the experimental X-ray crystallographic data of dimer molecules ([TCNE] $_2^{2-}$, [TCNQ] $_2^{2-}$ and [DDQ] $_2^{2-}$). All three dimer molecules exhibit a multicenter long π -bond stemming from the strong interaction of two SOMO orbitals of the monomers. The intradimer distances are around 2.8 – 3.1 Å which are in good agreement with the experimental crystallographic data.

BSSE correction in gas phase at B2PLYP-D/cc-pVTZ level of theory yields a dimerization of the most stable conformers of [TCNE] $_2^{2-}2\text{Na}^+$ and [DDQ] $_2^{2-}2\text{Na}^+$ in good agreement with the dimerization enthalpy from EPR experiments with an error of 5 to -28 kJ/mol. But for [TCNQ] $_2^{2-}2\text{Li}^+$ it reproduced a dimerization energy with too much overstabilization compared to the data from experiment that are measured in our institute. CASSCF calculations using CAS(2,2) for dimer and CAS(3,3) for monomer, reproduced the dimerization energy quite well for TCNE and TCNQ radical anions dimerization with an error of \sim -20 kJ/mol but do not reproduced dimerization energy for DDQ radical anion dimerization (an error of \sim 30 kJ/mol). The summary of an error of dimerization energy for radical anions dimerization (TCNE \bullet^- , DDQ \bullet^- and TCNQ \bullet^-) by BSSE B2PLYP-D and CASSCF methods is shown in following:

| Method | Error from experiment (kJ/mol) | | |
|---------------|--------------------------------|-------------------|--------------------|
| | TCNE ^{•-} | DDQ ^{•-} | TCNQ ^{•-} |
| BSSE B2PLYP-D | -28 | (+5) - (-22) | -130 |
| CASSCF | -22 | (+27) - (+30) | -22 |

An error of calculated dimerization energy may come from the lack of explicit solvent molecule and some effect of dielectric constant which is increasing when temperature decreased but in this calculation used dielectric constant of solvent at 20-25°C follow the default of the program package. The effect of the dielectric constants to the calculated dimerization energies are shown in Chapter 4.3.

The calculated UV/Vis spectrum of radical anion dimerization is hypsochromic shifted relative to the experiment around 0.6 eV. This error may come from the lack of explicit solvent molecules which is necessary for explain the interaction between dimer and monomer with solvent molecule. The inclusion of explicit solvent molecule is presented in Chapter 4.2 for PPD radical cation dimerization to see the interaction of dimer and monomer with explicit solvent resulting in more information in the calculated UV/Vis spectrum.

4.2 RADICAL CATION DIMERIZATION

Six radical cations were investigated in our theoretical calculation of dimerization which are p-phenylenediamine, *N,N*-dimethyl-p-phenylenediamine, 2,3,5,6-tetramethyl-p-phenylenediamine, *N,N,N',N'*-tetramethyl-p-phenylenediamine, 3,3',5,5'-tetramethylbenzidine and tetrathiofulvalene radical cations (PPD^{•+}, *N,N*-DMPPD^{•+}, 2,3,5,6-TMPPD^{•+}, *N,N,N',N'*-TMPPD^{•+}, TMB^{•+} and TTF^{•+}), respectively.

The dimerization of PPD radical cation (PPD^{•+}) is presented in more detail in this chapter including the discussion of solvent and its influence.

4.2.1 Paraphenylenediamine radical cation in EtOH/Et₂O (vol 2:1)

The optimized stable geometry of PPD radical cation monomer including bromide counter-ion (PPD^{•+}Br⁻) is shown in **Fig. 4.16**. The structural parameters of PPD^{•+}Br⁻ monomer correspond well with the experimental crystal structure of the amino benzene system (Wurster's salt)^[69, 70, 82], which shows crystal packing via N-H...N hydrogen bonds. The calculated bond lengths of PPD^{•+}Br⁻ monomer deviate from X-ray bond lengths by less than 0.07 Å (for C-N bond), which is an acceptable accordance. The bromide counter-ion is located near one of hydrogen atoms in NH₂ group in the most stable conformer with a Br-H distance of 2.27 Å. Bromide counter-ion produces a negative charge on those hydrogen atoms close to it.

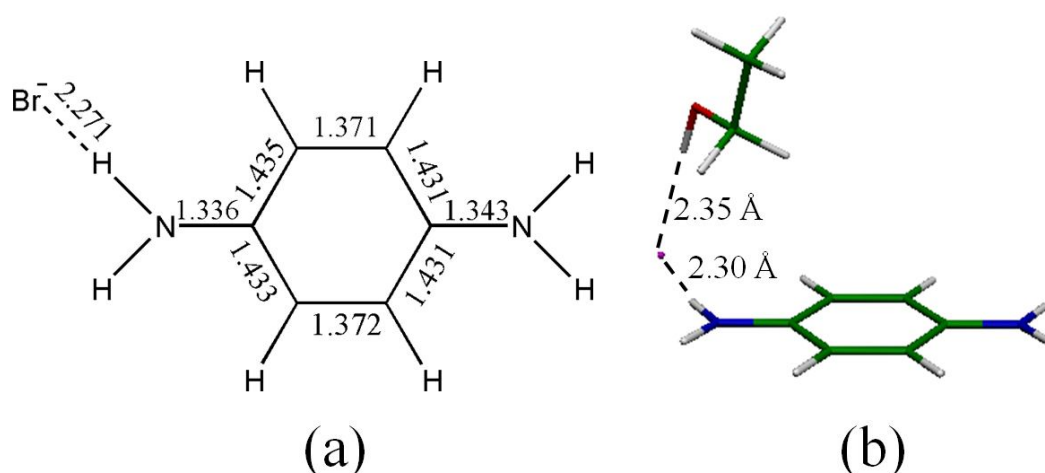


Figure 4.16: B3LYP-D optimized structural parameters of PPD^{•+} monomer (a) with Br⁻ counter-ion, (b) with Br⁻ counter-ion and one ethanol solvent molecule.

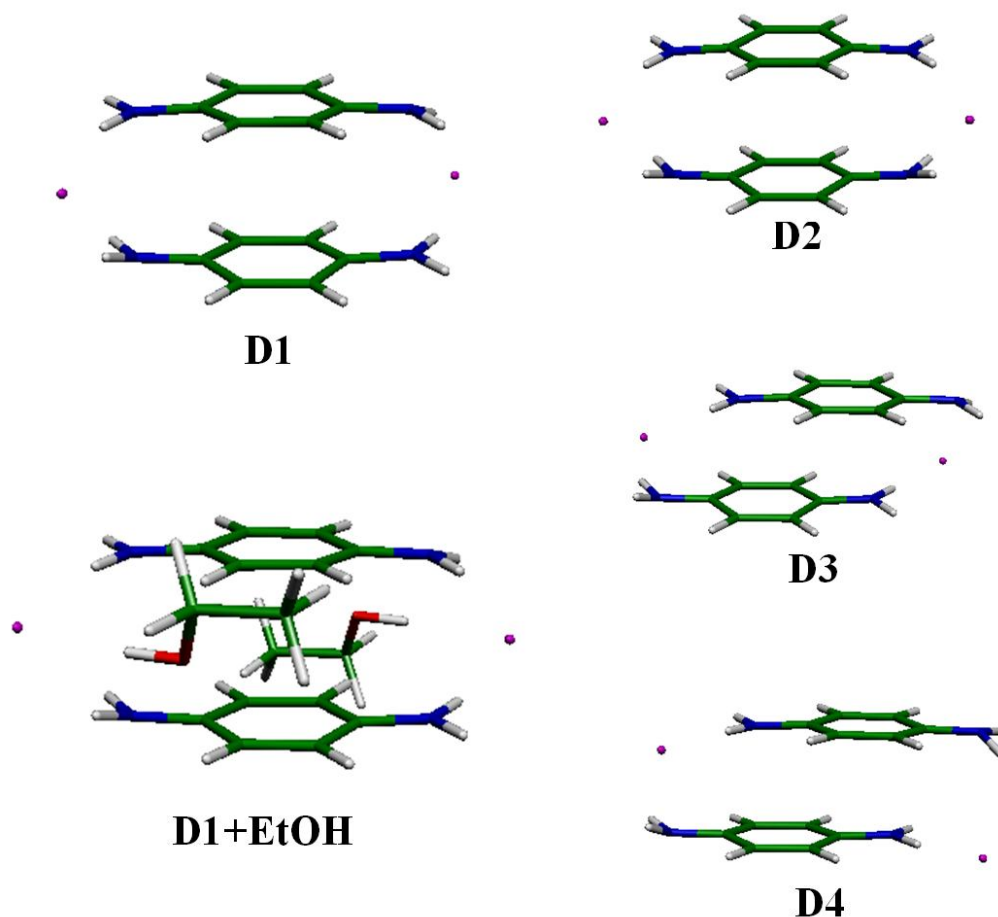


Figure 4.17: The B3LYP-D optimized geometries of $[PPD]_2^{2+} 2Br^-$ dimers **D1** - **D4** and the most stable conformer (**D1**) with two molecules of solvent ethanol (**D1+EtOH**).

Geometries

Four stable optimized geometries of dimers $[PPD]_2^{2+} 2Br^-$ were found after performing geometry optimization at UB3LYP-D/cc-pVDZ level of theory with broken symmetry as shown in **Fig. 4.17**. The two fragments arrange themselves in eclipsed and stacked positions with bromide counter-ions in cis and trans position. The energies of alpha and beta orbitals were degenerated after the optimization finished. Boltzmann distribution yields 96.25 % for conformer **D1**. Two monomers of $PPD^{\bullet+}$ align themselves in eclipsed position with the bromide counter-ions in trans position. The two benzene rings are slightly shifted (0.86 Å) along the short axis, as confirmed by other theoretical calculations for $[PPD]_2^{2+}$ with two bromide counter-ions^[32]. The two fragments try to avoid coulombic repulsion between the same charge and the monomeric units arrange their position to get electrostatic attraction of the opposite charge between the two fragments. Bromide counter-ions are interacting with the

nitrogen atoms in amino groups influencing the geometry of the NH₂ groups: in one fragment, the pyramidalization angle is almost zero, in the other fragment it is unsymmetrically pyramidal by 19-20° for one H-atom and less than 5° for the H on the opposite side of the bromide ion. The distance between bromide ion and the nearest hydrogen atom of amino group is 2.43 Å in dimer **D1**. The intradimer distance between the plane of the two fragments is 2.94 Å. Earlier Hückel calculations of D_{2h} symmetric [PPD]₂²⁺ dimers^[74] estimated the pi-pi distance by 2.75 Å. But with inclusion of the counter-ions, **D1** has somewhat larger distance and shows a clear deviation from D_{2h} symmetry. Our calculations do not include symmetry, but the resulting geometry **D1** closely resembles a C_i symmetric structure.

Orbital description

To get insight into the interaction of radical cation monomers in the dimer, we show the relevant CASSCF(3,3) orbitals for the monomer PPD^{•+}Br⁻ and the CAS(2,2) orbitals for the most stable [PPD]₂²⁺2Br⁻ dimer **D1** in **Fig. 4.18**. In CASSCF(2,2), the highest occupied molecular orbital (HOMO) is located in the intra-dimer region. It describes the radical-radical binding and reveals a long multicenter π -bond including two electrons at twelve centers (2e⁻/12c). The aromatic rings are strongly interacting with each other. No contribution from counter-ions is present in the CASSCF(2,2) HOMO orbital. In DFT, the electron distribution has changed: the orbitals with high electron density at bromide are inserted between the HOMO and LUMO orbitals resulting in a different orbital numbering. Moreover, the DFT HOMO orbital shows additional electron distribution at bromide ions to the interacting orbital as shown for the calculations including ethanol in **Fig. 4.18**.

Table 4.9: The intradimer distances, relative energies, Boltzmann distribution and dimerization energies of the most stable conformers of $[\text{PPD}]_2^{2+} \cdot 2\text{Br}^-$ dimers within COSMO model of solvation (EtOH/Et₂O vol2:1).

| PPD | dimer geometry | | B2PLYP-D cc-pVTZ | | UB3LYP-D cc-pVDZ | E _{dim} [kJ/mol] | | ΔH _{dim} [kJ/mol] |
|-----------|----------------------------|--|------------------------------|--------------------------------------|---------------------|------------------------------|--|-------------------------------|
| | ring geometry r (pi-pi) | bromine geometry ^a r(Br..N) r(Br..H(N)) | E _{rel} [kJ/mol] | N _i / N ₀ % | | BSSE UB2PLYP-D cc-pVTZ | CASSCF ^b MRMP2 ^c cc-pVTZ | exp. [2] |
| D1 | eclipsed 2.94 Å | trans 3.42 Å 2.43 Å | 0.00 | 96.25 | -94.70 | -198.47 | -74.68 (-248.76) | -52.40 |
| D2 | eclipsed 2.91 Å | cis 3.41 Å 2.41 Å | 12.83 | 0.54 | -93.15 | -186.58 | | |
| D3 | staggered 2.78 Å | trans 3.31 Å 2.29 Å | 8.60 | 2.99 | -88.39 | -189.87 | | |
| D4 | staggered 2.79 Å | cis 3.31 Å 2.28 Å | 15.10 | 0.22 | -88.97 | -184.07 | | |

^a distances are given to the closest nitrogen atom.

^b CASSCF(3,3)/CASSC(2,2) data are given.

^c MRMP2 calculation base on CASSCF(3,3)/CASSC(2,2) reference, Values in brackets.

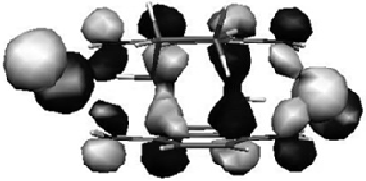
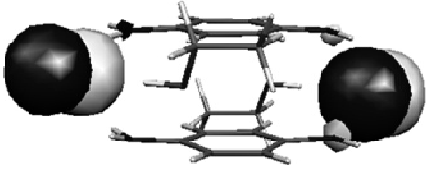
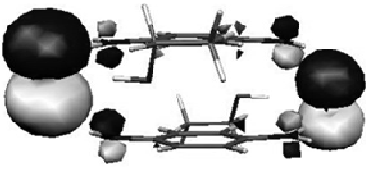
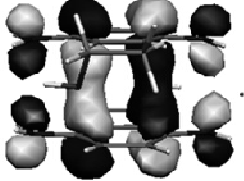
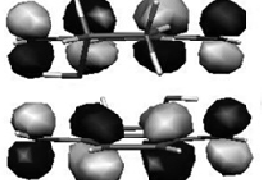
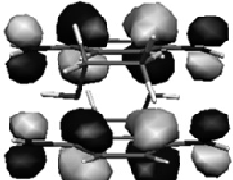
| PPD | DFT | CASSCF |
|--------|--|--|
| HOMO-6 |  |  |
| HOMO |  |  |
| LUMO |  |  |

Figure 4.18: The molecular orbitals computed by B3LYP-D and CASSCF methods of the most stable conformer $[PPD]_2^{2+} \cdot 2Br^-$ dimer **D1** with two ethanol solvent molecules.

Energetics

Dimerization energies calculated after eq.(3.1) for the different methods are presented in **Table 4.9** and compared with the dimerization enthalpy ΔH from temperature-dependent EPR measurements. All four stable geometries are stabilized after dimerization. We further discuss the data of the most relevant conformation **D1**. B3LYP-D/cc-pVDZ level computes the dimerization energy of -94.70 kJ/mol and BSSE corrected B2PLYP-D/cc-pVTZ method yields -198.47 kJ/mol for the dimer **D1**. The overestimation of dimerization energies might come from the strong electrostatic attraction between negative and positive atomic charge of the two fragments in the dimers and also from the strong interaction between bromide counter-ions with NH_2 groups in dimer.

MRMP2/CASSCF(2,2) using cc-pVTZ basis set shows around 14% character of double excitation in the dimer. CASSCF calculations using CAS(2,2) for dimer and CAS(3,3) for monomer yield dimerization energies of -74.68 kJ/mol (**D1**) that is well

corresponding with the dimerization enthalpy from temperature-dependent EPR spectroscopy (-52.40 kJ/mol)^[7]. Subsequent MRMP2 calculations receive a dimerization energy of -248.76 kJ/mol for dimer conformations **D1**.

For the dimers, CAS(2,2) seems to be the appropriate active space for reproducing experimental observed dimerization because it includes the relevant orbitals for the dimerization process. Therefore, for the other radical cations dimerization (*N,N*-DMPPD^{•+}, 2,3,5,6-TMPPD^{•+}, *N,N,N',N'*-TMPPD^{•+}, TMB^{•+} and TTF^{•+}) multireference MRMP2 calculations on the basis of dimer CAS(2,2) and monomer CAS(3,3) with the larger basis set (cc-pVTZ) were performed, although we know that this unsymmetric CAS spaces can only give the trends for the dimerization process.

Explicit solvent:

After adding one ethanol molecule to the monomer including bromide counter-ion, six geometries have been located with different interactions of ethanol with either bromide and/or the PPD^{•+} amino group. Focusing on the agreement with UV spectra interpretation, we choose the geometry with strong interaction of ethanol with bromide counter-ion (see **Fig. 4.17**) for construction of the dimer and further discussion, although is not the energetic minimum of monomers. The position of bromide counter-ion remains in the plane of PPD radical cation ring and ethanol molecule is located on top of bromide counter-ion. The distances between the bromide counter-ion to the alcohol group hydrogen atom (Br..H-O) and to the hydrogen atom of amino group (Br..H-N) are 2.35 Å and 2.30 Å, respectively. The Br..H-N distance is weakened and longer by 0.03 Å than without explicit ethanol solvent because the bromide counter-ion has additional interaction with ethanol.

In the dimer, two solvent molecules of ethanol were added to conformer **D1** starting from ethanol orientation like in the monomer. Ethanol molecules move to the plane of aromatic rings during optimization and are in side position of bromide counter-ions with a (Br..H(-O)) distance from bromide to alcohol hydrogen atom of 2.30 Å (see **Fig. 4.17**). This short distance is in the range of hydrogen bonding. The intramonomer distance of the dimer including ethanol is 3.057 Å, somewhat longer than for the dimer without ethanol (2.94 Å). This leads to the conclusion that the interaction of ethanol with PPD radical cation and bromide counter-ion is reduced at dimerization in favour of the interaction of the two PPD radical cations with each other.

Inclusion of explicit molecules of ethanol does not alter the frontier orbitals HOMO and LUMO in the DFT calculations as depicted in **Fig. 4.18**. The HOMO orbital of the dimer shows the same two electron twelve center ($2e^-/12c$) interaction as in the COSMO calculations with the electron additionally localized on bromide counter-ions. Discussion of the spectral characteristics will be performed on these geometries including the explicit ethanol solvent.

UV/Vis Calculations:

At low temperature another experimental finding for dimerization is that there appear new peaks in the UV spectra, significantly bathochromically shifted from the room temperature monomeric peak and assigned to the dimerization procedure. $\text{PPD}^{\bullet+}$ experimental UV/Vis spectra have been recorded for the bromine salt^[8]. Therefore the experimental data measured in ethanol were compared with calculations of the substituted $\text{PPD}^{\bullet+}$'s with inclusion of bromide counter-ion and the solvent ethanol. For $\text{PPD}^{\bullet+}$ also data in water are produced and compared to the respective UV spectrum in water^[10].

For $\text{PPD}^{\bullet+}$, the experimental maxima in UV/Vis absorption spectra are present at 500, 465, 380 and 322 nm (2.48, 2.66, 3.26 and 3.85 eV) in solvent ethanol representing the $\text{PPD}^{\bullet+}$ monomer. These peaks are not reasonably well described by our simulation of the monomer including the bromide counter-ion within the COSMO model of solvation. But with inclusion of one explicit solvent molecule of ethanol including specific interactions with the solvent, the monomer spectrum can be explained satisfactorily. In the UV/Vis calculation of $[\text{PPD}]_2^{2+}$ dimers and $\text{PPD}^{\bullet+}$ monomer, it was found that ethanol solvent plays an important role to the vertical excitation especially for the monomers. Therefore the calculations including bromide counter-ion and explicit ethanol solvent molecules will be discussed in this section. In the UV/Vis discussion we refer to the DFT orbitals as shown in **Figs. 4.18** and **4.19** for $[\text{PPD}]_2^{2+}$ dimers and $\text{PPD}^{\bullet+}$ monomers.

The vertical excitation process of the $\text{PPD}^{\bullet+}$ monomer takes place from SOMO to LUMO orbital, but also lower excitations from HOMO and HOMO-x ($x=1-4$) and from solvent to LUMO are involved. (see **Fig. 4.19** and **Table 4.10**). The experimental spectrum shows four relevant peaks in the monomer spectrum in the recorded range of

(2.48 eV – 3.85 eV). The calculated excitation energies of the monomer shift from (3.068 - 5.15 eV) for the pure PPD radical cation ($\text{PPD}^{\bullet+}$) to (2.74 - 4.45 eV) for $\text{PPD}^{\bullet+}\text{Br}^-$ with inclusion of counter-ion to (2.40 - 3.66 eV) with inclusion of counter-ion and explicit solvent molecule. The calculations underestimate the transition energy by approx. 0.6 eV when the stabilizing interaction with the counter-ion is neglected and the solvent is only described by the COSMO model. Neglecting the explicit interaction with the solvent still underestimates the transition energies by 0.27 eV. Inclusion of the solvent brings the energies to lower values corresponding well with the experimental spectrum.

In the DFT calculations the solvent orbitals are inserted energetically between the long-axis pi-orbital and the short-axis pi-orbitals. The bromide orbital oriented in xy is lying between the latter pi-orbital and the antibonding pi-orbital located on benzene ring. Interpretation of the excitations with respect to the orbitals in **Fig. 4.19** tells us, that the radical ion monomer has a strong interaction with the solvent and that the first two peaks in the spectrum mainly reflect excitation from the solvent to PPD radical cation. This is also reflected in the resulting convoluted absorption spectrum shown in **Fig. 4.20**.

The first two peaks (λ_1 and λ_2) of the monomer $\text{PPD}^{\bullet+}\text{Br}^-$ are two different linear combinations of transitions from ethanol C-O bond and from long-axis pi-orbital into the HOMO orbital located at the pi system including some electron distribution at bromide counter-ion ($\pi+\text{ethanol}\rightarrow\pi^*$ transition) resulting two lines at 515.7 nm (2.404 eV) and 451.8 nm (2.744 eV). λ_1 and λ_2 are not seen in the solvent water, because the C-O-bond orbital does not occur and the other contribution results in a very low oscillator strength (below 0.01).

The third peak λ_3 stems from transition of solvent beta orbital into the first antibonding pi beta LUMO (ethanol $\rightarrow\pi^*$ transition) yielding the absorption peak at 403.3 nm (3.074 eV) and can be modeled properly only with inclusion of explicit solvent molecules. The fourth peak λ_4 at 338.3 nm (3.664 eV) represents excitation from SOMO alpha orbital located at bromide counter-ion into the second antibonding pi alpha orbital (LUMO) located at the benzene ring (bromide $\rightarrow\pi^*$ transition). These two peaks are also present in the water spectrum with the same energy.

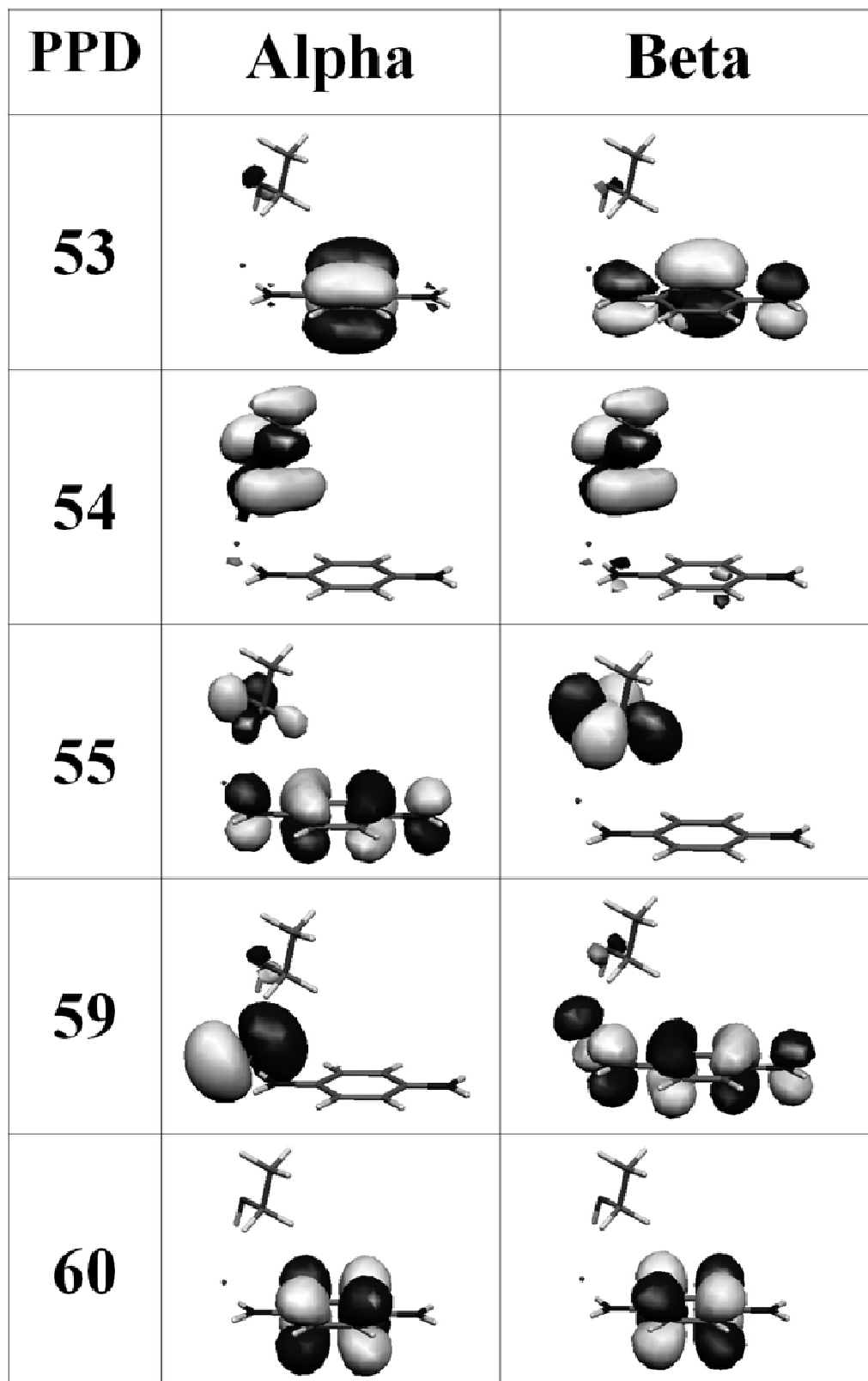


Figure 4.19: The molecular orbitals computed by B3LYP-D methods for PPD^{•+}Br⁻ monomer with one explicit molecules ethanol.

Table 4.10: TDA-B3LYP/cc-pVTZ transition energies and oscillator strengths of vertical excitations for dimers and monomers of all three PPD molecules with bromide counter-ions and explicit solvent ethanol.

| | | | PPD ^{•+} | N,N-DMPPD ^{•+} | 2,3,5,6-TMPPD ^{•+} | |
|----------------|-----------------|-------------|------------------------------------|------------------------------------|------------------------------------|------------------------------------|
| Dimer | λ_L | Exp. | 605 nm | 670 nm | 670 nm | |
| | | Calc. | 607.0 nm (2.042 eV) f=0.0466 | 652.8 nm (1.899 eV) f=0.1198 | 587.7 nm (2.110 eV) f=0.1056 | |
| | +Br+EtOH | λ_H | Exp. | 395 nm | 410 nm | 485 nm |
| | | | Calc. | 421.0 nm (2.945 eV) f=0.5512 | 454.1 nm (2.730 eV) f=0.8531 | 443.7 nm (2.794 eV) f=0.1654 |
| | | λ_1 | Exp. | 500 nm | 570 nm | 480 nm |
| | | | Calc. | 515.7 nm (2.404 eV) f=0.0146 | 540.7 nm (2.293 eV) f=0.0213 | 448.5 nm (2.764 eV) f=0.0594 |
| Monomer | λ_2 | Exp. | 465 nm | 523 nm | 450 nm | |
| | | Calc. | 451.8 nm (2.744 eV) f=0.0119 | 463.0 nm (2.678 eV) f=0.0501 | 311.3 nm (3.983 eV) f=0.0579 | |
| | +Br+EtOH | λ_3 | Exp. | 380 nm | 380 nm | |
| | | | Calc. | 403.3 nm (3.074 eV) f=0.0819 | 448.3 nm (2.766 eV) f=0.0391 | |
| | | λ_4 | Exp. | 322 nm | 324 nm | |
| | | | Calc. | 338.3 nm (3.664 eV) f=0.0429 | 337.8 nm (3.670 eV) f=0.0391 | |

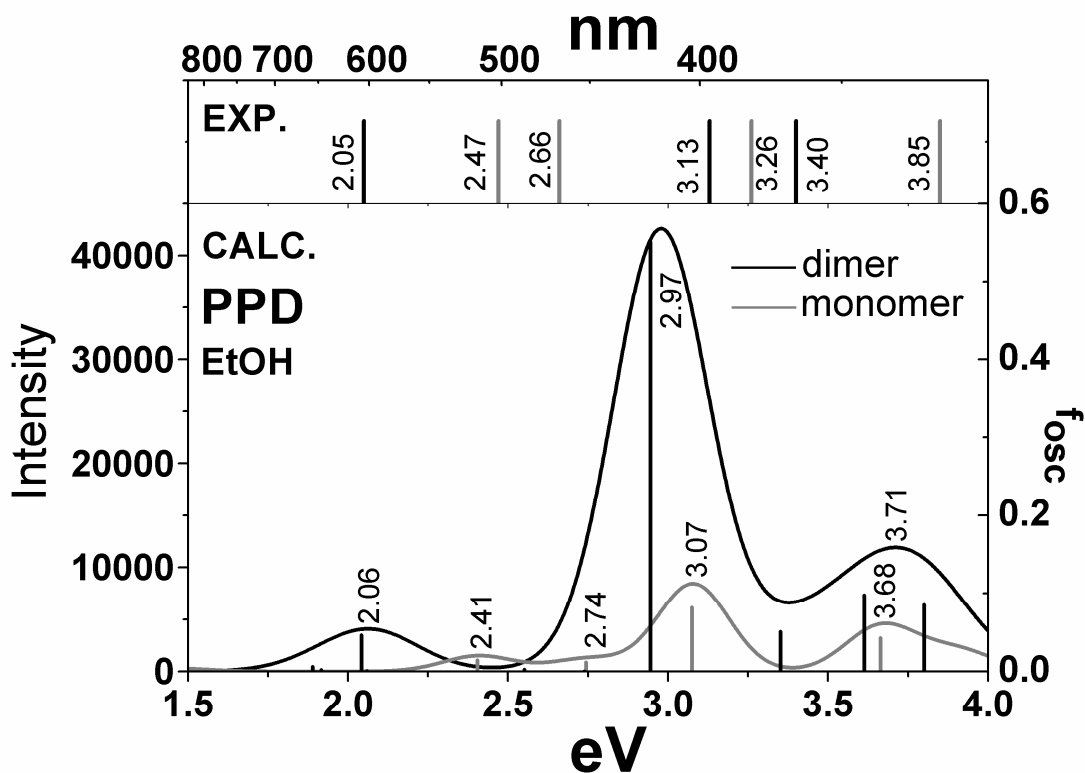


Figure 4.20: The TDA-B3LYP calculated vertical excitations (bottom, lines are shown with oscillator strengths) and convoluted UV/Vis spectrum (bottom) of the $[PPD]_2^{2+}2Br^-$ dimer (black) and PPD^+Br^- monomer (gray) with explicit solvent ethanol. The energies of experimental peak maxima^[8] are shown as vertical lines (top).

At lower temperature (143.15 K) new peaks appear and were assigned to the $[PPD]_2^{2+}2Br^-$ dimers^[8]. The experimental dimer spectra of $[PPD]_2^{2+}2Br^-$ show two main peaks^[8]. The first peak is attributed to λ_L (excitation from HOMO to LUMO orbital)^[3] which undergoes transition from the dimer stabilizing orbitals resulting in the strong dimer peak at 605 nm (2.05 eV). The second peak at 395 nm (3.13 eV)^[8] was attributed to λ_H (from HOMO-1 to LUMO orbital). In the recorded experimental range there is a third peak shown at 277 nm (4.47 eV). Ernstbrunner^[10] reported that in water the dimer peak (at ~600 nm) was already present at room temperature, but not in solvent methanol.

The vertical excitation process of dimer $[PPD]_2^{2+}2Br^-$ takes place mainly from the two interacting SOMO orbitals building the bonding HOMO orbital into the antibonding LUMO orbital as found in the CASSCF calculations (see **Fig. 4.18**). In DFT calculations, orbitals located at bromide counter-ion with different orientations (xy and z) shift between this strongly interacting orbital and the antibonding π^* orbital.

TDA-DFT calculations computes the two peak λ_L and λ_H of dimer resulting from linear combinations of orbitals located at the interacting orbital and the bromine counter-ion at 607 nm (2.042 eV) and at 421 nm (2.945 eV). The contributions and oscillator strengths are given in **Table 4.10**. For solvent water the same characteristics for the dimer found in our model (see **Fig. 4.21**), the peak λ_L is only slightly hypsochromic shifted by 0.14 eV to higher energies.

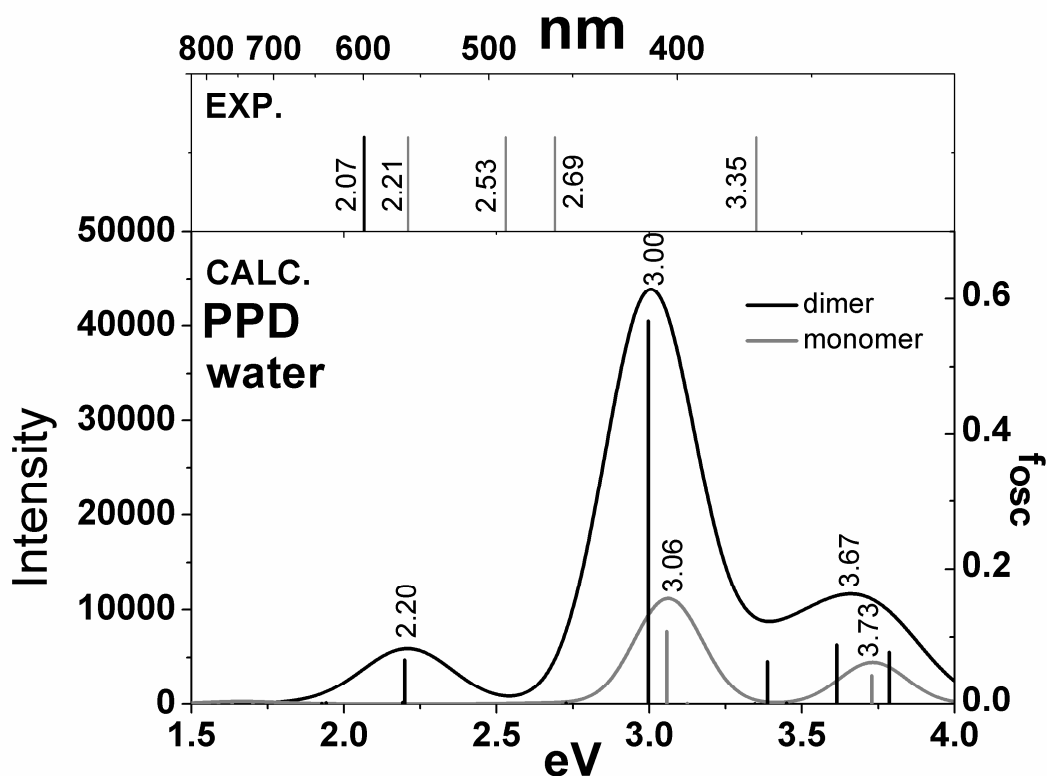


Figure 4.21: The TDA-B3LYP calculated vertical excitations (bottom, lines are shown with oscillator strengths) and convoluted UV/Vis spectrum (bottom) of the $[PPD]_2^{2+} 2Br^-$ dimer (black) and $PPD^+ Br^-$ monomer (gray) with explicit solvent water. The energies of experimental peak maxima^[10] are shown as vertical lines (top).

It is noticed for $PPD^+ Br^-$, that the monomer peak λ_3 is hidden under the higher energetic dimer peak λ_H in the convoluted spectrum. This is also the case for the next higher calculated peak which comes from excitations of the interacting orbital into the second antibonding orbital (LUMO+1) as well as from lower excitations. Comparison of the convoluted spectra with experimental data^[8, 10] confirms, that excitation energies for transitions with higher charge transfer character (λ_3 and λ_4 in monomers, λ_H in dimer) are underestimated by 0.15-0.2 eV with B3LYP method. Transitions with mainly pi character show good agreement with the experimental peak maxima.

4.2.2 *N,N*-Dimethyl-*p*-phenylenediamine radical cation in EtOH/Et₂O (vol 2:1)

Chloride counter-ion has been used for the calculation of the energetics of *N,N*-dimethyl-PPD and 2,3,5,6-tetramethyl-PPD radical cations dimerization to represent the data of temperature-dependent EPR experiment which was using perchlorate (ClO₄⁻) salt^[7]. For UV spectral characterization, bromide counter-ion has been used. There is no big difference in the geometries, except the counter-ion to *N,N*-DMPPD^{•+} distance. Substitution of two methyl groups changes the charge distribution in *N,N*-DMPPD^{•+} relative to the PPD^{•+}Cl⁻ monomer: the negative charge in the ring near NH₂ moves to the nitrogen atom on which the methyl groups are connected. The counter-ion is located near one amino hydrogen atom as in the unsubstituted PPD^{•+}. **Fig. 4.22** depicts the dimer structures of [N,N-DMPPD]₂²⁺.

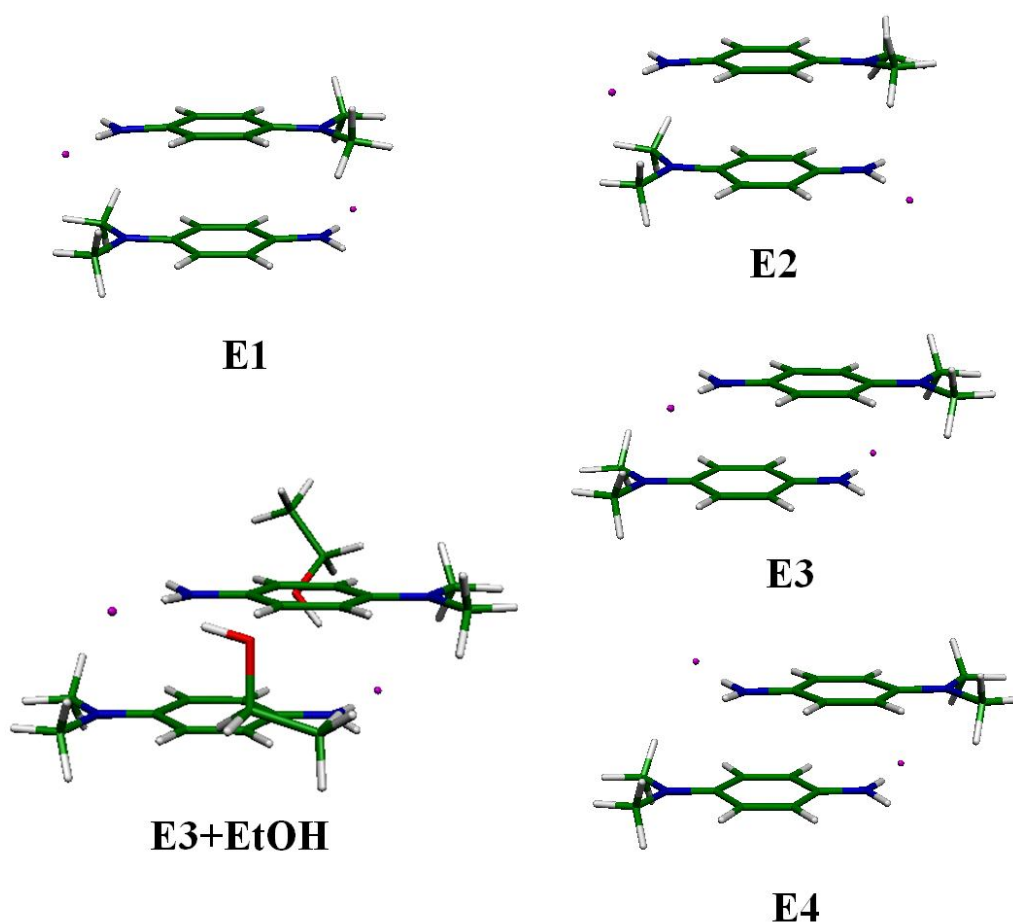


Figure 4.22: The most stable B3LYP-D dimers of [N,N-DMPPD]₂²⁺ with Cl⁻ counter-ions and with Br⁻ counter-ions and two explicit ethanol solvent molecules (bottom).

Four stable conformers of $[N,N\text{-DMPPD}]_2^{2+}2\text{Cl}^-$ dimer have been found after optimization. Like in $[\text{PPD}]_2^{2+}$ the two fragments arrange themselves in eclipsed and stacked positions with chloride counter-ions in cis and trans position. Boltzmann distribution yields 99.82 % for conformer **E3** that is the most stable dimer. The position of the π -stacked two fragments is shifted along the long fragment axis, with chloride counter-ion located in trans position of the dimer and a distance to the nearest amino hydrogen of 2.08 Å (see **Fig.4.22**). The intradimer distance between the two planes of monomer is 2.90 Å which is slightly larger than in π -stacking $[\text{PPD}]_2^{2+}$ dimer resulting from the lower electrostatic attraction. In contrast to $[\text{PPD}]_2^{2+}$, charge distribution in dimer **E3** shows that there is not much electrostatic attraction occurring but dispersion interaction plays an important role to stabilize this dimer to be the most stable conformer. The CASSCF(2,2) HOMO orbital of the $[N,N\text{-DMPPD}]_2^{2+}$ dimer **E3** (**Fig. 4.23**) has the same type of interacting electron distribution than in PPD conformer **D1**, but with shifted long axis it is exhibiting a multicenter $2e^-/14c$ interaction with the inclusion of one amino group. This is different from $[\text{PPD}]_2^{2+}$ insofar that two more atoms are involved in the multicenter long π -bond. DFT shows again additional electron distribution on chloride counter-ions, but in contrast to $[\text{PPD}]_2^{2+}$ it is orientated in p_z direction at the chlorine atoms participating in the π -interaction.

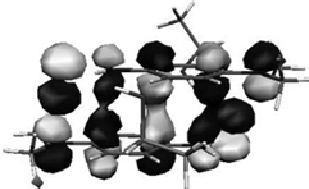
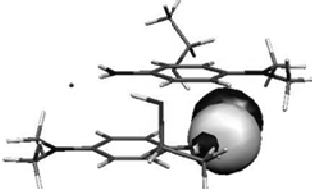
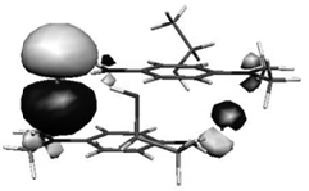
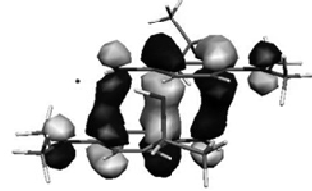
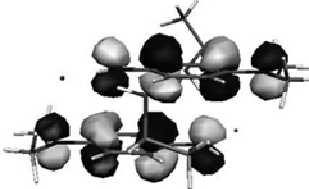
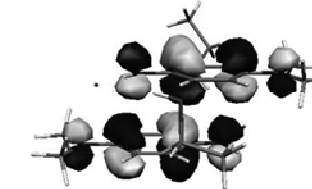
| N,N-DMPPD | DFT | CASSCF |
|---------------|---|--|
| HOMO-6 |  |  |
| HOMO |  |  |
| LUMO |  |  |

Figure 4.23: The molecular orbitals computed by B3LYP-D and CASSCF methods for $[N,N\text{-DMPPD}]_2^{2+} 2Br^-$ dimer with two explicit molecules of solvent ethanol.

The dimerization energies of $N,N\text{-DMPPD}^{\bullet+}$ are collected in **Table 4.11**. BSSE correction at B2PLYP-D/cc-pVTZ level of theory yields a dimerization energy of -36.15 kJ/mol which is in good agreement with the experimental dimerization enthalpy (-44.20 kJ/mol)^[7] from $N,N\text{-DMPPD}^{\bullet+}$ prepared with ClO_4^- counter-ions. Energy calculation with multireference methods as described for PPD radical cation dimerization, again confirms a stable dimer **E3**. CASSCF method results in a dimerization energy of -44.87 kJ/mol, corresponding also well with experiment. Second order perturbation based on this result again overstabilize the energetics (-220.68 kJ/mol with MRMP2).

Table 4.11: The intradimer distances, relative energies, Boltzmann distribution and dimerization energies of the most stable conformers of $[N,N\text{-DMPPD}]_2^{2+}2\text{Cl}^-$ dimer.

| N,N-DMPPD | dimer geometry | | B2PLYP-D cc-pVTZ | | E _{dim} [kJ/mol] | | ΔH _{dim} [kJ/mol] | |
|-----------|---------------------|--------------------------------|---------------------|---------------------------------|------------------------------|----------------------|----------------------------------|--------|
| | ring geometry | chlorine geometry ^a | E _{rel} | N _i / N ₀ | UB3LYP-D | BSSE | CASSCF ^b | exp. |
| | r (pi-pi) | r(Cl..N) r(Cl..H(N)) | [kJ/mol] | % | cc-pVDZ | UB2PLYP-D cc-pVTZ | (MRMP2 ^c) cc-pVTZ | [2] |
| E1 | eclipsed 3.24 Å | trans 3.12 Å 2.08 Å | 42.52 | 0.00 | -63.20 | 0.45 | | |
| E2 | eclipsed 3.23 Å | cis 3.11 Å 2.07 Å | 52.71 | 0.00 | -61.73 | 11.36 | | |
| E3 | staggered 2.90 Å | trans 3.12 Å 2.08 Å | 0.00 | 99.82 | -76.31 | -36.15 | -44.87 (-220.68) | -44.20 |
| E4 | staggered 2.90 Å | cis 3.11 Å 2.07 Å | 15.65 | 0.18 | -73.39 | -20.73 | | |

^a distances are given to the closest nitrogen atom.

^b CASSCF(3,3)/CASSC(2,2) data are given.

^c MRMP2 calculation base on CASSCF(3,3)/CASSC(2,2) reference, value in brackets.

UV/Vis calculations:

Chloride counter-ions were replaced by bromide counter-ions for monomer and dimer **E3** when adding explicit ethanol solvent to be in the same environment as in the UV-experiment^[8] and the geometries have been reoptimized. The optimized geometry of monomer shows that ethanol is located on top of bromide counter-ion lying in the plane of *N,N*-DMPPD radical cation. In monomer, the Br..H(-O) and Br..H(-N) distances are nearly the same as in the PPD^{•+} monomer, 2.36 Å and 2.37 Å, respectively. Optimization of dimer brings the two ethanol molecules aside the dimer and results in similar geometries as for [PPD]₂²⁺ (see **Fig. 4.22**). The intradimer distance between the two monomeric fragments is 2.91 Å which is longer by 0.01 Å than the dimer without ethanol using chloride counter-ions.

Kimura *et. al.* published the electronic absorption for [N,N-DMPPD]₂²⁺ dimers at 670 nm (1.85 eV) and for N,N-DMPPD^{•+} monomer at 570, 523, 380 and 324 nm (2.18, 2.37, 3.26 and 3.83 eV)^[8]. Both spectra are shifted bathochromically relative to the unsubstituted PPD, the monomer by approx. 0.3 eV for the first two peaks and the dimer by 0.2 eV for λ_L and 0.1 eV for λ_H . Substitution with two methyl groups at the amino group in [N,N-DMPPD]₂²⁺ does not only change the global minimum in the potential energy curve from eclipsed to stacked geometries, the UV spectrum also alters because of changed electron distribution. The interacting orbital shows no longer overlap of two monomer amino groups in CASSCF calculations. Moreover, in DFT the z-oriented bromine counter-ion now participates in the interaction of the two monomeric units. This is reflected in the computed transitions and shifts λ_L and λ_H to lower energies by 0.2 eV also in the calculations.

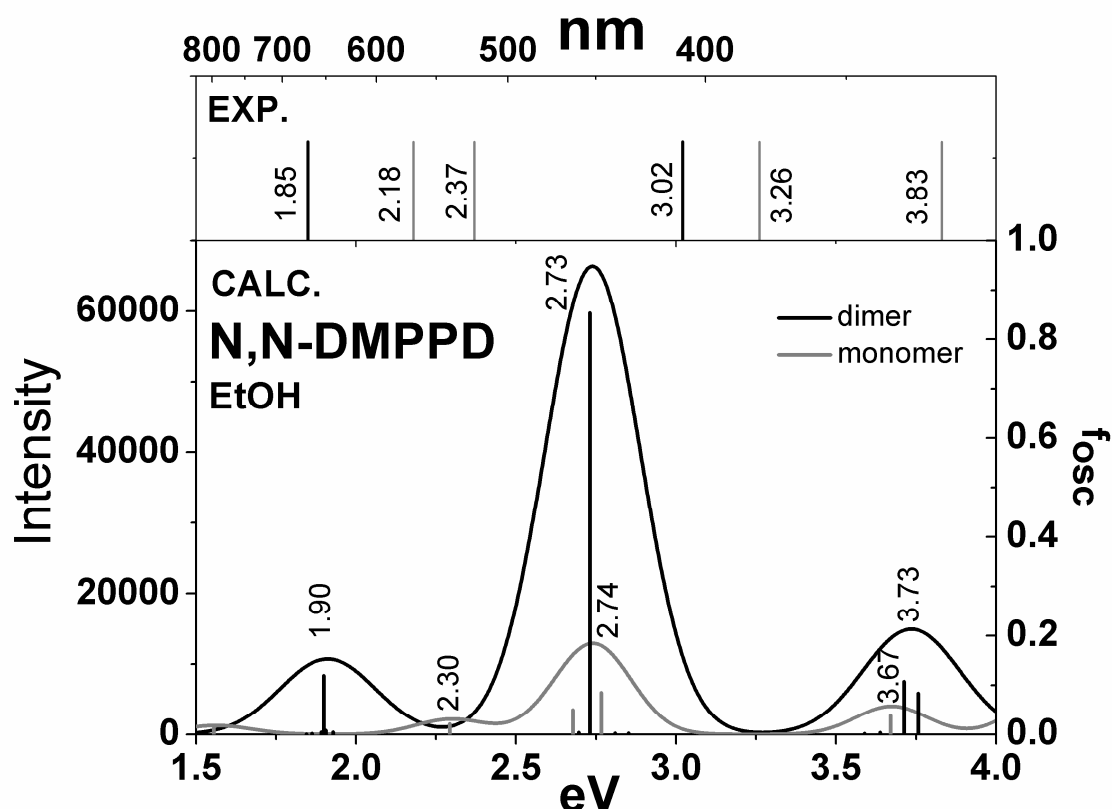


Figure 4.24: The TDA-B3LYP calculated vertical excitations (bottom, lines are shown with oscillator strengths) and convoluted UV/Vis spectrum (bottom) of the $[N,N\text{-DMPPD}]_2^{2+} 2\text{Br}^-$ dimer (black) and $N,N\text{-DMPPD}^{\bullet+} \text{Br}^-$ monomer (grey) with explicit solvent ethanol. The energies of experimental peak maxima [12] are shown as vertical lines (top).

TDA-DFT computes the dimer transitions at 652.8 nm (1.899 eV) for λ_L and at 454.1 nm (2.730 eV) for λ_H , respectively for $[N,N\text{-DMPPD}]_2^{2+}$ (see **Fig. 4.24**). λ_L has its main contribution from z-oriented bromine orbital (HOMO) into the antibonding π^* orbital (LUMO), but there are also transitions from the bonding orbital (HOMO-6) with small oscillator strength (665 nm, $f=0.0019$) hidden. The convoluted λ_L peak energy corresponds well with experiment. The second band λ_H is again a bromine to π^* excitation with larger CT character, therefore underestimating the experimental transition energy. The monomer transitions are calculated at 540.7, 463.0, 448.3 and 337.8 nm (2.293, 2.678, 2.766 and 3.670 eV). For the monomer we find the same characteristics as for $\text{PPD}^{\bullet+}$: λ_1 is also the ethanol C-O bond orbital exciting into the HOMO orbital. λ_2 and λ_3 are linear combinations of π orbitals to HOMO excitations, therefore shifted relative to $\text{PPD}^{\bullet+}$, but also lying under λ_H as in the experiment. The fourth peak for $N,N\text{-DMPPD}^{\bullet+}$ monomer is the same as in $\text{PPD}^{\bullet+}$.

4.2.3 2,3,5,6-Tetramethyl-p-phenylenediamine radical cation in EtOH/Et₂O (vol 2:1)

Substitution of PPD^{•+} with four methyl groups in the benzene ring does not change much compared to PPD^{•+}. The only difference to PPD^{•+} is, that in monomer 2,3,5,6-TMPPD^{•+}Cl⁻ negative charge is located on all six carbon atoms in the ring.

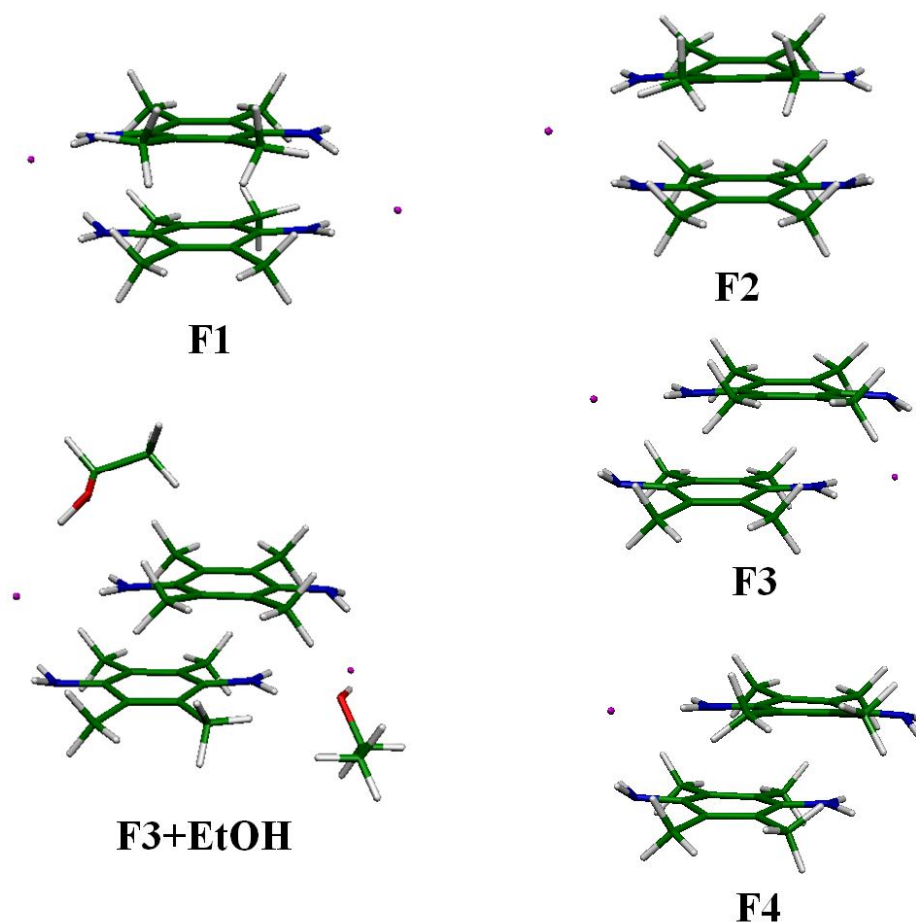


Figure 4.25: The most stable B3LYP-D dimers of $[2,3,5,6\text{-TMPPD}]_2^{2+}$ with 2Cl^- counterions and with Br^- counterions and two explicit ethanol solvent molecules (bottom).

Again four stable optimized geometries of $[2,3,5,6\text{-TMPPD}]_2^{2+}2\text{Cl}^-$ dimers have been found with the same arrangement of the two fragments as in $[\text{N,N-DMPPD}]_2^{2+}$. Conformer **F3**, shown in **Fig.4.25**, is the most stable conformer with 96.47 % Boltzmann distribution. As a result of methyl substitution and geometrical shifting of monomer fragments, the intradimer separation is 2.79 Å. This is shorter than in $[\text{PPD}]_2^{2+}$ and $[\text{N,N-DMPPD}]_2^{2+}$. **Fig. 4.26** depicts the HOMO orbital from CASSCF(2,2) calculations of $[2,3,5,6\text{-TMPPD}]_2^{2+}$. It shows the same strong interaction as in $[\text{N,N-DMPPD}]_2^{2+}$ with a multicenter long $2e^-/14c$ π -bond. DFT

HOMO orbital shows electron distribution on chlorine counter-ion pointing in xy direction.

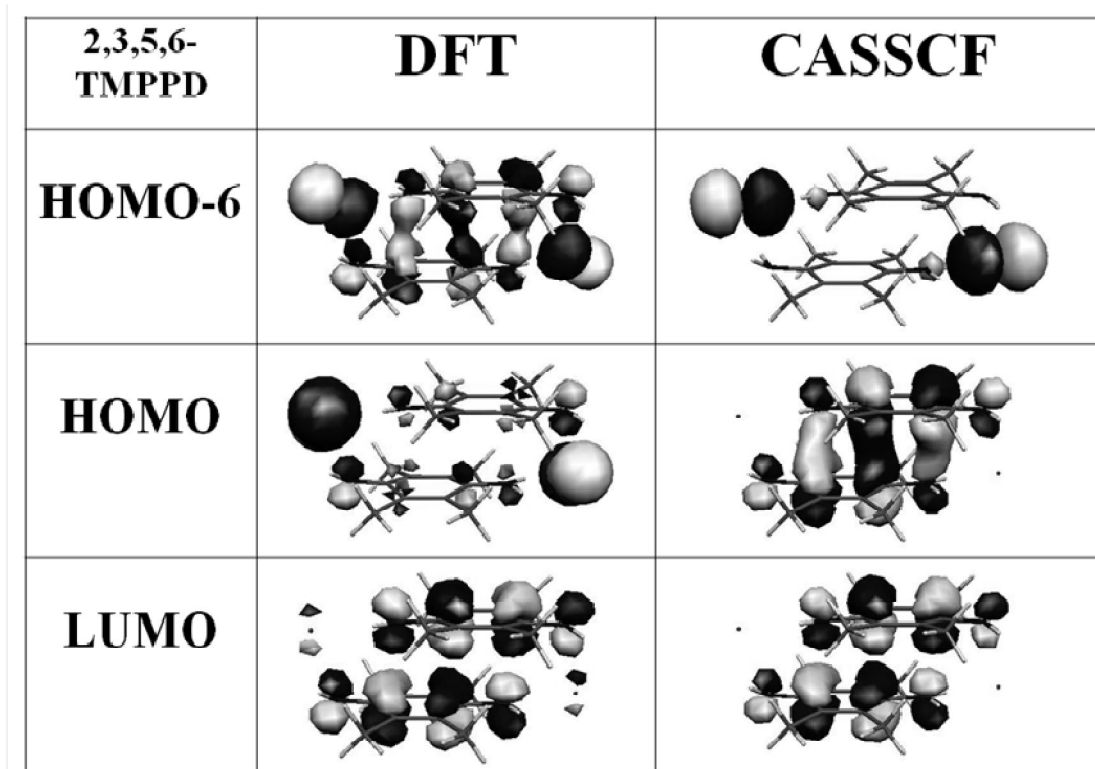


Figure 4.26: The molecular orbitals computed by B3LYP-D and CASSCF methods for the most stable conformer of $[2,3,5,6\text{-TMPPD}]_2^{2+} 2\text{Br}^-$ dimer by DFT and CASSCF methods.

The dimerization energies of $2,3,5,6\text{-TMPPD}^{\bullet+}$ are printed in **Table 4.12**. BSSE correction at B2PLYP-D/cc-pVTZ level of theory gives a dimerization energy of -14.33 kJ/mol, which underestimates the binding relative to the dimerization enthalpy earned from temperature-dependent EPR experiment (-58.20 kJ/mol)^[7] done with perchlorate counter-ion, but still reproduces the dimerization in this system. The energy difference may come from the strong electrostatic repulsion between the negative charges on carbon atoms in the benzene rings of the dimers. CASSCF calculation reproduces the dimerization energy (-57.42 kJ/mol) in good agreement with the experimental data.

Table 4.12: The intradimer distances, relative energies, Boltzmann distribution and dimerization energies of the most stable conformers of $[2,3,5,6\text{-TMPPD}]_2^{2+}2\text{Cl}^-$ dimers.

| 2,3,5,6-TMPPD | dimer geometry | | B2PLYP-D cc-pVTZ | | UB3LYP-D cc-pVDZ | E _{dim} [kJ/mol] | | ΔH _{dim} [kJ/mol] | |
|---------------|-------------------------------|---|------------------------------|--------------------------------------|---------------------|------------------------------|--------------------------------|-------------------------------|--|
| | ring geometry r (pi-pi) | chlorine geometry ^a r(Cl..N) r(Cl..H(N)) | E _{rel} [kJ/mol] | N _i / N ₀ % | | BSSE UB2PLYP-D cc-pVTZ | CASSCF ^b cc-pVTZ | exp. [2] | |
| F1 | eclipsed 3.09 Å | cis 3.27 Å 2.26 Å | 23.79 | 0.01 | -120.78 | 5.30 | | | |
| F2 | eclipsed 3.04 Å | trans 3.11 Å 2.18 Å | 28.39 | 0.00 | -116.09 | 14.26 | | | |
| F3 | staggered 2.79 Å | trans 3.12 Å 2.15 Å | 0.00 | 96.47 | -125.78 | -14.33 | -57.42 | -58.20 | |
| F4 | staggered 2.79 Å | cis 3.14 Å 2.15 Å | 8.20 | 3.52 | -126.50 | -7.56 | | | |

^a distances are given to the closest nitrogen atom.

^b CASSCF(3,3)/CASSCF(2,2) data are given.

For UV/Vis calculation chloride counter-ions were replaced by bromide counter-ions in monomer and dimer **F3** to model the same environment as in the UV/Vis experiment^[9]. In the monomer, ethanol sits atop amino group with a O-H..N distance of 2.09 Å. The bromide counter-ion moves out from the benzene plane with a resulting out-of-plane angle of 27.69°. Optimization of dimer can lead to an unsymmetrical geometry for the position of ethanol molecules: one is located atop bromide counter-ion, the other one is located in the plane of bromide counter-ion and the fragment, both showing strong interaction of ethanol with bromide counter-ion (O-H..Br). But the latter ethanol has an additional hydrogen bond to the amino group as shown in **Fig. 4.25**. The intradimer distance between the two monomeric fragments is 2.87 Å.

Addition of explicit ethanol molecules to the dimer can produce different geometries with different types of hydrogen-bond like interaction to bromine counter-ion or the amino group. These different dimer geometries show the peaks λ_L and λ_H with general agreement to experiment, but at slightly shifted positions responding to the different bonding situation in the solvent. Especially the transitions above 2.5 eV show a large response on different hydrogen bond patterns. The geometry in **Fig. 4.25** results in some splitting of the higher energy band λ_H at 443.7 nm (2.794 eV) and 430.1 nm (2.882 eV) representing excitations from the interacting orbital and from Br_{xy} orbitals into the LUMO orbital. While another geometry with symmetric orientation of ethanol would result in only one transition from Br_{xy} orbital into the LUMO orbital at 448.1 nm (2.767 eV). Interpretation would be rather cluttered when including all possible hydrogen bond patterns. For this reason we show in **Fig. 4.27** the convoluted UV spectrum of 2,3,5,6-TMPPD^{•+} monomer and [2,3,5,6-TMPPD]₂²⁺ dimer without explicit solvent and **Fig. 4.28** for 2,3,5,6-TMPPD^{•+} monomer and [2,3,5,6-TMPPD]₂²⁺ dimer with explicit solvent, are shown although the data including ethanol can be found in **Table 4.10** for geometry in **Fig. 4.25**. Keeping in mind that the energies show some systematic shift relative to experiment as already described in PPD radical cation dimerization, there is a general agreement of calculated and experimental spectrum.

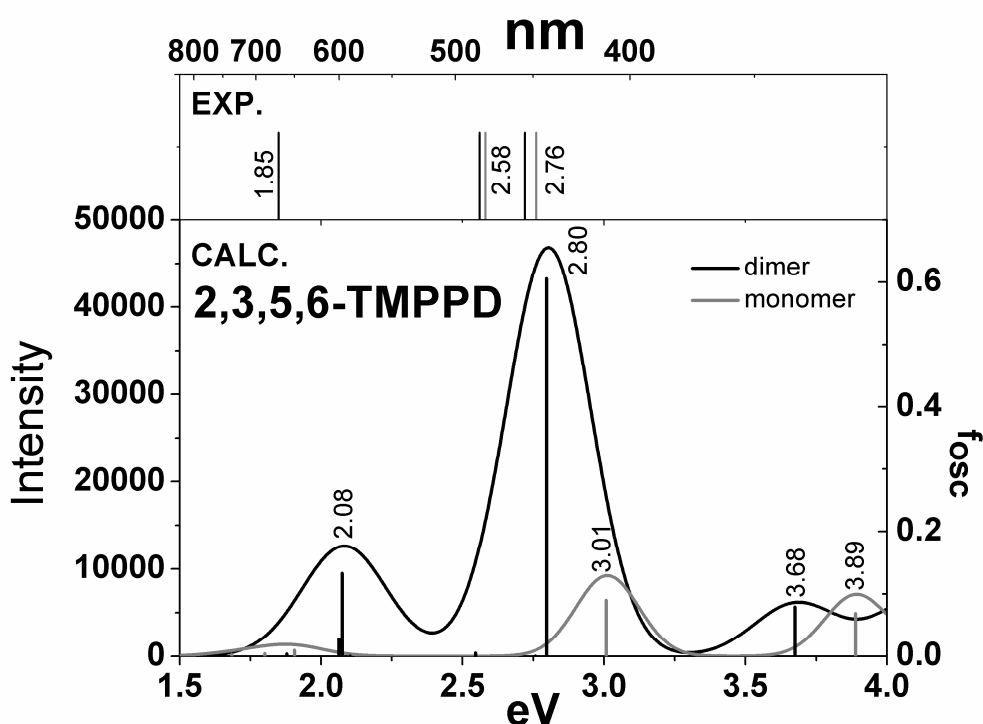


Figure 4.27: The TDA-B3LYP calculated vertical excitations (bottom, lines are shown with oscillator strengths) and convoluted UV/Vis spectrum (bottom) of the [2,3,5,6-TMPPD]₂²⁺ 2Br⁻ dimer (black) and 2,3,5,6-TMPPD^{•+} Br⁻ monomer (grey). The energies of experimental peak maxima^[9] are shown as vertical lines (top).

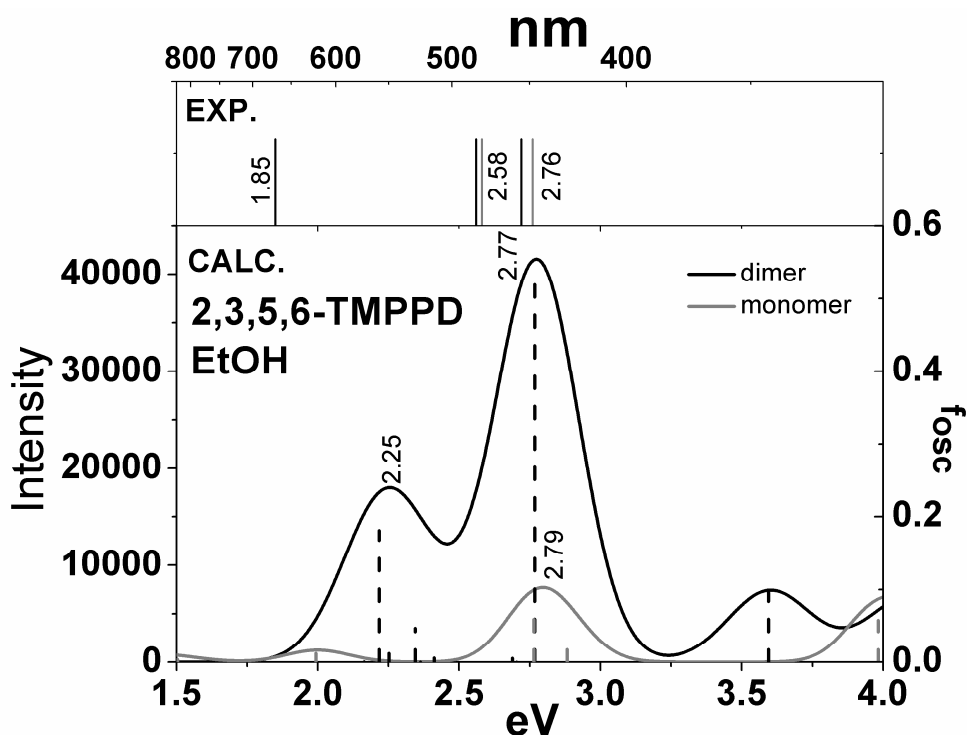


Figure 4.28: The TDA-B3LYP calculated vertical excitations (bottom, lines are shown with oscillator strengths) and convoluted UV/Vis spectrum (bottom) of the [2,3,5,6-TMPPD]₂²⁺ 2Br⁻ dimer (black) and 2,3,5,6-TMPPD^{•+} Br⁻ monomer (grey) with explicit solvent ethanol. The energies of experimental peak maxima^[9] are shown as vertical lines (top).

4.2.4 *N,N,N,N*-Tetramethyl-*p*-phenylenediamine radical cation in EtOH/Et₂O

(vol 2:1)

Four methyl groups were added to the amino groups in PPD^{•+}. This is changing the charge distribution in the radical monomer compared to PPD^{•+}. In monomer *N,N,N',N'*-TMPPD^{•+}Cl⁻, the positive charge is located on the two benzene carbon atoms near the amino nitrogen atoms. The optimized geometry of *N,N,N',N'*-TMPPD^{•+}Cl⁻ is shown in Fig. 4.29.

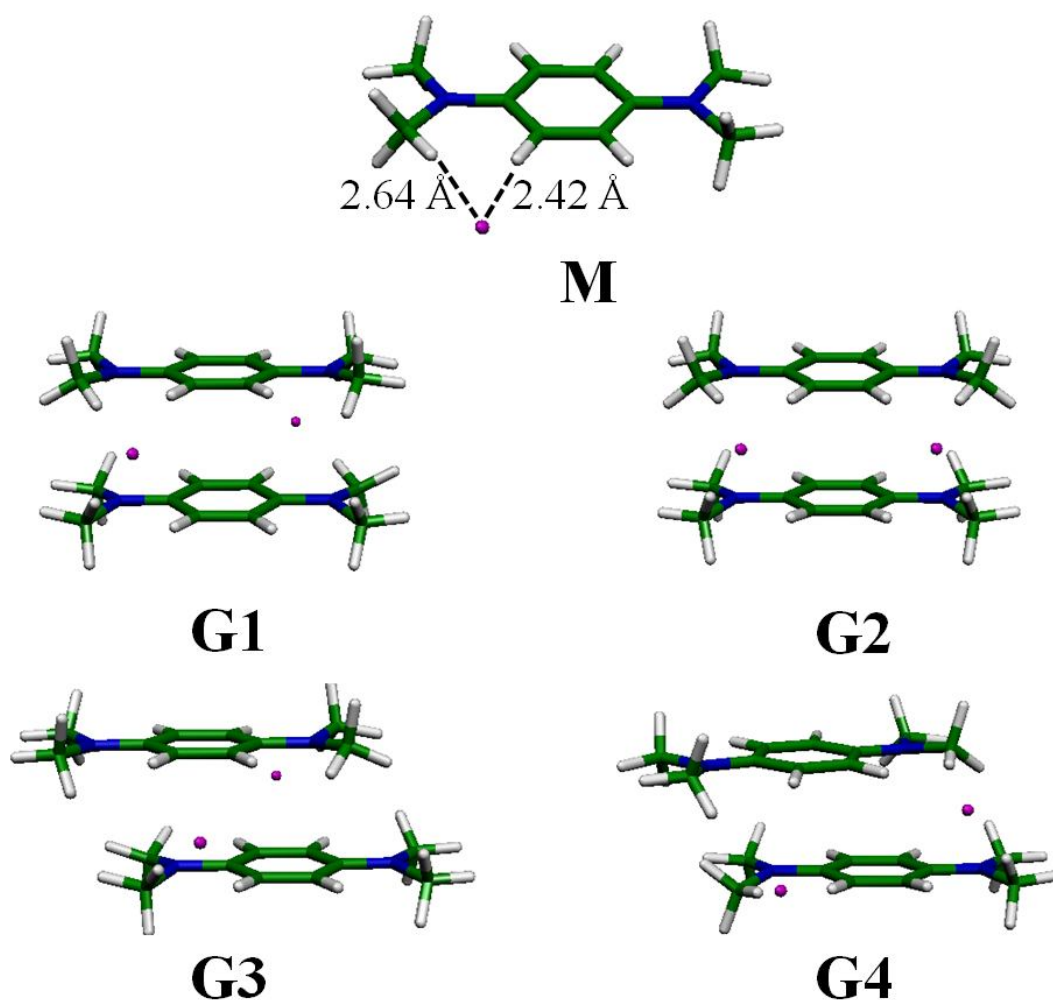


Figure 4.29: B3LYP-D optimized geometries of *N,N,N',N'*-TMPPD^{•+}Cl⁻ monomer and [*N,N,N',N'*-TMPPD]₂²⁺•2Cl⁻ dimers **G1** - **G4**.

Four stable optimized geometries (**G1-G4**) of $[N,N,N',N'\text{-TMPPD}]_2^{2+}2\text{Cl}^-$ dimers have been found with the same arrangement of the two fragments as in $[\text{PPD}]_2^{2+}2\text{Br}^-$. The most stable conformer is conformer **G1**, shown in **Fig. 4.29**, with 95.25 % in the Boltzmann distribution. Two monomer fragments are shifted along the short axis by 0.96 Å, similar to the most stable $[\text{PPD}]_2^{2+}2\text{Br}^-$ dimer and avoiding Coulombic repulsion between the same atomic charges on the two monomers in dimer. The intradimer separation of **G1** conformer is 3.22 Å which is longer than in $[\text{PPD}]_2^{2+}$, $[\text{N,N-DMPPD}]_2^{2+}$ and $[2,3,5,6\text{-TMPPD}]_2^{2+}$. The HOMO orbital from CASSCF(2,2) shows a strong interaction with $2e^-/12c$ multicenter long π -bond (shown in **Fig. 4.30**) while in contrast the HOMO orbital from DFT calculations shows that electron distribution is located on chlorine counter-ions in the xy direction, as already shown for $[2,3,5,6\text{-TMPPD}]_2^{2+}$.

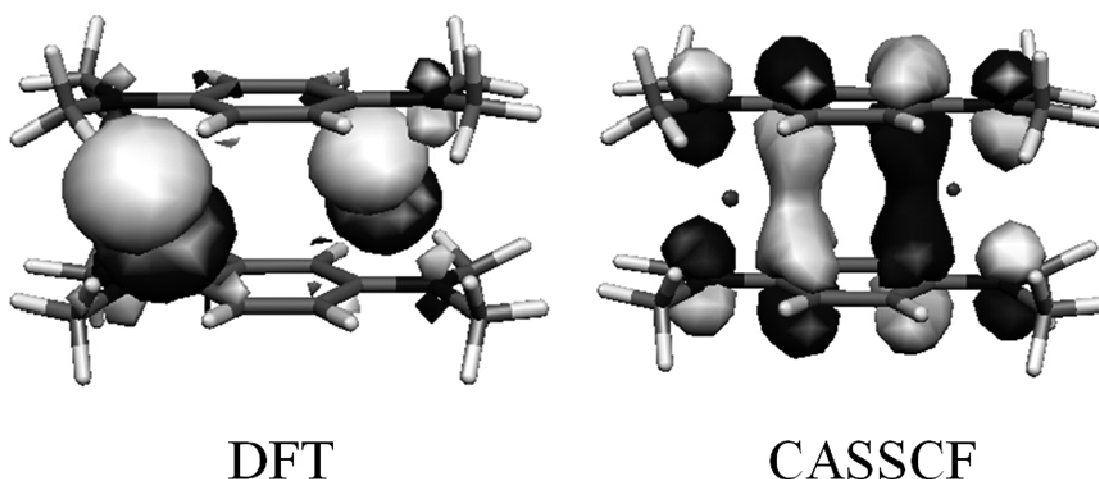


Figure 4.30: The HOMO orbitals computed by DFT and CASSCF methods of the most stable conformer $[N,N,N',N'\text{-TMPPD}]_2^{2+}2\text{Cl}^-$ dimer (**G1**).

BSSE correction at B2PLYP-D/cc-pVTZ level of theory yields a dimerization energy of -5.56 kJ/mol for conformer **G1**, which underestimates the experimental dimerization enthalpy (-29.6 kJ/mol)^[7] from $N,N,N',N'\text{-TMPPD}^{\bullet+}$ prepared with ClO_4^- counter-ions. Energy calculation with multireference methods confirms a stable dimer **G1** with CASSCF method yielding a dimerization energy of -93.22 kJ/mol. This is a larger overestimating over the EPR experimental detected heat of dimerization by around 60 kJ/mol. The dimerization energies of $[N,N,N',N'\text{-TMPPD}]_2^{2+}$ were shown in **Table 4.13**.

Table 4.13: The intradimer distances, relative energies, Boltzmann distribution and dimerization energies of the most stable conformers of $[N,N,N',N''\text{-TMPPD}]_2^{2+}2Cl^-$ dimers.

| N,N,N',N''- TMPPD | dimer geometry | | B2PLYP-D cc-pVTZ | | UB3LYP-D cc-pVDZ | E _{dim} [kJ/mol] | | ΔH _{dim} [kJ/mol] | |
|----------------------|----------------------------|---|------------------------------|--------------------------------------|---------------------|------------------------------|--------------------------------|-------------------------------|--|
| | ring geometry r (pi-pi) | chlorine geometry ^a r(Cl..H(benzene)) r(Cl..H(CH ₃)) | E _{rel} [kJ/mol] | N _i / N ₀ % | | BSSE UB2PLYP-D cc-pVTZ | CASSCF ^b cc-pVTZ | exp. [2] | |
| | | | | | | | | | |
| G1 | eclipsed 3.23 Å | trans 2.53 Å 2.65 Å | 0.00 | 95.25 | -89.87 | -5.56 | -93.22 | -29.60 | |
| G2 | eclipsed 3.33 Å | cis 2.61 Å 2.53 Å | 63.87 | 0.00 | -74.41 | 57.90 | | | |
| G3 | staggered 3.15 Å | trans 2.65 Å 2.60 Å | 7.43 | 4.75 | -75.46 | 7.70 | | | |
| G4 | staggered 3.20 Å | cis 2.59 Å 2.49 Å | 41.42 | 0.00 | -80.33 | 39.92 | | | |

^a distances are given to the closest nitrogen atom.

^b CASSCF(3,3)/CASSCF(2,2) data are given.

Sakata *et. al.* reported the UV/Vis spectroscopic data of N,N,N',N' -TMPPD $^{2+}$ with ClO_4^- counter-ions in ethanol solution^[13]. At 295 K, there are five absorption peaks at 600, 563, 526, 384 and 327 nm (2.07, 2.20, 2.36, 3.23 and 3.79 eV) which are assigned to the N,N,N',N' -TMPPD $^{2+}$ monomer. At low temperature (110 K), five absorption peaks of dimeric species occurred at 800, 540, 510, 370 and 308 nm (1.55, 2.30, 2.43, 3.35 and 4.03 eV). The calculated UV/Vis spectrum without ethanol explicit solvent of dimer **G1** and of the monomer is presented in **Fig. 4.31**. TDA-DFT show the dimer peaks at λ_L 795.2 nm (1.559 eV) and λ_H 524.8 nm (2.362 eV) which is corresponding well with the temperature-dependent UV/Vis experiment at 800 and 540 nm (1.55 and 2.30 eV), respectively. Both λ_L and λ_H peak have the main contribution from chlorine in xy direction exciting into the antibonding π^* orbital. Calculated monomer peaks correspond only partly with the experimental spectrum. Assuming that, the first two peaks might be attributed to ethanol-monomer interaction in the experiment, the spectrum might explain the missing of those peaks in the COSMO calculated spectrum.

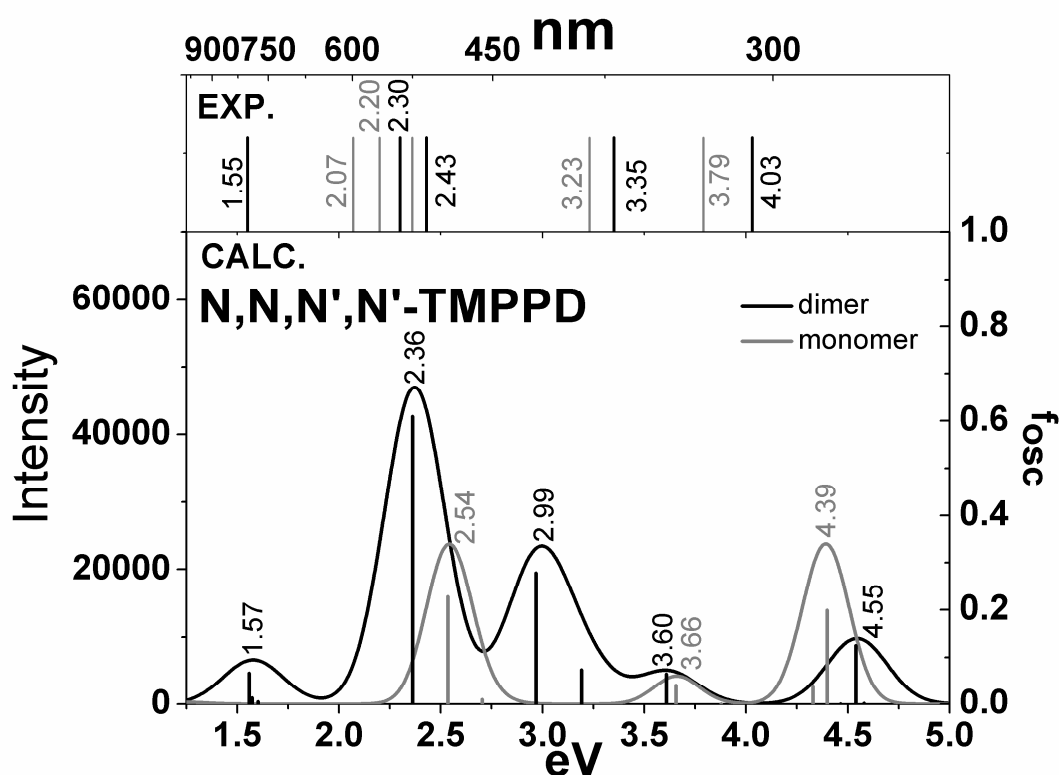


Figure 4.31: The TDA-B3LYP calculated vertical excitations (bottom, lines are shown with oscillator strengths) and convoluted UV/Vis spectrum (bottom) of the $[N,N,N',N'$ -TMPPD] $_2^{2+} 2Cl^-$ dimer (black) and N,N,N',N' -TMPPD $^{2+} Cl^-$ monomer (grey). The energies of experimental peak maxima [13] are shown as vertical lines (top).

4.2.5 Summary on substituted PPD's:

From the energetic calculations of all four molecules (PPD^{•+}, *N,N*-DMPPD^{•+}, 2,3,5,6-TMPPD^{•+} and *N,N,N',N'*-TMPPD^{•+}), it was found that dispersion correction is necessary for geometry optimization to get a stable structure of radical cation dimers. The counter-ions have been included as well as continuum solvation model for the surrounding. All four molecule dimers exhibit stable long multicenter π -bond (2.9±0.3 Å) in our calculations. Methyl substitution changes the geometry between the two monomer fragments from eclipsed [PPD]₂²⁺2Br⁻ to stacking orientation for [N,N-DMPPD]₂²⁺2Cl⁻ and [2,3,5,6-TMPPD]₂²⁺2Cl⁻ dimers. An exception is [N,N,N',N'-TMPPD]₂²⁺2Cl⁻ dimer which has an eclipsed arrangement of the two fragments like the PPD dimer. Substitution of PPD^{•+} with four methyl groups in 2,3,5,6-TMPPD^{•+} at the benzene ring does not alter the global minimum geometry relative to N,N-DMPPD^{•+} much, it shows the same orientation of the benzene rings. The interaction of two electron on twelve centers in [PPD]₂²⁺2Br⁻ and [N,N,N',N'-TMPPD]₂²⁺2Cl⁻ dimer becomes a two electron on fourteen center interaction in [N,N-DMPPD]₂²⁺2Cl⁻ and [2,3,5,6-TMPPD]₂²⁺2Cl⁻ dimers. Energy correction by CASSCF method using CAS(2,2) for dimers and CAS(3,3) for monomers with a triple zeta basis set (cc-pVTZ) can predict the dimerization energy of the radical cations corresponding well with the experimental enthalpy of dimerization^[7], especially for [N,N-DMPPD]₂²⁺2Cl⁻ and [2,3,5,6-TMPPD]₂²⁺2Cl⁻ dimers. For [PPD]₂²⁺2Br⁻ dimers CASSCF overstabilizes the dimer by around 20 kJ/mol. One possible reason is that bromide ion with its large number of electrons influences the energetics, because the dimer [PPD]₂²⁺2Cl⁻ shows better agreement with experiment for CASSCF and for B2PLYP-D energetics. In CASSCF method, selecting the proper active electrons and active orbitals in dimers and monomers is very important to reproduce dimerization energies to be in the same order of magnitude and well corresponding to the experimental dimerization enthalpies. MRMP2 calculation of dimerization energies on CASSCF reference of all four molecules shows that the calculated dimer of [N,N-DMPPD]₂²⁺ is less stable than [PPD]₂²⁺ and [2,3,5,6-TMPPD]₂²⁺ dimers which correlates well to the experimental fact that the dimerization enthalpy of [N,N-DMPPD]₂²⁺ is smaller than for the other two dimers^[7].

BSSE corrected dimerization energies with B2PLYP-D/cc-pVTZ can reproduce the experimental dimerization energies well for $[\text{N,N-DMPPD}]_2^{2+}$.

The calculated UV/Vis spectra of radical cation monomers and dication dimers of all four compounds (PPD, N,N-DMPPD, 2,3,5,6-TMPPD and N,N,N',N'-TMPPD) are corresponding well with the experimental data when including explicit solvent molecules ethanol or water showing that B3LYP/cc-pVTZ level with COSMO model is appropriate for the calculation of vertical excitation of PPD and substituted-PPD radical cation monomers and dication dimers. (The substituted methyl groups play an important role to the indicated dimer peaks in the range 600 -800 nm.) The monomer and dimer peaks of substituted-PPD radical cations are shift to the low energy (bathochromic shift) when compared to the monomer and dimer peak of unsubstituted-PPD radical cation which occurred around 600 nm. The second dimer peaks of all four dimers ($[\text{PPD}]_2^{2+}$, $[\text{N,N-DMPPD}]_2^{2+}$, $[\text{2,3,5,6-TMPPD}]_2^{2+}$, $[\text{N,N,N',N'-TMPPD}]_2^{2+}$) at higher energy have the highest oscillator strength. The first two monomer peaks of unsubstituted and substituted-PPD radical cations are coming from the interaction of monomers with the explicit solvents. This two peaks do not appear when computing monomer spectrum without explicit solvents. Therefore, especially for the description of the monomeric spectrum, but also for the appropriate description of dimers, inclusion of explicit solvent is necessary.

4.2.6 3,3',5,5'-Tetramethylbenzidine in acetonitrile

In 1990, H. Awano and H. Ohigashi have been reporting the spectrum of 3,3',5,5'-Tetramethylbenzidine radical cation perchlorate salt ($\text{TMB}^{\bullet+}(\text{ClO}_4)^-$) in acetonitrile by temperature dependent UV/Vis spectroscopy^[11]. They found that the intensity of the absorption bands around 370 and 660 nm (3.35 and 1.88 eV) were decreased while the absorption bands at approximately 450 and 800 nm (2.76 and 1.55 eV) were increased when rising temperature from 15°C to 60°C. They suggested that the absorption bands around 370 and 660 nm are the absorption bands of charge-transfer complex of $[\text{TMB}^{2+}\cdot\text{TMB}]$ while the absorption bands around 450 and 800 nm belong to TMB^{2+} (as in equation (4.1)). The estimated enthalpy change of complex formation is -66.2 kJ/mol.



In 1996, H. Awano and coworker published the experimental data of $\text{TMB}(\text{ClO})_4$ salt dimerization in acetonitrile using temperature-dependent EPR spectroscopy technique and compared the results with the earlier UV/Vis absorption spectra^[12]. They found that the previous work^[11] which suggested the charge-transfer complex of TMB^{2+} and TMB is partially corrected because EPR intensity is increasing when temperature is raised. The complex dissociated and the 3,3',5,5'-Tetramethylbenzidine radical cation occurred. So they supposed that the complex is a charge-transfer complex of $\text{TMB}^{\bullet+}$ radical cations according to equation (4.2).



The dimerization enthalpy obtained from EPR measurement is equal to -60 kJ/mol, well corresponding with the data from UV/Vis method.

Optimized geometry of $\text{TMB}^{\bullet+}\text{Cl}^-$ radical cation with chloride counter-ion is shown in **Fig. 4.32**. In $\text{TMB}^{\bullet+}\text{Cl}^-$ radical monomer, the two benzene rings are bending from the plane by around 11° . Chloride counter-ion is located in the plane of benzene ring near one amino hydrogen atom with a distance of 2.12 \AA .

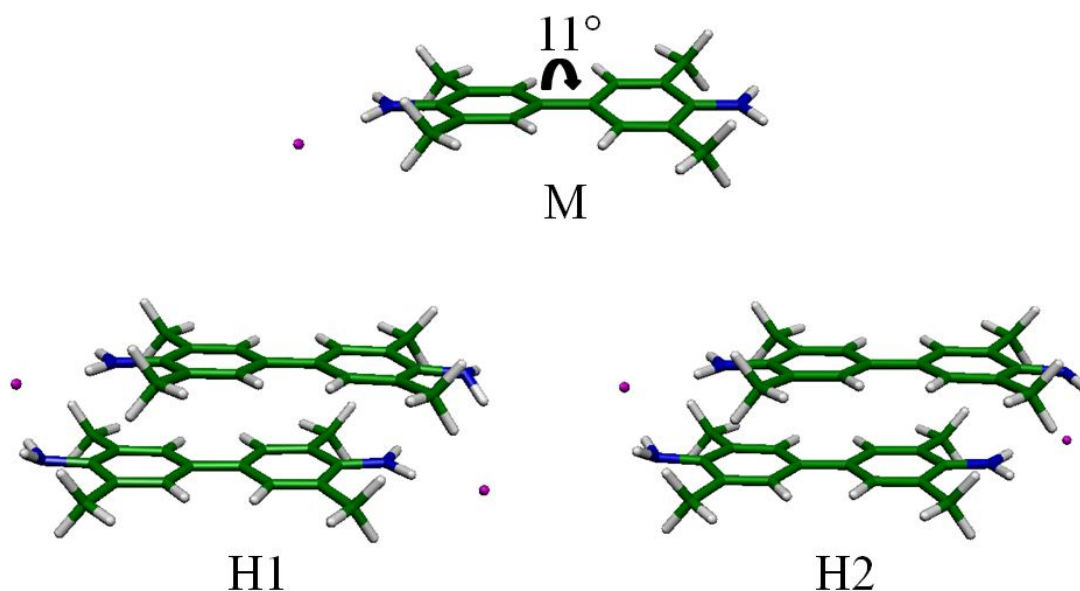


Figure 4.32: *B3LYP-D optimized structural parameters of $\text{TMB}^{\bullet+}\text{Cl}^-$ radical cation monomer and of $[\text{TMB}]_2^{2+}2\text{Cl}^-$ dimers.*

Two optimized geometries of $[\text{TMB}]_2^{2+}2\text{Cl}^-$ dimers are presented in **Fig. 4.32**. Only π -stacking geometries shifted along the long axis of two monomer fragments were found. The chloride counter-ions are located in cis- and trans positions of dimers (**H1** and **H2**, respectively). The intradimer separations between the two monomer fragments of these two dimers are 3.07 \AA and 3.06 \AA for **H1** and **H2**, respectively. Monomer fragments in these two dimers show that the two benzene rings are in plane with each other because of the strong interaction between two SOMO orbitals creating new multicenter long π -bond dimers. This is different from the $\text{TMB}^{\bullet+}\text{Cl}^-$ radical monomer.

Boltzmann distribution shows that conformer **H2** is the most stable conformer with 88.64 %. The HOMO orbital from CASSCF(2,2) show strong interaction with $2e^-/6c$ multicenter long π -bond (shown in **Fig. 4.33**).

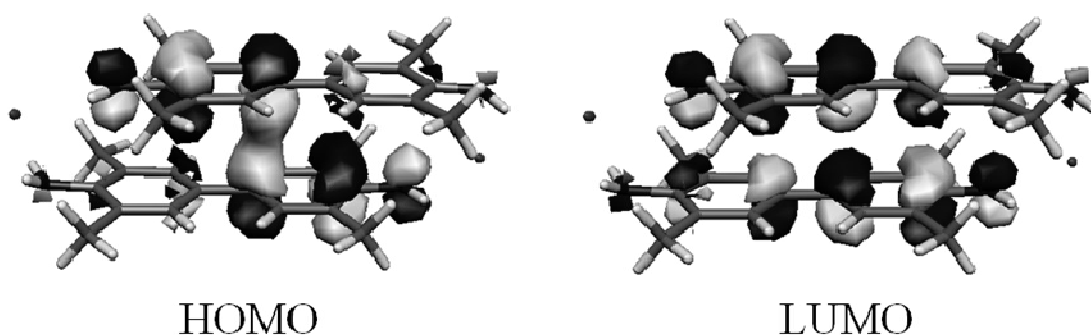


Figure 4.33: The HOMO and LUMO orbital computed by CASSCF methods of the most stable conformer $[TMB]_2^{2+} 2Cl^-$ dimer (H2).

Table 4.14 shows the dimerization energies of 3,3',5,5'-Tetramethylbenzidine compared to the enthalpy of dimerization from the experimental data. CASSCF calculation reproduced the dimerization energy for the most stable conformer (-48.38 kJ/mol) in the same magnitude of the UV/Vis and EPR experiments (-66.2 and -60.0 kJ/mol)^[11, 12]. BSSE correction at B2PLYP-D/cc-pVTZ level of theory fails to reproduce dimerization for this molecule. Stabilization of the structures including interaction of the solvent might be the reason for that energies. But UV/Vis data in the next paragraph confirm that the found geometries exist in acetonitrile.

Table 4.14: The intradimer distances, relative energies, Boltzmann distribution and dimerization energies of the most stable conformers of $[\text{TMB}]_2^{2+}2\text{Cl}^-$ dimers.

| TMB | dimer geometry | | B2PLYP-D cc-pVTZ | | UB3LYP-D cc-pVDZ | E_{dim} [kJ/mol] | | CASSCF ^b cc-pVTZ | ΔH_{dim} [kJ/mol] exp. |
|-----------|----------------------------|---|------------------------------|------------------|---------------------|------------------------------|---------|-----------------------------------|---|
| | ring geometry r (pi-pi) | chlorine geometry ^a r(Cl..N) r(Cl..H(N)) | E_{rel} [kJ/mol] | N_i / N_0 % | | BSSE UB2PLYP-D cc-pVTZ | | | |
| | H1 | staggered 3.07 Å | cis 3.17 Å 2.18 Å | 5.09 | | 11.36 | -134.20 | | |
| H2 | staggered 3.06 Å | tran 3.16 Å 2.18 Å | 0.00 | 88.64 | -135.56 | 1.71 | -48.38 | -66.2 (UV/Vis) ^[11] | |

^a distances are given to the closest nitrogen atom.

^b CASSCF(3,3)/CASSC(2,2) data are given.

UV/Vis spectrum of the most stable $\text{TMB}_2^{2+}2\text{Cl}^-$ dimer and TMB^+Cl^- monomer was computed by TDA-DFT method at B3LYP/cc-pVTZ level of theory in acetonitrile. The computed UV/Vis spectrum shows that there are two peaks of dimer and two peaks of monomer which have the same trend as in the experimental UV/Vis measurement^[11] (shown in Fig. 4.34).

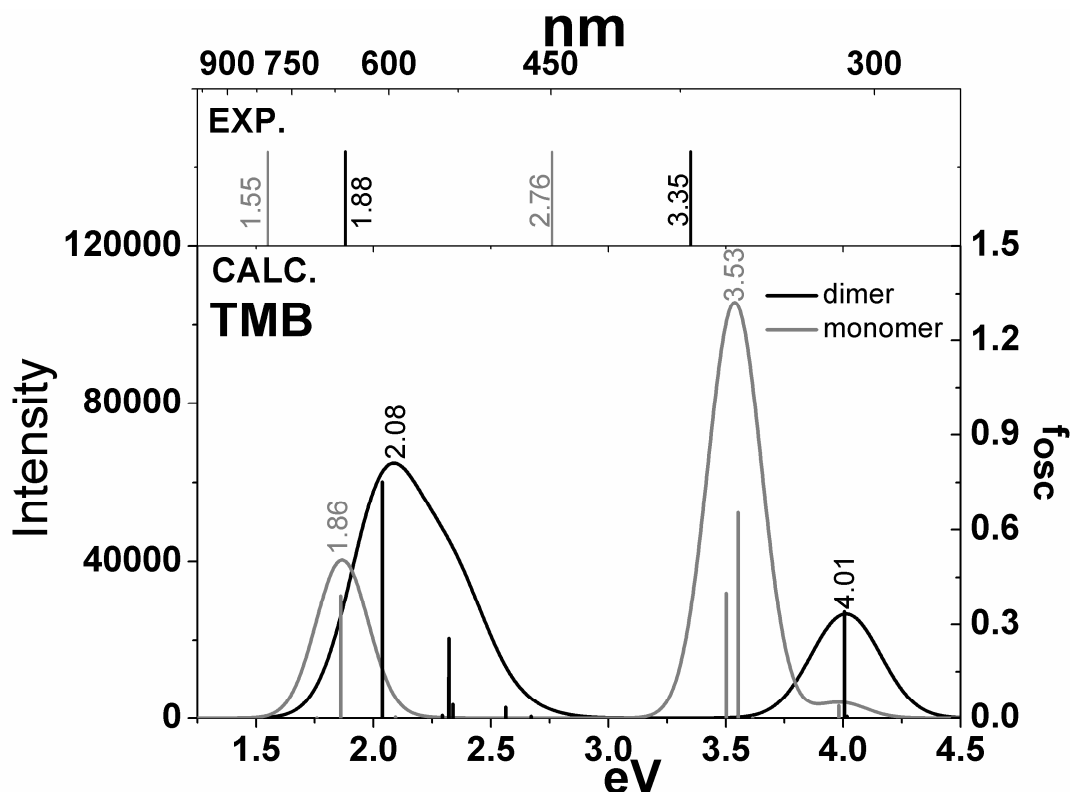


Figure 4.34: The TDA-B3LYP calculated vertical excitations (bottom, lines are shown with oscillator strengths) and convoluted UV/Vis spectrum (bottom) of the $[\text{TMB}]_2^{2+}2\text{Cl}^-$ dimer (black) and TMB^+Cl^- monomer (grey). The energies of experimental peak maxima are shown as vertical lines (top).

The first dimer peak is coming from the transition of $\text{HOMO} \rightarrow \text{LUMO}$ at 608 nm (2.04 eV) and the second peak come from $\text{HOMO}-2 \rightarrow \text{LUMO}+1$ transition at 309.5 nm (4.01 eV). Both dimer peaks describe the electron transition from chloride counter-ions to π -system located at the two benzene rings in each fragment (with some charge transfer character). The first monomer peak is a combination of $\text{HOMO} \rightarrow \text{LUMO}$ and $\text{SOMO} \rightarrow \text{LUMO}$ transitions at 666.6 nm (1.86 eV) while the second peak is the

transition of SOMO→LUMO at 349 nm (3.55 eV). Both transitions in monomer peaks are also charge transfer transitions from one chloride counter-ion to π -system located on two benzene rings. The computed UV/Vis spectrum shows a systematic shift (hypsochromic shift) relative to the experiment (shown in top of **Fig. 4.34**) by around 0.2 eV for the first indicated dimer and monomer peaks in the region 600-700 nm while the second dimer and monomer peaks in the UV region are shifted from experiment by around 0.7 eV. This might be due to solvent effects too.

4.2.7 Tetrathiofulvalene in acetone

Grampp et.al. studied the dimerization of tetrathiofulvalene radical cation ($\text{TTF}^{\bullet+}$) with perchlorate (ClO_4^-) counter-ion in acetone solvent with temperature-dependent EPR spectroscopy^[2] receiving the enthalpy of dimerization of -35.7 kJ/mol. UV/Vis spectroscopy was also used to measure the dimerization of TTF radical cation contemporary with EPR measurement by Kochi and co-worker^[48]. $\text{TTF}^{\bullet+}$ monomeric species (0.1-1.0 mM) shows absorption peaks at 438 and 582 nm (2.83 and 2.13 eV) at room temperature but in more concentration (> 5 mM) a new absorption band of dimer occurred at 752 nm (1.65 eV) and increasing as a function of concentration. While at temperature cooling to -100°C dimeric species TTF_2^{2+} shows absorption peaks at 395, 520 and 752 nm (3.14, 2.38 and 1.65 eV) and the intensity increase when the temperature decrease.

Fig. 4.35 shows the optimized geometry of $\text{TTF}^{\bullet+}\text{Cl}^-$ radical cation monomer. It was found that the most stable position of chloride counter-ion was located in the plane of monomer near hydrogen atom and sulphur atom with the distances 2.69 and 3.13 Å, respectively, and the two rings in the monomer are in plane with each other.

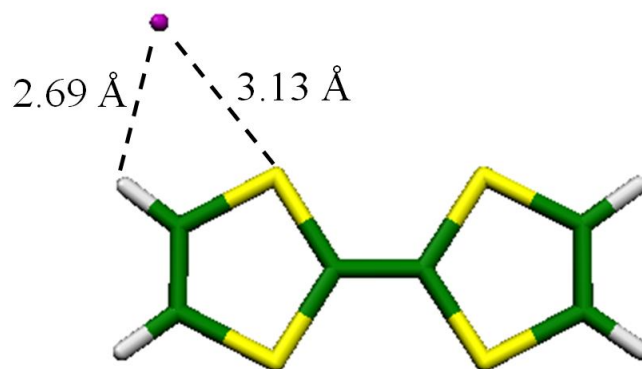


Figure 4.35: Optimized TTF radical cation monomer with chloride counter-ion.

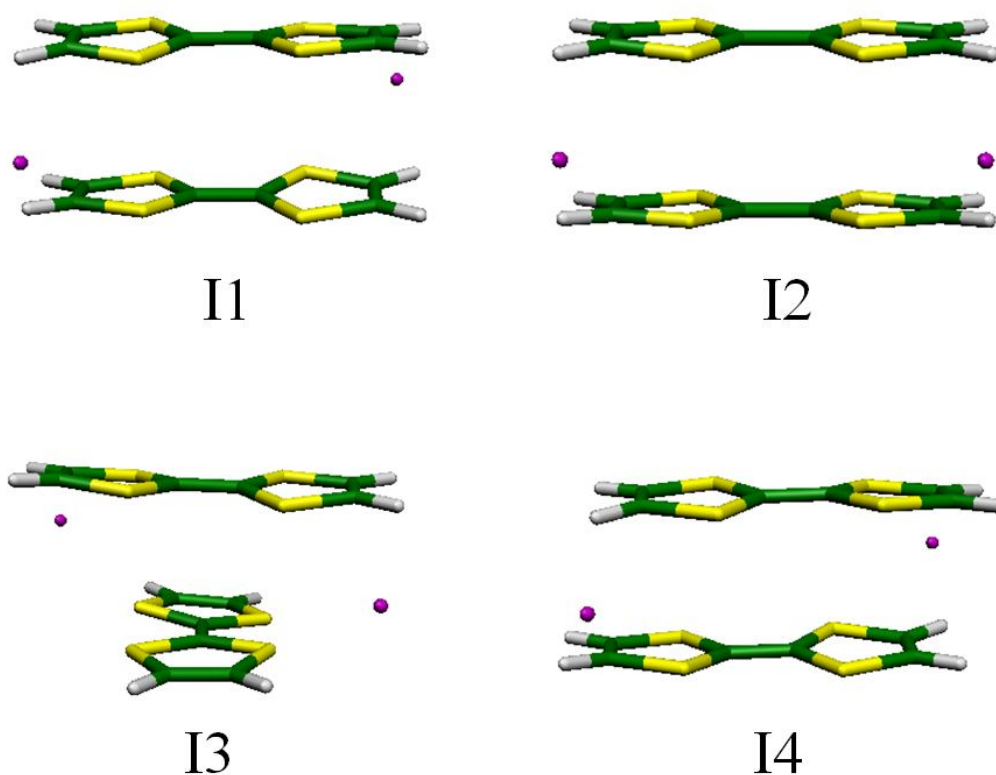


Figure 4.36: The B3LYP-D optimized geometries of $[TTF]_2^{2+}2Cl^-$ dimers.

Four optimized geometries of $TTF_2^{2+}2Cl^-$ dimers (**I1-I4**) are presented in **Fig. 4.36**. The intradimer distance of all four dimers is around 3.4 Å which is corresponding well with the theoretical work from Novoa's group^[28] and less than sum of the van der Waals radii of two sulphur atoms (3.6 Å)^[83]. Boltzmann distribution shows 50.44 % and 45.44 % for conformers **I1** and **I3**, respectively. Chloride counter-ions are located in trans position of monomers in these two conformers. The HOMO orbitals computed

by CASSCF method for these two conformers are presented in **Fig. 4.37** showing multicenter long π -bond with 2 electrons on 8 centers.

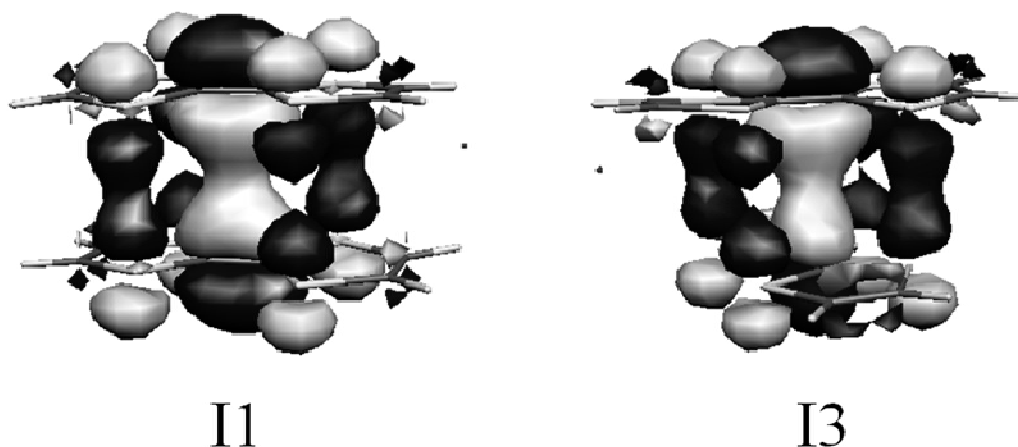


Figure 4.37: *The HOMO orbitals of two possible structure **I1** and **I3**.*

BSSE calculations in gas phase at B2PLYP-D/cc-pVTZ yield a dimerization energy of -51.94 and -63.39 kJ/mol for conformer **I1** and **I3**, respectively. CASSCF method results in a positive value, but it cannot reproduce the experimental dimerization enthalpy of -35.7 kJ/mol. Consecutively MRMP2 calculations on CAS reference give an overstabilization of the dimerization (-266.38 and -268.51 kJ/mol) as already known from other molecules.

Table 4.15: The intradimer distances, relative energies, Boltzmann distribution and dimerization energies of the most stable conformers of $[\text{TTF}]_2^{2+}2\text{Cl}^-$ dimers.

| TTF | dimer geometry | | B2PLYP-D cc-pVTZ | | UB3LYP-D cc-pVDZ | E_{dim} [kJ/mol] | | ΔH_{dim} [kJ/mol] | |
|-----------|----------------------------|--|------------------------------|------------------|---------------------|------------------------------|---|-------------------------------------|--|
| | ring geometry r (pi-pi) | chlorine geometry ^a r(Cl..H) r(Cl..S) | E_{rel} [kJ/mol] | N_i / N_0 % | | BSSE UB2PLYP-D cc-pVTZ | CASSCF ^b (MRMP2 ^c) cc-pVTZ | exp. [2] | |
| I1 | eclipsed 3.43 Å | trans 2.76 Å 3.37 Å | 0.00 | 50.44 | -88.38 | -51.94 | 49.34 (-266.38) | | |
| I2 | eclipsed 3.44 Å | cis 2.73 Å 2.38 Å | 12.56 | 0.32 | -86.98 | -40.05 | 122.90 (-254.47) | -35.7 | |
| I3 | crossed 3.44 Å | trans 2.81 Å 3.30 Å | 0.26 | 45.44 | -76.76 | -63.39 | 97.94 (-268.51) | | |
| I4 | staggered 3.36 Å | trans 2.82 Å 3.26 Å | 6.41 | 3.80 | -80.49 | -38.46 | 99.83 (-264.06) | | |

^a distances are given to the closest atom.

^b CASSCF(3,3)/CASSC(2,2) data are given.

^c MRMP2 calculation base on CASSCF(3,3)/CASSC(2,2) reference, values in brackets.

The computed UV/Vis spectrum of the two most stable conformer of dimers (**I1** and **I3**) and monomer is shown in Fig. 4.38.

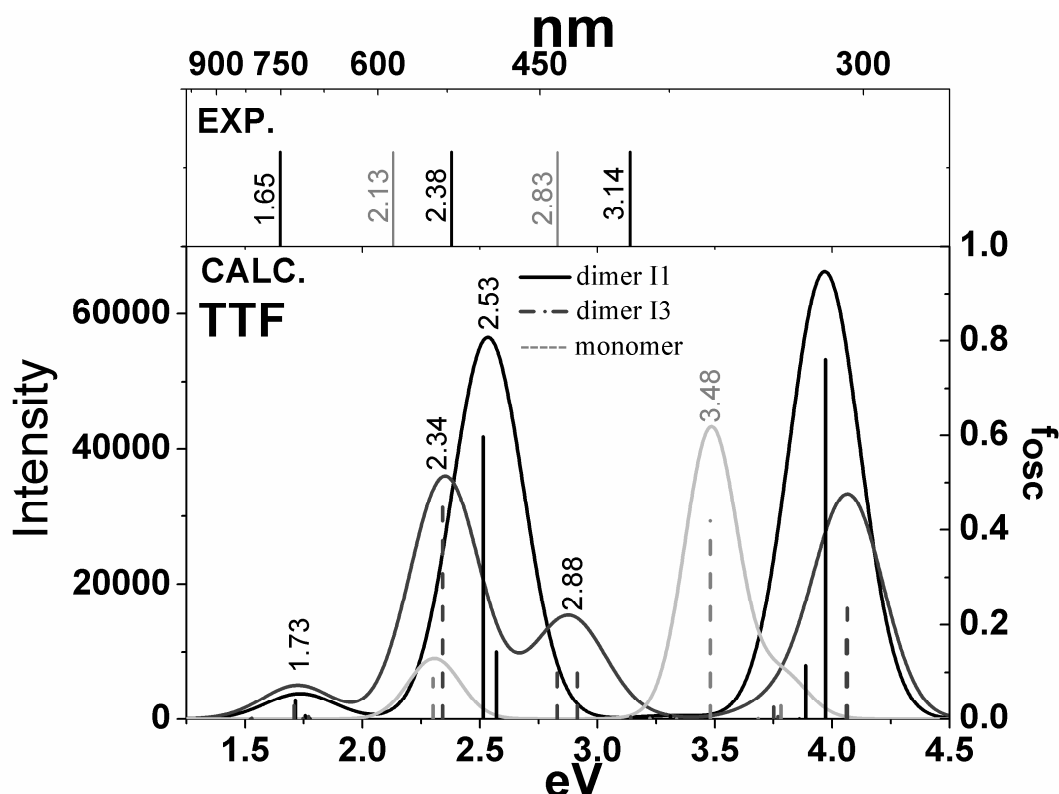


Figure 4.38: The TDA-B3LYP calculated vertical excitations (bottom, lines are shown with oscillator strengths) and convoluted UV/Vis spectrum (bottom) of the two most stable conformer of $[\text{TTF}]_2^{2+}2\text{Cl}^-$ dimer (**I1** and **I3**) (black) and $\text{TTF}^{\bullet+}\text{Cl}^-$ monomer (grey). The energies of experimental peak maxima are shown as vertical lines (top).

Both dimer conformers (**I1** and **I3**) show nearly the same dimer peaks around 730 nm (1.7 eV) which are corresponding well with the experimental UV/Vis data of indicated dimeric peak at 752 nm (1.63 eV)^[48]. These peaks in the two conformers are the combination of charge transfer chloride counter-ions to π -system in each fragment of dimers, described by $\text{HOMO} \rightarrow \text{LUMO} (\text{Cl} \rightarrow \pi^*)$ and $\text{HOMO}-1 \rightarrow \text{LUMO} (\text{Cl} \rightarrow \pi^*)$ transitions. The first monomer peak at 539 nm (2.30 eV) is assigned to the $\text{HOMO}-3 \rightarrow \text{LUMO}$ transition ($\pi \rightarrow \pi^* + \text{Cl}_z$) and correspond well with the first experimental monomeric peak at 582 nm (2.13 eV). The second peak of monomer at 356 nm (3.48 eV) stems from charge transfer transition from π -electron of two fulvalene ring to π -electron of one fulvalene ring and shows an error from the experiment of around 0.6 eV. The UV/vis spectrum of $[\text{TTF}]_2^{2+}$ dimer conformer **I3** is well corresponded with the experiment with an error approximately of 0.2 eV.

4.2.8 Summary of radical cation dimerization

Radical cation dimerization was investigated theoretically for six molecules ($\text{PPD}^{\bullet+}$, $\text{N,N-DMPPD}^{\bullet+}$, $2,3,5,6\text{-TMPPD}^{\bullet+}$, $\text{N,N,N',N'-TMPPD}^{\bullet+}$, $\text{TMB}^{\bullet+}$ and $\text{TTF}^{\bullet+}$, respectively).

Dispersion correction is very important in the optimization processes with B3LYP-D/cc-pVDZ level of theory to get stabilization of the molecular geometry of dimers corresponding to the experiment. The dimers of all six molecules exhibit multicenter long π -bond which is shorter than the sum of van der Waals radii but longer than a normal covalent bond. Density Functional Theory at B3LYP-D/cc-pVDZ level of theory is appropriate for the geometry optimization.

Two monomer fragments in dimers arrange themselves in eclipsed and stacking position with the intradimer distances around 2.8 – 3.4 Å for all dication dimers. Counter-ions are located either in cis or in trans position of the dimers, but the conformations with counter-ions in trans position yield lower energy for the dimers.

DFT HOMO orbitals are different from CASSCF HOMO orbitals: within the DFT method the electrons are localized on counter-ions and the interacting pi-system, while with CASSCF method the electrons are only localized in the interacting multicenter long π -bond. But for LUMO orbitals DFT and CASSCF give the same result that the electrons are localized in the antibonding π^* system of the two monomer fragments.

B3LYP-D/cc-pVDZ method calculates the energy of dimerization for all six molecules with some overstabilization compared to the experimental dimerization enthalpy from temperature-dependent EPR and UV/Vis measurement. Therefore energy correction is necessary for these calculations to improve the calculational results. BSSE correction at B2PLYP-D/cc-pVTZ in gas phase yields a dimerization energy in good agreement with experimental data for four of the investigated molecules ($[\text{N,N-DMPPD}]_2^{2+}$, $[2,3,5,6\text{-TMPPD}]_2^{2+}$, $[\text{N,N,N',N'-TMPPD}]_2^{2+}$ and $[\text{TTF}]_2^{2+}$). But for $[\text{PPD}]_2^{2+}$ the energy correction in gas phase results too much overstabilization and some destabilization for $[\text{TMB}]_2^{2+}$.

CASSCF calculations, based on CAS(2,2) for dimer and CAS(3,3) for monomer, yields a dimerization energy corresponding well with the experimental dimerization enthalpy for nearly all molecules ($[\text{PPD}]_2^{2+}$, $[\text{N,N-DMPPD}]_2^{2+}$, $[2,3,5,6\text{-TMPPD}]_2^{2+}$, $[\text{N,N,N',N'-TMPPD}]_2^{2+}$ and $[\text{TMB}]_2^{2+}$) except for $[\text{TTF}]_2^{2+}$.

Vertical transitions were computed at B3LYP/cc-pVTZ level of theory and after Gaussian broadening convoluted absorption spectra are shown. These calculated spectra show the indicated dimer peaks for all molecules in the range of 600 – 800 nm corresponding well with the experimental indicated dimer peaks from UV/Vis. These dimer peaks are coming from HOMO→LUMO transition while the second dimer peaks are coming from HOMO-1→LUMO transition in all compounds. This confirms the experimental assignment for those dimer peaks described in literature. The higher energy dimer peaks are also discussed in this work, although they were not discussed in the experiment. The computed monomer peaks show that the first two peaks are coming from the excitation from explicit solvent and to the π^* orbital of monomers. Without adding explicit solvent to monomer these first two peaks do not appear in the computed spectra. The other monomer peaks at higher energy could be described by even adding explicit solvent or not to the monomers. They come from transitions of SOMO alpha orbital located at counter-ion into LUMO alpha orbitals located at the benzene ring (counter-ion→ π^* transition), but are only partly described by the experimentalists.

The methyl substituted groups were added to PPD^{•+} and changed the structure of the most stable conformer of dimers. In the most stable conformer of [N,N-DMPPD]₂²⁺ and [2,3,5,6-TMPPD]₂²⁺ dimers, we found that the two monomer fragments in dimers arrange themselves in the π -stacked position which is different from [PPD]₂²⁺ dimer that the two monomer fragments arrange in the eclipsed position and slightly shift in the short axis of dimer molecule. The intradimer distance between two monomer fragments in [N,N-DMPPD]₂²⁺ and [2,3,5,6-TMPPD]₂²⁺ dimers are shorter than [PPD]₂²⁺ dimer by around 0.04 Å and 0.15 Å, respectively. But in [N,N,N',N'-TMPPD]₂²⁺ dimer, two monomer fragments arrange themselves in eclipsed position the same as [PPD]₂²⁺ dimer and the intradimer distance is longer by approximately 0.29 Å. That may come from the hindering between the methyl groups of two monomer fragments and the repulsion between the same charges on the atoms between two monomer fragments.

Moreover in substituted PPD dimer ([N,N-DMPPD]₂²⁺, [2,3,5,6-TMPPD]₂²⁺ and [N,N,N',N'-TMPPD]₂²⁺ dimers), we found that the substituted methyl groups are changing the position of the UV/Vis absorption peaks of dimers. There are two indicated dimer peaks, the first peak, λ_L , is the excitation from HOMO to LUMO

orbitals and the second peak, λ_H , is the excitation from HOMO-1 to LUMO orbitals. The position of the first and the second peak (λ_L and λ_H) of substituted PPD dimer were shifted from $[\text{PPD}]_2^{2+}$ dimer to lower energy (bathochromic shift) by around 65 nm to 195 nm (0.2-0.5 eV) depending on where is the position of substituted methyl groups. From this results, it can be concluded that the substituting methyl groups to PPD dimer results in the lower energy gap between the HOMO and LUMO orbitals in methyl substituted PPD dimers ($[\text{N,N-DMPPD}]_2^{2+}$, $[\text{2,3,5,6-TMPPD}]_2^{2+}$ and $[\text{N,N,N',N'-TMPPD}]_2^{2+}$).

UV/Vis vertical excitation calculations at B3LYP/cc-pVTZ level of theory using COSMO model of solvent mostly describe the UV/Vis spectra of dimers and monomers correct. But it has a problem that it cannot reproduce some absorption peaks that occurred from the transition from solvent molecules to dimers or monomers. Especially for the calculated UV/Vis spectra of monomers, it is obvious that COSMO model cannot reproduce two absorption peaks that occurred from the transition of electrons from solvent molecules to the π^* system of monomers. This problem can be solved by including explicit solvent molecules to dimers and monomers. Explicit solvent shifts the position of the calculated absorption peaks by around 0.1 eV compared to calculate without explicit solvent. Then the vertical excitation calculations can provide all information of the absorption peaks and correspond well to the experimental UV/Vis spectra.

4.3 EFFECT OF DIELECTRIC CONSTANT TO DIMERIZATION

ENERGY

Based on the knowledge that the dimerization process of PPD, substituted-PPD radical cations and all other radical ions molecules mostly occurred at low temperature (around -90°C) measured by temperature-dependent EPR spectroscopy^[7], it is necessary to include the T-dependence of the dielectric constant in my thesis.

Experimental Findings:

Table 4.16: List of experimental dielectric constants for solvents used in this study as a function of temperature. The default ORCA program values of (epsilon, refractive index) are given in brackets.

Dielectric constant of ethanol^[39]. (24.3, 1.361)

| | | | | | | | | | |
|---------------|-------|-------|-------|-------|-------|-------|-------|-------|-------|
| T [K] | 163.2 | 173.2 | 193.2 | 213.2 | 243.2 | 273.2 | 293.2 | 313.2 | 333.2 |
| $\epsilon(T)$ | 55.5 | 51.3 | 44.4 | 39.7 | 33.4 | 28.1 | 25.3 | 23.3 | 21.6 |
| T [K] | 363.2 | 393.2 | 423.2 | 453.2 | 483.2 | 503.2 | 513.2 | 523.2 | |
| $\epsilon(T)$ | 19.6 | 17.8 | 16.1 | 14.3 | 12.4 | 11.2 | 10.5 | 10.4 | |

Dielectric constant of methanol^[40]. (32.63, 1.329)

| | | | | | | | | | |
|---------------|-------|-------|-------|-------|-------|-------|-------|-------|-------|
| T [K] | 183.2 | 193.2 | 203.2 | 213.2 | 223.2 | 233.2 | 243.2 | 253.2 | 263.2 |
| $\epsilon(T)$ | 66.5 | 62.0 | 58.0 | 54.6 | 51.3 | 48.3 | 45.4 | 42.7 | 40.6 |
| T [K] | 273.2 | 283.2 | 293.2 | | | | | | |
| $\epsilon(T)$ | 37.9 | 35.4 | 33.6 | | | | | | |

Dielectric constant of diethyl ether^[41]. (a)

| | | | | | | | | |
|---------------|-------|-------|-------|-------|-------|-------|-------|-------|
| T [K] | 165.2 | 169.2 | 175.2 | 183.2 | 219.2 | 238.2 | 257.2 | 273.2 |
| $\epsilon(T)$ | 8.95 | 8.41 | 7.92 | 7.01 | 6.33 | 5.60 | 5.10 | 4.60 |

Dielectric constant of acetone^[42]. (20.7, 1.359)

| | | | | | | |
|---------------|-------|-------|-------|-------|-------|-------|
| T [K] | 204.2 | 233.2 | 253.2 | 273.2 | 293.2 | 313.2 |
| $\epsilon(T)$ | 31.31 | 28.42 | 25.91 | 23.65 | 21.45 | 19.38 |

Table 4.16 (continued)Dielectric constant of acetonitrile^[43]. (36.6, 1.344)

| | | | | | | | | | |
|---------------|-------|-------|-------|-------|-------|-------|-------|-------|-------|
| T [K] | 288.2 | 293.2 | 298.2 | 303.2 | 308.2 | 313.2 | 318.2 | 323.2 | 328.2 |
| $\epsilon(T)$ | 38.02 | 36.64 | 36.04 | 34.64 | 33.29 | 33.20 | 32.80 | 32.21 | 31.78 |
| T [K] | 333.2 | | | | | | | | |
| $\epsilon(T)$ | 31.08 | | | | | | | | |

Dielectric constant of dichloromethane^[44]. (9.08, 1.424)

| | | | | | | | | | |
|---------------|-------|-------|-------|-------|-------|-------|-------|--|--|
| T [K] | 184.1 | 192.5 | 217.6 | 244.3 | 264.6 | 298.0 | 306.0 | | |
| $\epsilon(T)$ | 15.9 | 11.98 | 13.02 | 11.34 | 10.27 | 8.93 | 8.47 | | |

Dielectric constant of tetrahydrofuran^[45]. (7.25, 1.407)

| | | | | | | | | | |
|---------------|-------|-------|-------|-------|-------|-------|-------|-------|-------|
| T [K] | 203.2 | 213.2 | 223.2 | 233.2 | 243.2 | 253.2 | 263.2 | 273.2 | 283.2 |
| $\epsilon(T)$ | 11.58 | 10.98 | 10.43 | 9.91 | 9.43 | 9.00 | 8.60 | 8.23 | 7.88 |
| T [K] | 298.2 | | | | | | | | |
| $\epsilon(T)$ | 7.39 | | | | | | | | |

Dielectric constant of propionitrile^[84]. (b)

| | | | | | | | | | |
|---------------|-------|-------|-------|-------|-------|-------|-------|-------|-------|
| T [K] | 213.2 | 233.2 | 253.2 | 273.2 | 293.2 | 303.2 | 313.2 | 333.2 | 353.2 |
| $\epsilon(T)$ | 41.6 | 38.3 | 35.1 | 32.2 | 29.7 | 28.6 | 27.5 | 25.2 | 23.0 |
| T [K] | 373.2 | 393.2 | 413.2 | 433.2 | 453.2 | 473.2 | | | |
| $\epsilon(T)$ | 21.0 | 19.2 | 17.4 | 15.7 | 14.0 | 12.4 | | | |

Dielectric constant of butyronitrile^[85]. (b)

| | | | | |
|---------------|-------|-------|-------|-------|
| T [K] | 293.2 | 303.2 | 313.2 | 333.2 |
| $\epsilon(T)$ | 24.83 | 23.73 | 22.79 | 20.83 |

Dielectric constant of water^[86]. (80.4, 1.330)

| | | | | | | | | | |
|---------------|-------|-------|-------|-------|-------|-------|-------|-------|-------|
| T [K] | 273.2 | 323.2 | 373.2 | 423.2 | 473.2 | 523.2 | 543.2 | 573.2 | 593.2 |
| $\epsilon(T)$ | 88.15 | 70.50 | 55.55 | 43.89 | 34.59 | 26.75 | 23.86 | 19.66 | 16.88 |
| T [K] | 623.2 | | | | | | | | |
| $\epsilon(T)$ | 12.61 | | | | | | | | |

Table 4.16 (continued)Dielectric constant of EtOH/Et₂O (v/v 2:1) mixture. ^(c)

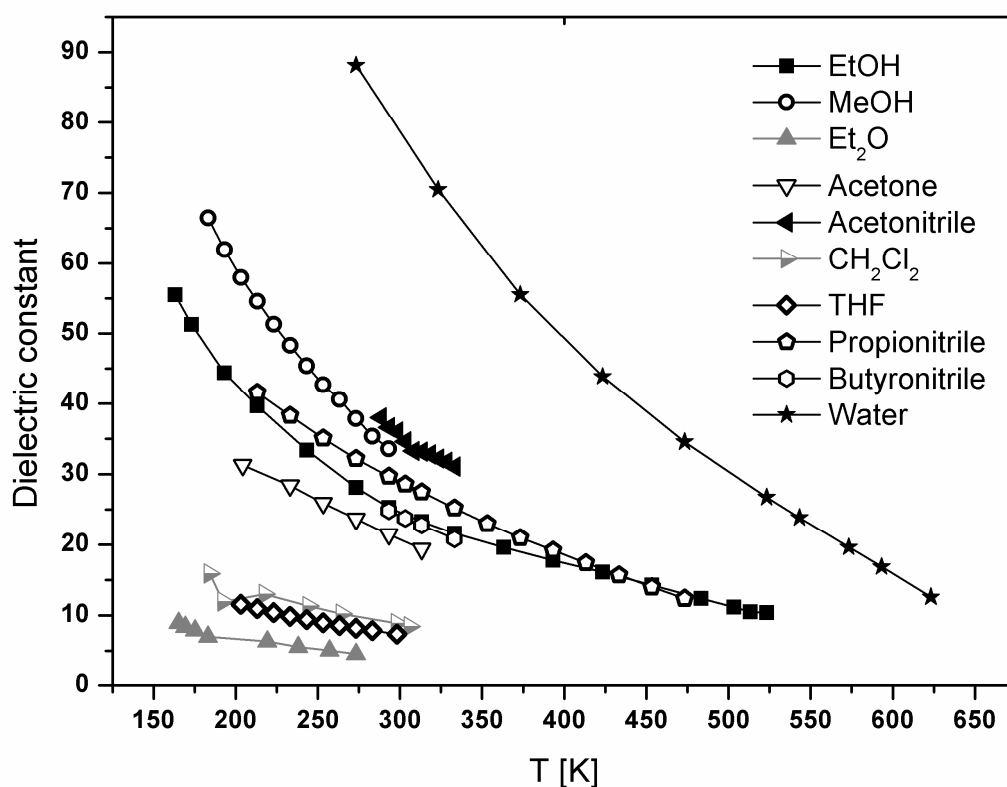
| | | | |
|---------------|-----|-------|-------|
| T [K] | 183 | 193 | 298 |
| $\epsilon(T)$ | | 34.68 | 16.93 |

(a) These pure solvents are not used in this study.

(b) A mixture of propionitrile/butyronitrile (1:1) will be used in a future EPR experiment for TCNQ. Data for completeness of solvent list.

(c) The dielectric constant of ethanol and diethyl ether mixture v/v 2:1 at low temperature are calculated by using the dielectric constant of pure ethanol at 193 K and pure diethyl ether at 183 K and further extrapolation by using the mol fraction according to the procedure for room temperature^[46, 47].

The plot of the dielectric constants of all solvent molecules (ethanol, methanol, diethyl ether, acetone, acetonitrile, dichloromethane, tetrahydrofuran, propionitrile, butyronitrile and water) against temperature is shown in **Fig. 4.39**. For all solvent molecules, the dielectric constant is increasing when the temperature decreases, especially for the polar solvents (ethanol, methanol, acetonitrile and acetone) the dielectric constant is changing much when temperature changes.

**Figure 4.39:** The plot of dielectric constants of solvents against temperature.

Theoretical calculations for ϵ -dependence:

The effect of dielectric constant change to the dimerization energy has been investigated for all molecules of this work. The COSMO model of solvation was used for optimization within the B3LYP-D/cc-pVDZ method with the dielectric constant at room temperature. Then, single point calculation on the energetics has been performed by using B2PLYP-D/cc-pVTZ method at different dielectric constants ($\epsilon_{298} - \epsilon_{T_{dim}}$) for these geometries. Data in Chapter 4 contain also the BSSE correction for gas phase, while data in this chapter (**Tables 4.17-4.18**, **Figs. 4.40-4.41**) do not contain any BSSE correction to see the pure effect of dielectric constant. The default values for dielectric constant of the program ORCA (see **Table 4.16**) have been used as room temperature values, and the dielectric constants at dimerization temperature were used for the second energy value in **Tables 4.17-4.18**. The standard refractive indices have been used for all calculations, as it does not change so much with temperature and has a minor effect on the energies.

Radical cations and dication dimers of four molecules (PPD, N,N-DMPPD, 2,3,5,6-TMPPD, N,N,N',N'-TMPPD) have been tested for the effect of dielectric constant in a range of $\epsilon=16.93$ to 150 to dimerization energy. Dimerization energies of these four molecules were calculated in ethanol and diethyl ether mixing solvent^[46] v/v 2:1 at B2PLYP-D/cc-pVTZ level of theory with COSMO solvent model. The dimerization energies of the most stable dimers of [PPD]₂²⁺ with bromine counter-ion (**D1**) and of the substituted PPD's with chlorine counter-ions (**E3** of [N,N-DMPPD]₂²⁺, **F3** of [2,3,5,6-TMPPD]₂²⁺ and **G1** of [N,N,N',N'-TMPPD]₂²⁺) varying with dielectric constant are shown in **Fig. 4.40** and **Table 4.17**.

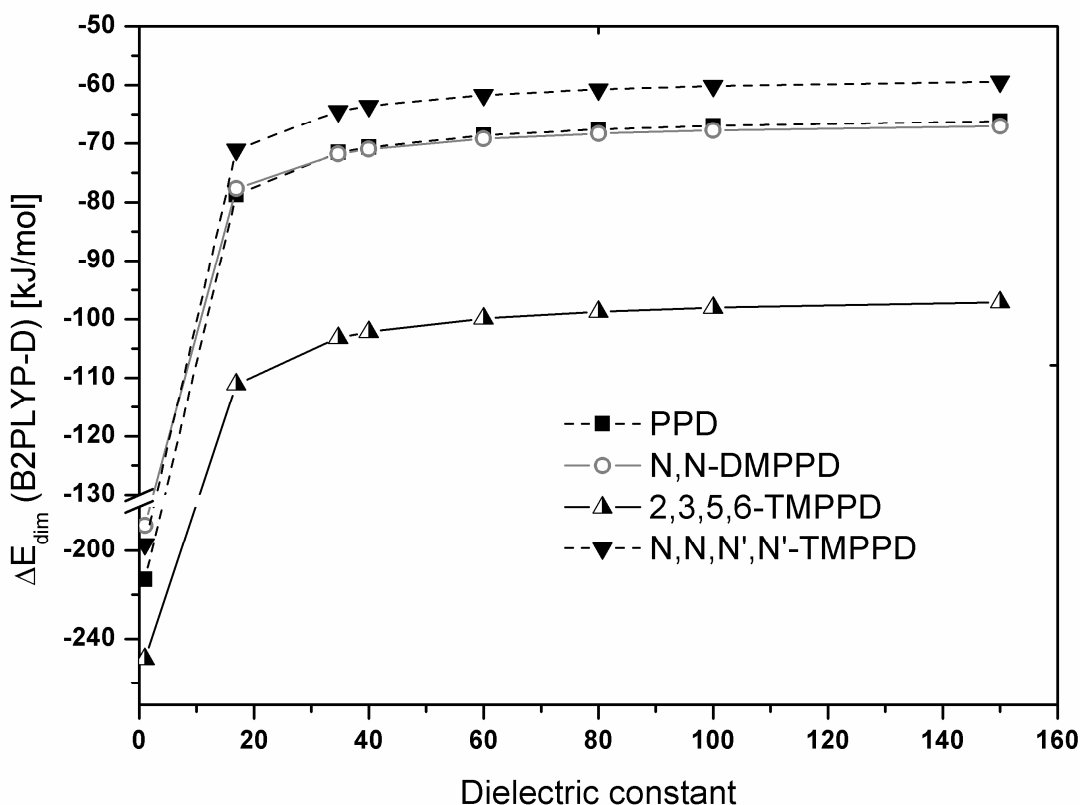


Figure 4.40: Dimerization energies of cationic radicals in various dielectric constants.

Fig. 4.40 and **Table 4.17** show that dimerization energies calculated at B2PLYP-D/cc-pVTZ level of theory within the COSMO model of solvation for all four radical cations molecules (PPD^{•+}, N,N-DMPPD^{•+}, 2,3,5,6-TMPPD^{•+}, N,N,N',N'-TMPPD^{•+}) decrease and converge to the experimental dimerization enthalpies when dielectric constants is increasing. The dimerization energies change significantly by approximately 7-9 kJ/mol in the range of dielectric constant from 16.93 to 40. A steep decrease of dimerization energy is found for the gas phase calculations ($\epsilon = 1$). At higher dielectric constants ($\epsilon > 40$) the curve is flattening. The energy value at $\epsilon = 80$, which is water, can be taken as close to the converged energy. When looking at the calculated dimerization energies using the dielectric constant at the dimerization temperature 193 K ($\epsilon = 34.68$), it was found that the calculated dimerization energies at 193 K are higher than the calculated dimerization energies at room temperature ($\epsilon = 16.93$) by around 6-8 kJ/mol and go to the direction of the experimental dimerization enthalpies measured by temperature-dependent EPR spectroscopy^[7].

Although the calculated dimerization energies are overstabilizing the dimer relative to experiment, the error relative to experiment is reduced from 26-53 to 19-44 kJ/mol.

Keeping in mind, that the B2PLYP-D data do not contain any other temperature effect than the dielectric constant effect in COSMO model, and that they are compared to experimental enthalpies, the agreement is reasonable well given.

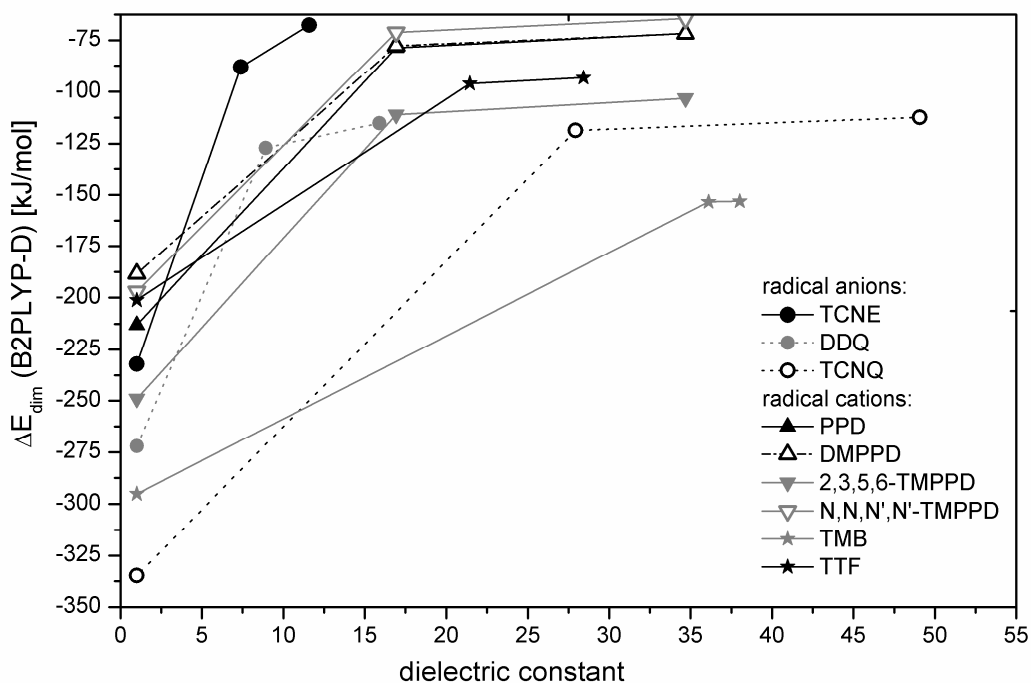


Figure 4.41: Dimerization energies, kJ/mol, of radical ions dimerization versus dielectric constant in gas phase, room temperature and dimerization temperature of solvent.

The calculated dimerization energies of the other investigated radical ions molecules ($\text{TCNE}^{\bullet-}$, $\text{DDQ}^{\bullet-}$, $\text{TCNQ}^{\bullet-}$, $\text{PPD}^{\bullet+}$, $\text{N,N-DMPPD}^{\bullet+}$, $\text{2,3,5,6-TMPPD}^{\bullet+}$, $\text{N,N,N',N'-TMPPD}^{\bullet+}$, $\text{TMB}^{\bullet+}$ and $\text{TTF}^{\bullet+}$) (see **Table 4.18**) were calculated at room temperature and at dimerization temperature using the optimized geometries of dimers and monomers from Chapters 4.1 and 4.2. The dielectric constants at indicated dimerization temperature are larger than the dielectric constants at room temperature for radical anions and radical cations. This fact is also presented in **Fig. 4.41**. Generally, the difference of dimerization energies using the high dielectric constants or using the low dielectric constants are smaller for the radical cations, while they can become up to 20 kJ/mol for radical anions, with the largest value for $\text{TCNE}^{\bullet-}$. The slope of the ϵ - and T-dependent energetics is almost the same for all radical cations. Only the radical anions $\text{TCNE}^{\bullet-}$ and $\text{DDQ}^{\bullet-}$ show larger changes of dimerization energy with changing dielectric constant, but they were solvated in low- ϵ solvents

THF ($\epsilon_{298} = 7.39$) and CH_2Cl_2 ($\epsilon_{298} = 8.93$), respectively. The radical anion $\text{TCNQ}^{\bullet-}$, which was solvated in a EtOH/MeOH (v/v 4:1) mixture with higher dielectric constant ($\epsilon_{298} = 27.93$) shows less change with dielectric constant.

So, there appears the question, whether dimerization energy shows a higher dependence of temperature in low dielectric constant. It would be interesting to test, whether the radical anion $\text{TCNQ}^{\bullet-}$ shows a different behaviour in solvents with very low or very high dielectric constant.

Table 4.17: Dimerization energies, ΔE_{dim} , of cationic radicals for various dielectric constants compared to experimental dimerization enthalpies, ΔH_{dim} .

| Substance | ΔE_{dim} (kJ/mol) | | | | | | | $\Delta H_{\text{dim}}^{[7]}$ (kJ/mol) |
|-------------------------------|----------------------------------|-------------------------------|--------------------|--------------------|--------------------|---------------------|---------------------|---|
| | $\epsilon = 16.93$ (298 K) | $\epsilon = 34.68$ (193 K) | $\epsilon = 40.00$ | $\epsilon = 60.00$ | $\epsilon = 80.00$ | $\epsilon = 100.00$ | $\epsilon = 150.00$ | |
| PPD ^{•+} | -78.71 | -71.59 | -70.67 | -68.66 | -67.64 | -67.03 | -66.21 | -52.4 |
| N,N-DMPPD ^{•+} | -77.72 | -71.79 | -70.98 | -69.23 | -68.35 | -67.81 | -67.10 | -44.2 |
| 2,3,5,6-TMPPD ^{•+} | -111.10 | -103.18 | -102.15 | -99.88 | -98.73 | -98.04 | -97.12 | -58.2 |
| N,N,N',N'-TMPPD ^{•+} | -71.09 | -64.45 | -63.59 | -61.70 | -60.75 | -60.18 | -59.41 | -29.6 |

Table 4.18: The calculated dimerization energies, ΔE_{dim} (kJ/mol), of anionic and cationic radicals at B2PLYP-D/cc-pVTZ level of theory at room temperature and at dimerization temperature.

| Substance | Solvent | $\epsilon(T_{\text{room}})$ | T_{dim} | $\epsilon(T_{\text{dim}})$ | B2PLYP-D/cc-pVTZ | | EXP. | |
|-----------|-------------------------------|---------------------------------|------------------|----------------------------|--|---|---------|-------|
| | | | | | $\Delta E_{\text{dim}}(T_{\text{room}})$ | $\Delta E_{\text{dim}}(T_{\text{dim}})$ | | |
| Anion | TCNE ^{•-} | THF | 7.39 (298 K) | 183 K | 11.58 (T=203 K) | -88.03 | -67.62 | -33.4 |
| | DDQ ^{•-} | CH ₂ Cl ₂ | 8.93 (298 K) | 171 K | 15.90 (T=184.1 K) | -127.04 | -115.08 | -24.0 |
| | TCNQ ^{•-} | EtOH:MeOH v 4:1 | 27.93 (298 K) | 190 K | 49.08 (T=193.2 K) | -118.64 | -112.29 | -34.2 |
| Cation | PPD ^{•+} | EtOH:Et ₂ O v 2:1 | 16.93 (298 K) | 183 K | 34.68 (T=193 K) | -78.71 | -71.59 | -52.4 |
| | PPD ^{•+} | Water | 80.0 (298 K) | 298 K | | -67.64 | | |
| | N,N-DMPPD ^{•+} | EtOH:Et ₂ O v 2:1 | 16.93 (298 K) | 183 K | 34.68 (T=193 K) | -77.72 | -71.79 | -44.2 |
| | 2,3,5,6-TMPPD ^{•+} | EtOH:Et ₂ O v 2:1 | 16.93 (298 K) | 183 K | 34.68 (T=193 K) | -111.10 | -103.18 | -58.2 |
| | N,N,N',N'-TMPPD ^{•+} | EtOH:Et ₂ O v 2:1 | 16.93 (298 K) | 183 K | 34.68 (T=193 K) | -71.09 | -64.45 | -29.6 |
| | TMB ^{•+} | Acetonitrile | 36.1 (293 K) | 288 K | 38.02 (T=288 K) | -153.40 | -153.12 | -60.0 |
| | TTF ^{•+} | Acetone | 21.45 (293 K) | 233 K | 28.42 (T=233 K) | -96.07 | -93.29 | -35.7 |

At low temperature the dielectric constant is not the same as at room temperature, but computer programs have standard values for dielectric constant which are valid at temperatures between 20 and 25°C. As dimerization of ionic radicals is a temperature-dependent reaction, this might be one error when comparing calculated dimerization energies (electronic energies or Gibbs free energies) with experimental dimerization enthalpies measured at low temperature. The dielectric constant used in the calculation of dimerization energy must be taken from the value at dimerization temperature which is larger than the value at room temperature to correct the calculated dimerization energy to agree well with experimental data.

Another one problem is that dielectric constant at low temperature can be found mostly for pure solvents from the literature data but not often for mixing solvents. So the extrapolation of dielectric constant for mixing solvents by using mol fraction is necessary for the calculation.

From the presented information, it can be concluded that dielectric constant is one of many factors that influence the dimerization energy. This may be one reason of the error in the energy calculations at low or high temperature compared to experimental data.

Further work can be done for testing, whether radical anions show a larger dependence on the dielectric constant than radical cations. T-dependent EPR experiments on the dimerization of radical anion TCNQ^{•-} in different (high ϵ) solvents are in preparation in our institute, but not matter of this thesis.

5. CONCLUSIONS

Theoretical investigations on the dimerization of ionic radicals (both anions and cations) in solution have been performed in this study to understand the process of dimerization in solution.

Density Functional method including dispersion interaction at B3LYP-D/cc-pVDZ level of theory was chosen to the geometry optimization process for dimers and monomers. The optimized geometries of dimers and monomers of all nine radical ions (TCNE^{•-}, DDQ^{•-}, TCNQ^{•-}, PPD^{•+}, N,N-DMPPD^{•+}, 2,3,5,6-TMPPD^{•+}, N,N,N',N'-TMPPD^{•+}, TMB^{•+} and TTF^{•+}) correspond well with the results from the X-ray crystallographic data. The dimers of all nine molecules exhibit multicenter long π -bonds which show intradimer distances in the range of 2.8 - 3.4 Å longer than normal covalent bond, but shorter than the sum of the van der Waals radii in ionic radical dimers. It can be concluded that B3LYP-D/cc-pVDZ level of theory is appropriate for the geometry optimization of ionic radicals dimerization to find good structural parameters in good agreement with the experimental data.

In the geometry optimization process, it was found that dispersion interaction and electrostatic attraction from the counter-ions play an important role to stabilize the dimers. The counter-ions located in trans-position of dimers are more stable than located in cis-position.

The most stable conformer of [DDQ]₂²⁻ dimer in acetone and dichloromethane show a lateral rotation of one monomer fragment with respect to another monomer fragment. The most stable conformer of [TCNQ]₂²⁻, [PPD]₂²⁺, [N,N,N',N'-TMPPD]₂²⁺ dimers arrange the two monomer fragments in eclipsed position and slightly shifted along the short axis of dimer by approximately of 0.9 Å to avoid electrostatic repulsion between the same charges on the atoms in each monomer fragment.

The strongly bonding HOMO orbitals in dimers show strong interactions of the two radical electrons in the SOMO orbitals generating the multicenter long π -bond dimers. The HOMO orbitals of dication dimers calculated from DFT and CASSCF exhibit a difference in electron distribution of dimers and monomers. In DFT orbitals the

electron distribution is localized on the counter-ions atoms, but in CASSCF orbitals the electrons are localized only in the interacting bonds. This difference does not occur in dianion dimers.

Basis set superposition error correction at B2PLYP-D/cc-pVTZ level in gas phase yields dimerization energies corresponding well with the temperature-dependent EPR-experiments, except for TCNQ and PPD which are calculated with too much overstabilization and TMB, which shows much destabilization. Gas phase CASSCF energy calculations using CAS(2,2) for dimer and CAS(3,3) for monomer with cc-pVTZ basis set show approximately 15% character of double excitation, which can be neglected using a proper DFT method like B2PLYP-D. The CASSCF dimerization energies are also in good agreement with the experimental values, especially for dimers $[\text{N,N-DMPPD}]_2^{2+}2\text{Cl}^-$ and $[\text{2,3,5,6-TMPPD}]_2^{2+}2\text{Cl}^-$. MRMP2 calculations without basis set superposition error correction yield a overstabilization of dimers. The summary of the calculated dimerization energy by various methods of calculations for all investigated molecules compared to the experimental data is shown in **Table 5.1**. No uniform picture is seen for the energetics. The BSSE error is up to 300 kJ/mol, therefore it must be included. Using ϵ_{Tdim} instead of ϵ_{298} is more important for the anions, where this effect can become up to 20 kJ/mol. From data of PPD radical cation dimerization, it is seen that the energetics is also very much dependent on the counter-ion. Chloride gives different errors relative to experiment than bromide counter-ion. One reason might be the different stacking.

Table 5.1: Dimerization energies for different calculation methods and errors relative to experiment. Effects of different dielectric constants are also given.

| Solvent | radical ion | Counter ion | Geometry | ΔE_{dim} calculated for $\epsilon = 1$ | | | effect of method or of different ϵ | | | errors relative to exp | | | | ΔH_{dim} |
|---------------------------------|--------------------------|-----------------|------------|--|------------------------------|-------------------------|---|--|---|-------------------------|--------------|---|---|-------------------------|
| | | | | B2PLYP-D/ cc-pVTZ | BSSE B2PLYP-D/ cc-pVTZ | CASSCF (3,3/2,2) | BSSE correction | effect of ϵ_{298} instead of gas phase | effect of ϵ_{Tdim} instead of ϵ_{298} | of BSSE- B2PLYP-D | of CASSCF | of ΔE_{dim} (ϵ_{298}) from Tab.4.18 | of ΔE_{dim} (ϵ_{Tdim}) from Tab.4.18 | experiment |
| | | | | ΔE_{dim} | ΔE_{dim} | ΔE_{dim} | | | | | | | | ΔH_{dim} |
| THF | TCNE^{•-} | Na ⁺ | A2 | -232.07 | -54.52 | -55.72 | +177.55 | +144.04 | +20.41 | -21.12 | -22.32 | -54.63 | -34.22 | -33.4 |
| CH ₂ Cl ₂ | DDQ^{•-} | Na ⁺ | B6m | -272.09 | -46.88 | +53.75 | +225.21 | +145.05 | +11.96 | -22.88 | +77.75 | -103.04 | -91.08 | -24.0 |
| EtOH / MeOH | TCNQ^{•-} | Li ⁺ | C1 | -334.81 | -164.77 | -54.99 | +170.04 | +216.17 | +6.35 | -130.57 | -20.79 | -84.44 | -78.09 | -34.2 |

Table 5.1: (continued)

| Solvent | radical ion | Counter ion | Geometry | ΔE_{dim} calculated for $\epsilon = 1$ | | | effect of method or of different ϵ | | | errors relative to exp | | | | ΔH_{dim} |
|-----------------------------|--|------------------------------------|-----------|--|------------------------------|---------------------|---|--|---|-------------------------|------------------|---|---|-------------------------|
| | | | | B2PLYP-D/ cc-pVTZ | BSSE B2PLYP-D/ cc-pVTZ | CASSCF (3,3/2,2) | BSSE correction | effect of ϵ_{298} instead of gas phase | effect of ϵ_{Tdim} instead of ϵ_{298} | of BSSE- B2PLYP-D | of CASSCF | of ΔE_{dim} (ϵ_{298}) from Tab.4.18 | of ΔE_{dim} (ϵ_{Tdim}) from Tab.4.18 | experiment |
| EtOH / Et ₂ O | PPD^{•+} | Br ⁻ Cl ⁻ | D1 | -213.12 -202.57 | -198.47 -19.45 | -74.68 -118.37 | +14.65 +183.12 | +134.41 - | +7.12 - | -146.07 +32.95 | -22.28 -65.97 | -26.31 - | -19.19 - | -52.4 |
| EtOH / Et ₂ O | N,N- DMPPD^{•+} | Cl ⁻ | E3 | -188.37 | -36.15 | -44.87 | +152.22 | +110.65 | +5.93 | +8.05 | -0.67 | -33.52 | -21.59 | -44.2 |
| EtOH / Et ₂ O | 2,3,5,6- TMPPD^{•+} | Cl ⁻ | F3 | -249.02 | -14.33 | -57.42 | +234.69 | +137.92 | +7.92 | +43.87 | +0.78 | -52.9 | -44.98 | -58.2 |
| EtOH / Et ₂ O | N,N,N',N'- TMPPD^{•+} | Cl ⁻ | G1 | -197.06 | -5.56 | -93.22 | +191.50 | +125.97 | +6.64 | +24.04 | -63.62 | -41.49 | -34.85 | -29.6 |
| ACN | TMB^{•+} | Cl ⁻ | H2 | -295.17 | +1.71 | -48.38 | +296.88 | +141.77 | +0.28 | +61.71 | +11.62 | -93.4 | -93.12 | -60.0 |
| Acetone | TTF^{•+} | Cl ⁻ | I1 | -201.01 | -51.94 | +49.34 | +149.07 | +104.94 | +2.78 | -16.24 | +85.04 | -60.37 | -57.59 | -35.7 |

Counter-ions and explicit solvent effect are necessary for the proper description of vertical excitations, especially for a comparison of monomer calculations with experiment. Strong interaction was found for the monomers with the solvent in the molecules (PPD^{•+}, N,N-DMPPD^{•+} and 2,3,5,6-TMPPD^{•+}). The solvent is included in the vertical transitions, which cannot be described properly without explicit solvent molecules, using only COSMO model of solvation. During the dimerization process, the strongly interacting orbitals of the two monomer units become the dominant transition representing the main feature of the UV/Vis spectra and interaction of the monomer units with explicit solvent does not contribute to the dimer spectrum anymore.

Although DFT method describes a different electron distribution than CASSCF method shifting the counter-ion orbitals energetically between the interacting orbitals, the main orbitals contributing to the vertical transitions feature the same characteristics. The experimental spectrum can be modeled well by B3LYP method with deviations of less than 0.1 eV for transitions between pi-orbitals and approx. 0.2 eV for solvent to pi-system transitions.

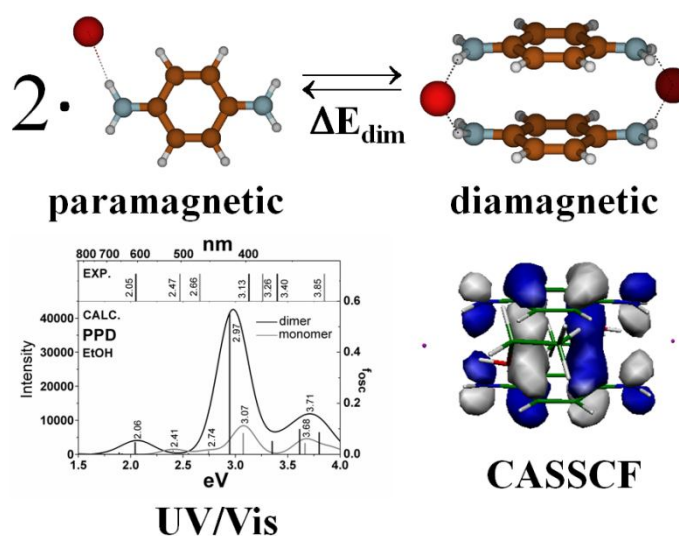
The dielectric constant plays an important role for the energetic correction of the calculated dimerization energy. Dielectric constants of solvents are temperature dependent and they increase when temperature decreased for the solvents used in this work. The dimerization process occurred at temperatures below room temperature. By default, the computer programs use default dielectric constants for the COSMO model of solvation. Those dielectric constants are taken from database at 20-25°C which are smaller than the dielectric constants at low dimerization temperature. This results in the overstabilization of the calculated dimerization energy. Using the proper dielectric constants at dimerization temperature yields 6-20 kJ/mol higher dimerization energies which are closer to the experimental enthalpies of dimerization. More experimental work on dielectric constants at low temperature and measurements of radical ion dimerization with solvents in a larger range of dielectric constants are necessary to confirm this theoretical finding.

PUBLICATION

Part of Chapter 4.2 of this thesis is published in *Spectrochimica Acta Part A* (2011)
doi: 10.1016/j.saa.2011.08.048.

Authors: Kraiwan Punyain, Anne-Marie Kelterer*, Günter Grampp

Title: Theoretical studies on the dimerization of substituted paraphenylenediamine radical cations



Abstract:

Organic radical cations form dicationic dimers in solution, observed experimentally as diamagnetic species in temperature-dependent EPR and low temperature UV/Vis spectroscopy. Dimerization of paraphenylenediamine, *N,N*-dimethyl-paraphenylenediamine and 2,3,5,6-tetramethyl-paraphenylenediamine radical cation in ethanol/diethylether mixture was investigated theoretically according to geometry, energetics and UV/Vis spectroscopy. Density Functional Theory including dispersion correction describes stable dimers after geometry optimization with conductor-like screening model of solvation and inclusion of the counter-ion. Energy corrections were done on double-hybrid Density Functional Theory with perturbative second-order correlation (B2PLYP-D) including basis set superposition error (BSSE), and multireference Møller-Plesset second-order perturbation theory method (MRMP2) based on complete active space method (CASSCF(2,2)) single point calculation, respectively. All three dication π -dimers exhibit long multicenter π -bonds around $2.9 \pm 0.1 \text{ \AA}$ with strongly interacting orbitals. Substitution with methyl groups does not

influence the dimerization process substantially. Dispersion interaction and electrostatic attraction from counter-ion play an important role to stabilize the dication dimers in solution. Dispersion-corrected double hybrid functional B2PLYP-D and CASSCF(2,2) can describe the interaction energetics properly.

Vertical excitations were computed with Tamm-Dancoff approximation for time-dependent Density Functional Theory (TDA-DFT) at the B3LYP level with the cc-pVTZ basis set including ethanol solvent molecules explicitly. A strong interaction of the counter-ion and the solvent ethanol with the monomeric species is observed, whereas in the dimers the strong interaction of both radical cation species is the dominating factor for the additional peak in UV/Vis spectra.

APPENDIX

The optimized structure of TCNE radical anion monomer

| | | | |
|----|-----------|-----------|-----------|
| C | -0.003363 | 0.698034 | -1.541013 |
| C | 0.000332 | -0.745736 | -1.513334 |
| C | 1.175079 | 1.456968 | -1.721860 |
| C | -1.235196 | 1.362447 | -1.380369 |
| C | 1.182685 | -1.505169 | -1.664282 |
| C | -1.228147 | -1.409713 | -1.327706 |
| N | 2.155042 | 2.078188 | -1.870413 |
| N | -2.310393 | 1.810458 | -1.238593 |
| N | 2.165448 | -2.126897 | -1.790510 |
| N | -2.300902 | -1.857005 | -1.166508 |
| Na | -3.955408 | -0.025795 | -0.977038 |

The most stable optimized structure of TCNE dimer (A2)

| | | | |
|----|-----------|-----------|-----------|
| C | -0.015568 | -0.690091 | 1.480203 |
| C | -0.001576 | 0.750417 | 1.451505 |
| C | 0.014406 | 0.692557 | -1.479805 |
| C | 0.000491 | -0.747948 | -1.451379 |
| C | 1.213842 | -1.376248 | 1.561960 |
| C | -1.258646 | -1.352722 | 1.548334 |
| C | 1.240966 | 1.415352 | 1.506317 |
| C | -1.231521 | 1.439255 | 1.492802 |
| C | 1.257497 | 1.355164 | -1.547889 |
| C | -1.214949 | 1.378782 | -1.561834 |
| C | 1.230576 | -1.436570 | -1.492280 |
| C | -1.241918 | -1.413134 | -1.506229 |
| N | 2.304294 | -1.802166 | 1.588548 |
| N | -2.357355 | -1.757505 | 1.563229 |
| N | 2.339536 | 1.820689 | 1.515715 |
| N | -2.321920 | 1.866192 | 1.489623 |
| N | 2.356223 | 1.759889 | -1.562263 |
| N | -2.305327 | 1.804906 | -1.588535 |
| N | 2.321302 | -1.862670 | -1.490251 |
| N | -2.340294 | -1.819017 | -1.515110 |
| Na | 3.424819 | -0.031795 | 0.019267 |
| Na | -3.424791 | 0.034151 | -0.018976 |

The optimized structure of DDQ radical anion monomer (in acetone & CH₂Cl₂)

DDQ radical anion monomer in acetone

| | | | |
|----|-----------|-----------|-----------|
| C | 1.906846 | 0.275063 | -0.033918 |
| C | 1.289363 | -1.070450 | -0.055436 |
| C | -0.068167 | -1.260064 | -0.052962 |
| C | -1.011287 | -0.133779 | -0.028693 |
| C | -0.415414 | 1.189421 | -0.006847 |
| C | 0.969635 | 1.391417 | -0.008872 |
| O | 3.137149 | 0.442797 | -0.036510 |
| O | -2.255601 | -0.306306 | -0.025452 |
| Cl | -0.785071 | -2.847574 | -0.078904 |
| Cl | 2.405069 | -2.403893 | -0.083942 |
| C | -1.349731 | 2.262850 | 0.019295 |
| N | -2.195304 | 3.068426 | 0.036980 |
| C | 1.524145 | 2.704521 | 0.014974 |
| N | 1.962982 | 3.784499 | 0.039640 |
| Na | -3.985480 | 1.171492 | 0.042623 |

DDQ radical anion monomer in CH₂Cl₂

| | | | |
|----|-----------|-----------|-----------|
| C | 1.907738 | 0.274461 | -0.034395 |
| C | 1.288404 | -1.071234 | -0.056371 |
| C | -0.069580 | -1.259133 | -0.051707 |
| C | -1.010730 | -0.132314 | -0.024263 |
| C | -0.413662 | 1.189952 | -0.003456 |
| C | 0.971603 | 1.392261 | -0.007533 |
| O | 3.137404 | 0.440453 | -0.038447 |
| O | -2.256540 | -0.303491 | -0.018935 |
| Cl | -0.788402 | -2.846228 | -0.077887 |
| Cl | 2.402061 | -2.404944 | -0.088437 |
| C | -1.349571 | 2.261878 | 0.022358 |
| N | -2.201378 | 3.061213 | 0.039324 |
| C | 1.524817 | 2.705898 | 0.015185 |
| N | 1.957874 | 3.788191 | 0.037335 |
| Na | -3.970903 | 1.171457 | 0.029202 |

The most stable optimized structure of DDQ dimer (in acetone & CH₂Cl₂)

The most stable optimized structure of DDQ dimer in acetone

(B5)

| | | | |
|----|-----------|-----------|-----------|
| C | -1.566459 | -0.468139 | -1.322810 |
| C | -1.013496 | -1.820513 | -1.096521 |
| C | 0.332682 | -2.061909 | -1.091820 |
| C | 1.320349 | -0.983786 | -1.308226 |
| C | 0.776897 | 0.328047 | -1.628185 |
| C | -0.599529 | 0.576925 | -1.633942 |
| O | -2.792659 | -0.245034 | -1.281885 |
| O | 2.547675 | -1.194964 | -1.253919 |
| Cl | 0.988056 | -3.651025 | -0.863237 |
| Cl | -2.179297 | -3.085198 | -0.865171 |
| C | 1.719166 | 1.315597 | -2.041969 |
| N | 2.502032 | 2.102520 | -2.397710 |
| C | -1.133949 | 1.831627 | -2.051561 |
| N | -1.583729 | 2.846835 | -2.405458 |
| C | -1.255986 | 1.400922 | 1.169900 |
| C | -0.834975 | 0.058343 | 1.590577 |
| C | 0.486203 | -0.316210 | 1.662727 |
| C | 1.571217 | 0.601530 | 1.302225 |
| C | 1.160714 | 1.960031 | 0.946409 |
| C | -0.173705 | 2.340826 | 0.887926 |
| O | -2.455772 | 1.740576 | 1.099037 |
| O | 2.775284 | 0.270287 | 1.340819 |
| Cl | 0.972310 | -1.878213 | 2.245354 |
| Cl | -2.124949 | -1.010026 | 2.078397 |
| C | 2.211519 | 2.897366 | 0.710258 |
| N | 3.074455 | 3.656399 | 0.524300 |
| C | -0.550762 | 3.681544 | 0.575773 |
| N | -0.853676 | 4.777765 | 0.326270 |
| Na | 4.304350 | -0.718329 | 0.054467 |
| Na | -4.164814 | 0.453725 | 0.370343 |

(B7)

| | | | |
|---|-----------|-----------|-----------|
| C | -0.141943 | -0.014859 | 0.129605 |
| C | -0.018779 | -0.019299 | 1.579856 |
| C | 1.121583 | 0.009482 | -0.626907 |
| C | 1.220035 | -0.153200 | 2.203409 |
| C | 2.342457 | -0.080314 | -0.009763 |
| C | 2.466629 | -0.263948 | 1.445984 |
| C | -0.835489 | -2.779463 | 1.228426 |
| C | 0.493373 | -2.876885 | 0.642608 |
| C | -1.972714 | -2.653739 | 0.433334 |
| C | 0.545932 | -3.002835 | -0.824041 |
| C | -1.905638 | -2.641907 | -1.028064 |
| C | -0.578842 | -2.919780 | -1.603591 |
| O | -2.909204 | -2.408019 | -1.732039 |

| | | | |
|----|-----------|-----------|-----------|
| O | 1.525707 | -2.845522 | 1.348750 |
| O | 3.557695 | -0.502551 | 2.002869 |
| O | -1.258325 | -0.039913 | -0.435054 |
| Cl | 0.965312 | 0.164655 | -2.346926 |
| Cl | 3.835078 | -0.036779 | -0.893147 |
| C | -1.229693 | 0.151982 | 2.314950 |
| N | -2.237049 | 0.296692 | 2.881472 |
| C | 1.354422 | -0.323364 | 3.610157 |
| N | 1.576928 | -0.578718 | 4.727178 |
| Na | -3.516672 | -0.287391 | -0.729767 |
| Na | 2.904446 | -2.525405 | 3.156477 |
| Cl | -0.526603 | -3.083192 | -3.329978 |
| Cl | 2.120618 | -3.268890 | -1.499945 |
| C | -3.262024 | -2.397765 | 0.979277 |
| N | -4.336970 | -2.080221 | 1.304969 |
| C | -0.904081 | -2.852418 | 2.651901 |
| N | -0.924219 | -2.918498 | 3.814580 |

The most stable optimized structure of DDQ dimer in CH₂Cl₂ (**B6m**)

| | | | |
|----|-----------|-----------|-----------|
| C | -1.273789 | -0.492987 | -1.777844 |
| C | -0.129496 | -1.281193 | -2.264846 |
| C | 1.153304 | -0.824723 | -2.135378 |
| C | 1.487089 | 0.470475 | -1.496173 |
| C | 0.355534 | 1.286680 | -1.088738 |
| C | -0.953678 | 0.810545 | -1.189002 |
| O | -2.444516 | -0.908376 | -1.866894 |
| O | 2.669560 | 0.832204 | -1.327541 |
| Cl | 2.512106 | -1.729751 | -2.733686 |
| Cl | -0.510566 | -2.805507 | -2.994056 |
| C | 0.629002 | 2.608506 | -0.628737 |
| N | 0.836182 | 3.698932 | -0.274640 |
| C | -2.102100 | 1.552503 | -0.793810 |
| N | -3.119385 | 2.011565 | -0.453899 |
| C | -1.400543 | 0.081211 | 1.771595 |
| C | -0.626262 | -1.013818 | 1.181441 |
| C | 0.768632 | -0.970333 | 1.114516 |
| C | 1.527042 | 0.186544 | 1.570591 |
| C | 0.739500 | 1.278084 | 2.185593 |
| C | -0.626134 | 1.228701 | 2.275518 |
| O | -2.643762 | 0.043539 | 1.841020 |
| O | 2.766721 | 0.249460 | 1.459949 |
| Cl | -1.554344 | 2.513055 | 2.977707 |
| Cl | 1.656055 | 2.612184 | 2.789750 |
| C | -1.415784 | -2.120057 | 0.766415 |
| N | -2.187303 | -2.919899 | 0.409415 |
| C | 1.569250 | -2.055049 | 0.662710 |
| N | 2.335519 | -2.865549 | 0.317499 |
| Na | 3.961750 | -0.791906 | -0.246539 |
| Na | -3.826713 | -0.666895 | -0.018676 |

The optimized structure of TCNQ radical anion monomer

| | | | |
|----|-----------|-----------|-----------|
| C | -0.916410 | -1.126090 | -0.003664 |
| C | 0.405038 | -0.736859 | -0.004942 |
| C | 0.771949 | 0.642583 | -0.002016 |
| C | -0.281715 | 1.604691 | 0.002638 |
| C | -1.603805 | 1.216758 | 0.003844 |
| C | -1.971824 | -0.163481 | 0.000593 |
| H | -1.163661 | -2.189646 | -0.006058 |
| H | 1.186689 | -1.499673 | -0.008325 |
| H | -0.033482 | 2.667974 | 0.005178 |
| H | -2.386382 | 1.978283 | 0.007363 |
| C | -3.344832 | -0.566868 | 0.001278 |
| C | 2.150370 | 1.051415 | -0.004024 |
| C | -4.400080 | 0.380639 | 0.004211 |
| N | -5.259029 | 1.175361 | 0.006639 |
| C | -3.720891 | -1.934227 | -0.002364 |
| N | -4.015026 | -3.066928 | -0.005368 |
| C | 2.530380 | 2.417558 | -0.001566 |
| N | 2.825747 | 3.550004 | 0.000587 |
| C | 3.196538 | 0.112717 | -0.010199 |
| N | 4.060351 | -0.677466 | -0.015598 |
| Li | 5.534667 | -2.044131 | 0.008847 |

The most stable optimized structure of TCNQ dimer (C1)

| | | | |
|---|-----------|-----------|-----------|
| C | 1.419751 | -0.098087 | 1.602163 |
| C | 0.772315 | -1.263495 | 1.095882 |
| C | -0.598467 | -1.367289 | 1.073870 |
| C | -1.427672 | -0.309345 | 1.548370 |
| C | -0.780612 | 0.859246 | 2.063268 |
| C | 0.588802 | 0.960257 | 2.091685 |
| C | 1.428579 | 0.307021 | -1.559081 |
| C | 0.783873 | -0.862382 | -2.075126 |
| C | -0.585358 | -0.965810 | -2.104352 |
| C | -1.418504 | 0.090741 | -1.614645 |
| C | -0.773395 | 1.257107 | -1.107588 |
| C | 0.597196 | 1.363233 | -1.084580 |
| H | 1.375331 | -2.087738 | 0.711939 |
| H | 1.054434 | 1.863089 | 2.491610 |
| H | -1.387499 | 1.684543 | 2.441203 |
| H | -1.061143 | -2.270863 | 0.674253 |
| H | -1.049120 | -1.869282 | -2.504993 |
| H | 1.392426 | -1.686388 | -2.453214 |
| H | -1.378104 | 2.080078 | -0.723555 |
| H | 1.057974 | 2.267384 | -0.684088 |
| C | 2.852878 | 0.428562 | -1.524568 |
| C | -2.843432 | -0.009981 | -1.641599 |
| C | -2.852184 | -0.428346 | 1.515098 |
| C | 2.844886 | -0.000106 | 1.628715 |
| C | 3.508813 | 1.162918 | 2.097586 |

| | | | |
|----|-----------|-----------|-----------|
| N | 4.039757 | 2.130266 | 2.482957 |
| C | 3.663012 | -1.081900 | 1.245985 |
| N | 4.324659 | -1.995170 | 0.930267 |
| C | -3.494258 | -1.644285 | 1.157545 |
| N | -4.002512 | -2.656957 | 0.869068 |
| C | -3.690583 | 0.640502 | 1.878507 |
| N | -4.381071 | 1.551508 | 2.138320 |
| C | 3.693629 | -0.637608 | -1.890533 |
| N | 4.385709 | -1.546675 | -2.152888 |
| C | 3.492165 | 1.645021 | -1.163826 |
| N | 3.997742 | 2.658231 | -0.872559 |
| C | -3.663984 | 1.070674 | -1.260884 |
| N | -4.327979 | 1.982949 | -0.947209 |
| C | -3.504806 | -1.175483 | -2.107969 |
| N | -4.033606 | -2.144965 | -2.490928 |
| Li | 5.180611 | -2.883242 | -0.733505 |
| Li | -5.182464 | 2.877517 | 0.712930 |

The optimized structure of PPD radical cation monomer

| | | | |
|----|-----------|-----------|-----------|
| C | -0.067471 | -0.000164 | 0.006069 |
| C | -0.030143 | 0.000182 | 1.438879 |
| C | 1.170329 | -0.000122 | -0.721628 |
| C | 1.169810 | 0.000265 | 2.105114 |
| C | 2.367374 | 0.000044 | -0.052161 |
| C | 2.402965 | 0.000122 | 1.378923 |
| H | -0.972438 | 0.000378 | 1.991534 |
| H | 1.199261 | 0.000491 | 3.197120 |
| H | 1.125867 | -0.000218 | -1.813552 |
| H | 3.310945 | 0.000022 | -0.602898 |
| N | -1.229268 | -0.000636 | -0.654833 |
| N | 3.577263 | 0.000078 | 2.031547 |
| H | -1.242644 | -0.000254 | -1.694861 |
| H | -2.108601 | -0.000370 | -0.146021 |
| H | 4.456585 | -0.000164 | 1.525491 |
| H | 3.612946 | -0.000253 | 3.045418 |
| Br | -0.920773 | 0.003787 | -3.943730 |

The most stable optimized structure of PPD dimer (**D1**)

| | | | |
|---|-----------|-----------|-----------|
| C | -1.371403 | 1.491150 | -0.574061 |
| C | -0.309115 | 1.801843 | -1.494804 |
| C | 0.992173 | 1.812363 | -1.074745 |
| C | 1.316838 | 1.542458 | 0.302619 |
| C | 0.251886 | 1.328484 | 1.230371 |
| C | -1.051892 | 1.289576 | 0.806761 |
| C | -1.371771 | -1.495787 | -0.293219 |
| C | -0.303564 | -1.282962 | -1.217461 |
| C | 0.998704 | -1.244818 | -0.789084 |
| C | 1.313630 | -1.446802 | 0.592911 |

| | | | |
|----|-----------|-----------|-----------|
| C | 0.247951 | -1.755880 | 1.510133 |
| C | -1.051894 | -1.764362 | 1.085737 |
| H | -0.557829 | 1.990382 | -2.541370 |
| H | -1.870019 | 1.086743 | 1.500437 |
| H | 0.496909 | 1.160135 | 2.280619 |
| H | 1.808457 | 1.996978 | -1.775279 |
| H | 1.819334 | -1.043341 | -1.480199 |
| H | -0.544620 | -1.115182 | -2.268702 |
| H | 0.492897 | -1.944804 | 2.557509 |
| H | -1.871091 | -1.947209 | 1.783324 |
| N | -2.645450 | -1.467717 | -0.701328 |
| N | 2.580824 | -1.340641 | 1.006152 |
| N | -2.639568 | 1.384134 | -0.983450 |
| N | 2.592108 | 1.515300 | 0.707351 |
| H | -2.855373 | -1.241308 | -1.668085 |
| H | -3.402497 | -1.341621 | -0.013803 |
| H | 3.326489 | -1.115070 | 0.332080 |
| H | 2.829198 | -1.532489 | 1.971353 |
| H | -2.889750 | 1.569727 | -1.949405 |
| H | -3.383040 | 1.153291 | -0.309184 |
| H | 3.345729 | 1.382042 | 0.017092 |
| H | 2.801988 | 1.267482 | 1.669002 |
| Br | -4.619833 | 0.071450 | 1.481209 |
| Br | 4.572413 | -0.047405 | -1.454462 |

The optimized structure of N,N-DMPPD radical cation monomer

| | | | |
|----|-----------|-----------|-----------|
| C | 1.082685 | 0.841337 | -0.001767 |
| C | 0.027175 | 1.807003 | -0.000390 |
| C | -1.289277 | 1.416403 | 0.000402 |
| C | -1.651636 | 0.028082 | 0.000166 |
| C | -0.588499 | -0.936381 | -0.001020 |
| C | 0.727314 | -0.547219 | -0.002056 |
| H | -2.059380 | 2.185669 | 0.002165 |
| H | 0.280261 | 2.869717 | 0.000412 |
| H | -0.814229 | -2.001373 | -0.002037 |
| H | 1.532016 | -1.286133 | -0.003393 |
| N | 2.369152 | 1.206406 | -0.002828 |
| N | -2.952706 | -0.358442 | 0.001023 |
| H | 2.622136 | 2.189739 | -0.002614 |
| H | 3.124270 | 0.483761 | -0.002561 |
| Cl | 4.384639 | -1.163591 | -0.001240 |
| C | -4.028132 | 0.634848 | -0.004840 |
| H | -4.991925 | 0.115465 | -0.012332 |
| H | -3.979015 | 1.272605 | 0.892410 |
| H | -3.966496 | 1.274962 | -0.899456 |
| C | -3.311279 | -1.777997 | 0.007168 |
| H | -2.923571 | -2.285135 | -0.890932 |
| H | -2.908117 | -2.280811 | 0.900672 |
| H | -4.402347 | -1.868912 | 0.016913 |

The most stable optimized structure of DMPPD dimer (E3)

| | | | |
|----|-----------|-----------|-----------|
| C | -0.172652 | -1.017914 | -1.075642 |
| C | 0.813243 | -0.204340 | -1.723912 |
| C | 0.269241 | -1.932603 | -0.061689 |
| C | 2.135992 | -0.278617 | -1.374846 |
| C | 1.594805 | -2.015230 | 0.280573 |
| C | 2.583833 | -1.182921 | -0.350479 |
| C | -0.308508 | 1.900729 | 0.119041 |
| C | 0.129124 | 0.983309 | 1.132672 |
| C | -1.632873 | 1.986319 | -0.226617 |
| C | -0.859806 | 0.169794 | 1.776307 |
| C | -2.624903 | 1.154554 | 0.400272 |
| C | -2.181437 | 0.246642 | 1.423346 |
| H | 0.492563 | 0.494957 | -2.498137 |
| H | 2.842077 | 0.390964 | -1.858619 |
| H | -0.478064 | -2.565348 | 0.420661 |
| H | 1.887429 | -2.725207 | 1.051826 |
| H | -1.922205 | 2.699113 | -0.996508 |
| H | 0.441038 | 2.533699 | -0.359548 |
| H | -2.889181 | -0.427143 | 1.898868 |
| H | -0.542552 | -0.532557 | 2.549158 |
| N | 3.891772 | -1.272645 | -0.021066 |
| N | -1.469540 | -0.929024 | -1.383212 |
| N | 1.425102 | 0.891883 | 1.442706 |
| N | -3.931541 | 1.247098 | 0.066700 |
| H | -1.770143 | -0.327287 | -2.142308 |
| H | -2.165949 | -1.554980 | -0.923208 |
| H | 2.123108 | 1.520264 | 0.988208 |
| H | 1.723362 | 0.287945 | 2.201017 |
| Cl | 3.280146 | 2.875283 | -0.090283 |
| Cl | -3.314611 | -2.906406 | 0.173319 |
| C | 4.890545 | -0.425432 | -0.680732 |
| H | 4.630832 | 0.639963 | -0.565160 |
| H | 5.867172 | -0.610070 | -0.220428 |
| H | 4.958004 | -0.667289 | -1.754657 |
| C | 4.333454 | -2.197195 | 1.022343 |
| H | 3.864251 | -1.954703 | 1.990747 |
| H | 4.085047 | -3.239040 | 0.762846 |
| H | 5.419797 | -2.116229 | 1.133328 |
| C | -4.365136 | 2.157252 | -0.992704 |
| H | -5.449844 | 2.070841 | -1.114623 |
| H | -4.123672 | 3.203219 | -0.743358 |
| H | -3.884416 | 1.904723 | -1.952850 |
| C | -4.934507 | 0.403085 | 0.724047 |
| H | -4.704187 | -0.664404 | 0.568896 |
| H | -4.968709 | 0.610962 | 1.806154 |
| H | -5.917793 | 0.627580 | 0.296927 |

The optimized structure of 2,3,5,6-TMPPD radical cation monomer

| | | | |
|----|-----------|-----------|-----------|
| C | -2.200634 | 0.392365 | -0.001895 |
| C | -1.178544 | 1.406362 | -0.031158 |
| C | 0.150935 | 1.022293 | -0.026853 |
| C | 0.472253 | -0.386638 | 0.006878 |
| C | -0.558203 | -1.401133 | 0.036858 |
| C | -1.885826 | -1.013067 | 0.032370 |
| N | -3.497116 | 0.770783 | -0.006264 |
| N | 1.759039 | -0.765751 | 0.011227 |
| H | -3.764265 | 1.746485 | -0.031561 |
| H | -4.248010 | 0.092720 | 0.011887 |
| H | 2.583613 | -0.128504 | -0.013435 |
| H | 1.991426 | -1.752384 | 0.033401 |
| Cl | 4.574936 | 0.556649 | -0.068992 |
| C | -1.644263 | 2.841703 | -0.064831 |
| H | -2.271920 | 3.023208 | -0.956485 |
| H | -2.266263 | 3.066712 | 0.820827 |
| H | -0.819800 | 3.561615 | -0.085115 |
| C | 1.309241 | 1.984161 | -0.054710 |
| H | 1.959871 | 1.831821 | 0.823309 |
| H | 1.955480 | 1.787479 | -0.927064 |
| H | 0.997397 | 3.033711 | -0.080171 |
| C | -3.050393 | -1.972457 | 0.061109 |
| H | -3.683402 | -1.784496 | 0.947520 |
| H | -3.689387 | -1.830499 | -0.829589 |
| H | -2.743817 | -3.023190 | 0.087241 |
| C | -0.101401 | -2.838572 | 0.070906 |
| H | 0.517857 | -3.067739 | -0.815321 |
| H | 0.526917 | -3.022890 | 0.961183 |
| H | -0.929561 | -3.554358 | 0.093240 |

The most stable optimized structure of 2,3,5,6-TMPPD dimer (F3)

| | | | |
|---|-----------|-----------|-----------|
| C | 0.258044 | 0.354529 | -1.402086 |
| C | -0.677901 | -0.700553 | -1.723072 |
| C | -0.194507 | 1.673007 | -1.016939 |
| C | -2.027854 | -0.484361 | -1.532604 |
| C | -1.545916 | 1.877830 | -0.806094 |
| C | -2.457554 | 0.770516 | -0.961344 |
| C | 0.205835 | -1.650898 | 1.000312 |
| C | -0.246944 | -0.332456 | 1.385291 |
| C | 1.557162 | -1.855461 | 0.788835 |
| C | 0.688803 | 0.723091 | 1.705118 |
| C | 2.468797 | -0.748210 | 0.944721 |
| C | 2.038919 | 0.506407 | 1.516095 |
| N | -3.773924 | 0.939468 | -0.695140 |
| N | 1.570744 | 0.116090 | -1.520381 |
| N | -1.559790 | -0.094815 | 1.504132 |
| N | 3.785303 | -0.916952 | 0.678674 |
| H | -4.060537 | 1.780589 | -0.206181 |

| | | | |
|----|-----------|-----------|-----------|
| H | -4.305703 | 0.110512 | -0.414410 |
| H | 1.883581 | -0.779082 | -1.876767 |
| H | 2.328751 | 0.818960 | -1.442661 |
| H | -2.316963 | -0.798523 | 1.427261 |
| H | -1.873406 | 0.799395 | 1.862199 |
| H | 4.071949 | -1.757183 | 0.188179 |
| H | 4.316620 | -0.087428 | 0.398700 |
| Cl | -4.346983 | -1.505967 | 1.468827 |
| Cl | 4.356669 | 1.528633 | -1.484621 |
| C | -3.106316 | -1.468266 | -1.911543 |
| H | -3.595746 | -1.876106 | -1.009094 |
| H | -3.889439 | -0.948435 | -2.490417 |
| H | -2.729237 | -2.300589 | -2.516170 |
| C | -0.110843 | -1.974189 | -2.296323 |
| H | 0.424379 | -1.768474 | -3.240649 |
| H | 0.616099 | -2.423662 | -1.601665 |
| H | -0.876696 | -2.730278 | -2.494919 |
| C | 0.856056 | 2.745424 | -0.898987 |
| H | 1.650254 | 2.439636 | -0.201271 |
| H | 1.352437 | 2.897789 | -1.873219 |
| H | 0.453778 | 3.705885 | -0.560517 |
| C | -2.148977 | 3.198114 | -0.392117 |
| H | -1.416818 | 4.011439 | -0.353430 |
| H | -2.948276 | 3.491476 | -1.095387 |
| H | -2.617074 | 3.121926 | 0.607271 |
| C | 0.122491 | 1.997810 | 2.276838 |
| H | -0.615839 | 2.438877 | 1.588942 |
| H | -0.398810 | 1.796183 | 3.229818 |
| H | 0.887015 | 2.759526 | 2.458463 |
| C | 3.117034 | 1.490163 | 1.896670 |
| H | 2.739861 | 2.319515 | 2.505358 |
| H | 3.901422 | 0.969053 | 2.472647 |
| H | 3.605024 | 1.901706 | 0.995128 |
| C | -0.844516 | -2.723617 | 0.883156 |
| H | -1.342451 | -2.873313 | 1.857017 |
| H | -1.637727 | -2.419955 | 0.183355 |
| H | -0.441675 | -3.685074 | 0.548215 |
| C | 2.160321 | -3.175328 | 0.373701 |
| H | 2.960216 | -3.468929 | 1.076176 |
| H | 1.428335 | -3.988811 | 0.334856 |
| H | 2.627624 | -3.098292 | -0.626001 |

The optimized structure of N,N,N',N'-TMPPD radical cation monomer

| | | | |
|----|-----------|-----------|-----------|
| C | -0.781379 | -1.043743 | 0.012215 |
| C | 0.359162 | -1.912025 | 0.035572 |
| C | 1.641640 | -1.415484 | 0.022850 |
| C | 1.895401 | -0.007302 | -0.014746 |
| C | 0.754557 | 0.857247 | -0.040100 |
| C | -0.527996 | 0.366368 | -0.027270 |
| H | 2.466909 | -2.125213 | 0.039456 |
| H | 0.231092 | -2.992514 | 0.061981 |
| H | 0.880246 | 1.938681 | -0.068077 |
| H | -1.342664 | 1.096329 | -0.047602 |
| N | -2.039138 | -1.553835 | 0.028454 |
| N | 3.159652 | 0.484807 | -0.025877 |
| C | 3.396451 | 1.928319 | -0.077128 |
| H | 4.475783 | 2.111570 | -0.100063 |
| H | 2.945550 | 2.368321 | -0.980826 |
| H | 2.972485 | 2.428553 | 0.808687 |
| C | 4.313145 | -0.414615 | 0.015101 |
| H | 4.296517 | -1.034251 | 0.926001 |
| H | 4.327214 | -1.078305 | -0.864738 |
| H | 5.230964 | 0.182639 | 0.016398 |
| C | -3.256817 | -0.743670 | -0.006291 |
| H | -3.854422 | -1.033407 | -0.886460 |
| H | -3.852830 | -0.952205 | 0.897831 |
| H | -3.053476 | 0.332240 | -0.053675 |
| C | -2.257485 | -3.000791 | 0.077646 |
| H | -3.335964 | -3.191751 | 0.104465 |
| H | -1.834398 | -3.492524 | -0.812675 |
| H | -1.801063 | -3.437215 | 0.979907 |
| Cl | -2.870006 | 2.969368 | -0.066221 |

The most stable optimized structure of N,N,N',N'-TMPPD dimer (**G1**)

| | | | |
|---|-----------|-----------|-----------|
| C | -1.469447 | -0.028738 | -1.689358 |
| C | -0.395581 | -0.743061 | -2.316192 |
| C | 0.901798 | -0.302509 | -2.243257 |
| C | 1.236860 | 0.908034 | -1.552125 |
| C | 0.161395 | 1.628394 | -0.942953 |
| C | -1.133889 | 1.177812 | -0.995101 |
| C | -1.237849 | -0.908715 | 1.550030 |
| C | -0.162373 | -1.628876 | 0.940317 |
| C | 1.133068 | -1.178904 | 0.993292 |
| C | 1.469001 | 0.026997 | 1.688339 |
| C | 0.394877 | 0.742561 | 2.313619 |
| C | -0.902409 | 0.301731 | 2.241055 |
| H | -0.588096 | -1.673116 | -2.847314 |
| H | -1.892905 | 1.763084 | -0.473225 |
| H | 0.350215 | 2.556218 | -0.407235 |
| H | 1.682728 | -0.921546 | -2.679033 |
| H | 1.892459 | -1.763799 | 0.471376 |

| | | | |
|----|-----------|-----------|-----------|
| H | -0.350918 | -2.556551 | 0.404320 |
| H | 0.587058 | 1.673352 | 2.843547 |
| H | -1.683582 | 0.921074 | 2.676035 |
| N | -2.518405 | -1.355804 | 1.489462 |
| N | 2.747500 | 0.480558 | 1.760412 |
| N | -2.747622 | -0.483889 | -1.758841 |
| N | 2.517106 | 1.355568 | -1.490991 |
| C | -3.080330 | -1.629563 | -2.607291 |
| H | -2.501215 | -2.520210 | -2.320894 |
| H | -4.144960 | -1.857785 | -2.488502 |
| H | -2.879114 | -1.406482 | -3.668014 |
| C | -3.886051 | 0.270337 | -1.230476 |
| H | -3.604552 | 0.910904 | -0.386738 |
| H | -4.328823 | 0.898338 | -2.023967 |
| H | -4.649428 | -0.442073 | -0.888492 |
| C | 3.588967 | 0.670076 | -2.218686 |
| H | 4.549917 | 1.093700 | -1.905435 |
| H | 3.585200 | -0.408740 | -1.995194 |
| H | 3.474481 | 0.816880 | -3.306678 |
| C | 2.821571 | 2.663267 | -0.912010 |
| H | 2.459300 | 3.478086 | -1.562007 |
| H | 2.357981 | 2.777196 | 0.076303 |
| H | 3.907023 | 2.757500 | -0.797133 |
| C | 3.078167 | 1.626715 | 2.609193 |
| H | 4.145882 | 1.846793 | 2.503673 |
| H | 2.509345 | 2.520371 | 2.311343 |
| H | 2.861311 | 1.409067 | 3.667859 |
| C | 3.887144 | -0.277494 | 1.239841 |
| H | 4.319786 | -0.909225 | 2.035850 |
| H | 3.610985 | -0.914780 | 0.391761 |
| H | 4.655894 | 0.432803 | 0.905640 |
| C | -3.588364 | -0.676396 | 2.225975 |
| H | -4.550441 | -1.098412 | 1.914158 |
| H | -3.468957 | -0.831362 | 3.312316 |
| H | -3.586789 | 0.403918 | 2.009974 |
| C | -2.826053 | -2.659890 | 0.903556 |
| H | -2.348293 | -2.774420 | -0.077560 |
| H | -2.481978 | -3.479593 | 1.557355 |
| H | -3.910515 | -2.742734 | 0.771096 |
| Cl | 3.223438 | -2.861873 | -1.375738 |
| Cl | -3.227404 | 2.854679 | 1.379064 |

The optimized structure of TMB radical cation monomer

| | | | |
|----|-----------|-----------|-----------|
| C | 1.561197 | 0.043916 | 0.023087 |
| C | 2.140104 | -1.255059 | -0.063518 |
| C | 3.504917 | -1.470312 | -0.064674 |
| C | 4.385051 | -0.342159 | 0.033961 |
| C | 3.840311 | 0.980506 | 0.131780 |
| C | 2.468138 | 1.139345 | 0.119561 |
| C | 0.124059 | 0.241666 | 0.010626 |
| C | -0.786108 | -0.849579 | 0.146658 |
| C | -2.156347 | -0.695392 | 0.134426 |
| C | -2.704416 | 0.626989 | -0.036285 |
| C | -1.813274 | 1.753869 | -0.168190 |
| C | -0.452465 | 1.538529 | -0.139056 |
| H | 1.495437 | -2.128901 | -0.158866 |
| H | 2.083636 | 2.154762 | 0.211758 |
| H | -0.400179 | -1.858022 | 0.293413 |
| H | 0.195749 | 2.405751 | -0.263889 |
| C | -2.384460 | 3.135985 | -0.346104 |
| H | -1.585089 | 3.885022 | -0.426489 |
| H | -3.005018 | 3.199671 | -1.257498 |
| H | -3.028723 | 3.417235 | 0.505734 |
| C | -3.079389 | -1.870316 | 0.310908 |
| H | -3.770763 | -1.974547 | -0.541212 |
| H | -2.510361 | -2.803596 | 0.424913 |
| H | -3.723779 | -1.740557 | 1.196936 |
| C | 4.767639 | 2.162552 | 0.251847 |
| H | 4.202470 | 3.102375 | 0.319312 |
| H | 5.405687 | 2.083982 | 1.150054 |
| H | 5.443019 | 2.234345 | -0.619131 |
| C | 4.082017 | -2.857827 | -0.173934 |
| H | 3.286543 | -3.612931 | -0.236309 |
| H | 4.718989 | -2.958600 | -1.070685 |
| H | 4.711822 | -3.100943 | 0.700349 |
| N | -4.030721 | 0.815238 | -0.069569 |
| H | -4.748700 | 0.063589 | -0.034118 |
| H | -4.401942 | 1.750360 | -0.195651 |
| N | 5.724008 | -0.525536 | 0.034076 |
| H | 6.134364 | -1.447838 | -0.030996 |
| H | 6.368647 | 0.251446 | 0.102248 |
| Cl | -6.565169 | -1.025426 | -0.201300 |

The most stable optimized structure of TMB dimer (**H2**)

| | | | |
|---|-----------|-----------|-----------|
| C | -1.936970 | -1.264898 | 0.398494 |
| C | -2.504492 | -1.047211 | 1.688525 |
| C | -3.848321 | -0.791426 | 1.882973 |
| C | -4.713434 | -0.706637 | 0.742278 |
| C | -4.199767 | -1.026055 | -0.558805 |
| C | -2.850464 | -1.273163 | -0.697658 |
| C | -0.521511 | -1.487624 | 0.204546 |
| C | 0.401137 | -1.529985 | 1.295255 |
| C | 1.753490 | -1.737850 | 1.130532 |
| C | 2.273120 | -1.903937 | -0.202994 |
| C | 1.364295 | -1.927240 | -1.321683 |
| C | 0.024495 | -1.711879 | -1.096028 |
| H | -1.864940 | -1.067832 | 2.570254 |
| H | -2.490879 | -1.493930 | -1.701279 |
| H | 0.037801 | -1.401852 | 2.313800 |
| H | -0.633548 | -1.723686 | -1.962961 |
| C | 1.883760 | -2.221434 | -2.704318 |
| H | 1.072121 | -2.191329 | -3.443759 |
| H | 2.650313 | -1.496021 | -3.019573 |
| H | 2.347689 | -3.222435 | -2.748266 |
| C | 2.686593 | -1.827953 | 2.308228 |
| H | 3.493658 | -1.083242 | 2.243280 |
| H | 2.145394 | -1.673459 | 3.251920 |
| H | 3.180347 | -2.814170 | 2.345954 |
| C | -5.138636 | -1.112412 | -1.734533 |
| H | -4.607070 | -1.443301 | -2.638144 |
| H | -5.952446 | -1.829026 | -1.526875 |
| H | -5.612641 | -0.137963 | -1.941321 |
| C | -4.416806 | -0.569359 | 3.261327 |
| H | -3.640430 | -0.669929 | 4.031954 |
| H | -4.861595 | 0.437186 | 3.362315 |
| H | -5.217854 | -1.295263 | 3.484678 |
| N | 3.587411 | -2.054168 | -0.410287 |
| H | 4.318927 | -2.088367 | 0.319461 |
| H | 3.933186 | -2.205558 | -1.350114 |
| N | -6.028928 | -0.397563 | 0.885929 |
| H | -6.335943 | -0.049692 | 1.788511 |
| H | -6.475135 | 0.096665 | 0.107289 |
| C | 0.514498 | 1.491455 | -0.193298 |
| C | -0.031689 | 1.716314 | 1.107051 |
| C | -1.371290 | 1.933682 | 1.332326 |
| C | -2.279852 | 1.910816 | 0.213496 |
| C | -1.760189 | 1.742385 | -1.119685 |
| C | -0.407908 | 1.533558 | -1.284126 |
| C | 1.930169 | 1.269195 | -0.387102 |
| C | 2.843440 | 1.276722 | 0.709196 |
| C | 4.193198 | 1.031927 | 0.570360 |
| C | 4.707661 | 0.715776 | -0.731076 |
| C | 3.842370 | 0.799831 | -1.871930 |

| | | | |
|----|-----------|-----------|-----------|
| C | 2.498255 | 1.053703 | -1.677301 |
| H | 0.626094 | 1.727089 | 1.974178 |
| H | -0.044619 | 1.403944 | -2.302477 |
| H | 2.483112 | 1.494471 | 1.713227 |
| H | 1.858810 | 1.074672 | -2.559118 |
| C | 4.410946 | 0.579025 | -3.250356 |
| H | 3.634667 | 0.679838 | -4.021030 |
| H | 5.212059 | 1.304934 | -3.473450 |
| H | 4.855933 | -0.427420 | -3.351898 |
| C | 5.131604 | 1.117352 | 1.746570 |
| H | 5.942906 | 1.837582 | 1.541712 |
| H | 4.598859 | 1.443659 | 2.651168 |
| H | 5.608093 | 0.143433 | 1.950106 |
| C | -2.693039 | 1.832450 | -2.297551 |
| H | -2.153124 | 1.670750 | -3.240796 |
| H | -3.504302 | 1.092647 | -2.229537 |
| H | -3.180698 | 2.821543 | -2.339614 |
| C | -1.890594 | 2.229186 | 2.714758 |
| H | -1.079067 | 2.198676 | 3.454307 |
| H | -2.353489 | 3.230683 | 2.758201 |
| H | -2.657803 | 1.504501 | 3.030112 |
| N | 6.023823 | 0.410527 | -0.875835 |
| H | 6.473433 | -0.079927 | -0.097073 |
| H | 6.331781 | 0.064203 | -1.778632 |
| N | -3.594191 | 2.062123 | 0.420384 |
| H | -3.939648 | 2.215395 | 1.360018 |
| H | -4.325119 | 2.097713 | -0.309821 |
| Cl | 6.348485 | -2.251720 | 1.106989 |
| Cl | -6.355680 | 2.258000 | -1.098789 |

The optimized structure of TTF radical cation monomer

| | | | |
|----|-----------|-----------|-----------|
| C | 2.439258 | 1.849903 | -0.070575 |
| C | 0.196946 | 0.574238 | -0.061090 |
| C | 2.774541 | 0.542739 | -0.073779 |
| C | -1.158871 | 0.226015 | -0.054893 |
| C | -3.752273 | 0.243171 | -0.042325 |
| C | -3.409675 | -1.060764 | -0.045205 |
| S | -1.704166 | -1.441664 | -0.053866 |
| S | -2.451779 | 1.410892 | -0.047381 |
| S | 1.480695 | -0.630487 | -0.068765 |
| S | 0.737013 | 2.238628 | -0.061644 |
| H | -4.110164 | -1.896721 | -0.042654 |
| H | -4.772642 | 0.628139 | -0.037037 |
| H | 3.780847 | 0.123150 | -0.079403 |
| H | 3.144980 | 2.681325 | -0.073017 |
| Cl | 3.940762 | -2.564981 | -0.081989 |

The most stable optimized structure of TTF dimer (**II**)

| | | | |
|----|-----------|-----------|-----------|
| C | -3.249133 | -1.683934 | 0.416464 |
| C | -0.671833 | -1.718749 | 0.246098 |
| C | -2.812575 | -1.739042 | 1.692092 |
| C | 0.653397 | -1.716791 | -0.201998 |
| C | 2.794235 | -1.734605 | -1.647855 |
| C | 3.230597 | -1.672046 | -0.372540 |
| S | 2.023465 | -1.608639 | 0.883668 |
| S | 1.068710 | -1.755350 | -1.905108 |
| S | -1.087026 | -1.751713 | 1.949505 |
| S | -2.042255 | -1.621297 | -0.839948 |
| H | 4.265637 | -1.603638 | -0.037854 |
| H | 3.434212 | -1.760999 | -2.530351 |
| H | -3.452354 | -1.764203 | 2.574766 |
| H | -4.284583 | -1.619819 | 0.082096 |
| C | -3.255500 | 1.670733 | 0.410638 |
| C | -0.678425 | 1.715696 | 0.239926 |
| C | -2.819074 | 1.733458 | 1.685939 |
| C | 0.646817 | 1.717978 | -0.208153 |
| C | 2.787568 | 1.741622 | -1.654021 |
| C | 3.224201 | 1.685544 | -0.378475 |
| S | 2.017381 | 1.620466 | 0.877942 |
| S | 1.061973 | 1.752233 | -1.911343 |
| S | -1.093625 | 1.754217 | 1.943172 |
| S | -2.048507 | 1.607723 | -0.845715 |
| H | 4.259697 | 1.624471 | -0.043755 |
| H | 3.427476 | 1.768660 | -2.536536 |
| H | -3.458920 | 1.760071 | 2.568521 |
| H | -4.290768 | 1.601182 | 0.076805 |
| Cl | -4.713381 | -0.013246 | -2.118225 |
| Cl | 4.690193 | 0.014018 | 2.151971 |

REFERENCES

- [1] R. Chang, *J Phys Chem* **1970**, *74*, 2029.
- [2] G. Grampp, S. Landgraf, K. Rasmussen, S. Strauss, *Spectrochim Acta A Mol Biomol Spectrosc* **2002**, *58*, 1219.
- [3] J. M. Lu, S. V. Rosokha, J. K. Kochi, *J Am Chem Soc* **2003**, *125*, 12161.
- [4] S. V. Rosokha, J. Lu, T. Y. Rosokha, J. K. Kochi, *Phys Chem Chem Phys* **2009**, *11*, 324.
- [5] S. V. Rosokha, J. Lu, B. Han, J. K. Kochi, *New J. Chem.* **2009**, *33*, 545.
- [6] S. V. Rosokha, J. Zhang, J. Lu, J. K. Kochi, *J. Phys. Org. Chem.* **2009**, *23*, 395.
- [7] G. Grampp, W. Jaenicke, *Ber. Bunsenges. Phys. Chem.* **1984**, *88*, 325.
- [8] K. Kimura, H. Yamada, H. Tsubomura, *J Chem Phys* **1968**, *48*, 440.
- [9] K. Yokoyama, S. Maeda, *Chem. Phys. Lett.* **1977**, *48*, 59.
- [10] E. E. Ernstbrunner, R. B. Girling, W. E. Grossman, E. Mayer, K. P. J. Williams, R. E. Hester, *J. Raman Spectrosc.* **1981**, *10*, 161.
- [11] H. Awano, H. Ohigashi, *Bull. Chem. Soc. Jpn.* **1990**, *63*, 2101.
- [12] H. Awano, O. Ichihara, K. Sawada, H. Ohigashi, *Ber. Bunsenges. Phys. Chem.* **1996**, *100*, 1700.
- [13] T. Sakata, S. Nagakura, *Bull. Chem. Soc. Jpn.* **1969**, *42*, 1497.
- [14] R. H. Boyd, W. D. Phillips, *J. Chem. Phys.* **1965**, *43*, 2927.
- [15] J. J. Novoa, P. Lafuente, R. E. Del Sesto, J. S. Miller, *Angew Chem Int Ed Engl* **2001**, *40*, 2540.
- [16] R. E. D. Sesto, J. S. Miller, P. Lafuente, J. J. Novoa, *Chem. Eur. J.* **2002**, *8*, 4894.
- [17] J. J. Novoa, J. Ribas-Arino, W. W. Shum, J. S. Miller, *Inorg Chem* **2007**, *46*, 103.
- [18] J. Jakowski, J. Simons, *J Am Chem Soc* **2003**, *125*, 16089.
- [19] M. Strohmeier, D. H. Barich, D. M. Grant, J. S. Miller, R. J. Pugmire, J. Simons, *J. Phys. Chem. A.* **2006**, *110*, 7962.
- [20] Y. Jung, Head-Gordon, M., *Phys Chem Chem Phys* **2004**, *6*, 2008.
- [21] Y. M. Rhee, R. A. D. Jr., R. C. Lochan, M. Head-Gordon, *Chem.Phys.Lett.* **2006**, *426*, 197.

- [22] M. A. Carvajal, I. Garcia-Yoldi, J. J. Novoa, *J.Mol. Struct. (Theochem)* **2005**, 727, 181.
- [23] I. Garcia-Yoldi, F. Mota, J. J. Novoa, *J Comput Chem* **2007**, 28, 326.
- [24] I. Garcia-Yoldi, J. S. Miller, J. J. Novoa, *J Phys Chem A* **2007**, 111, 8020.
- [25] J. S. Miller, J. J. Novoa, *Acc Chem Res* **2007**, 40, 189.
- [26] I. Garcia-Yoldi, J. S. Miller, J. J. Novoa, *Phys Chem Chem Phys* **2008**, 10, 4106.
- [27] F. Mota, J. S. Miller, J. J. Novoa, *J Am Chem Soc* **2009**, 131, 7699.
- [28] I. Garcia-Yoldi, J. S. Miller, J. J. Novoa, *J Phys Chem A* **2009**, 113, 484.
- [29] I. Garcia-Yoldi, J. S. Miller, J. J. Novoa, *Theor Chem Acc* **2009**, 123, 137.
- [30] Y. Li, H. Li, X. Zhao, M. Chen, *J. Phys. Chem. A* **2010**, 114, 6972.
- [31] F. Rodriguez-Roperro, J. Casanovas, D. Zanuy, C. Aleman, *Chem. Phys. Lett* **2010**, 488, 177.
- [32] T. Kamisuki, C. Hirose, *Spectrochim Acta A Mol Biomol Spectrosc* **2000**, 56A, 2141.
- [33] S. Sinnecker, A. Rajendran, A. Klamt, M. Diedenhofen, F. Neese, *J Phys Chem A* **2006**, 110, 2235.
- [34] B. G. Lone, P. B. Undre, S. S. Patil, P. W. Khirade, S. C. Mehrotra, *Journal of Molecular Liquids* **2008**, 141, 47.
- [35] A. Chmielewska, M. Zurada, K. Klimaszewski, A. Bald, *J. Chem. Eng. Data* **2009**, 54, 801.
- [36] G. Moumouzias, G. Ritzoulis, *J. Chem. Eng. Data* **1997**, 1997, 710.
- [37] F. I. El-Dossoki, *J. Chin. Chem. Soc.* **2007**, 54, 1129.
- [38] H. M. Amber, R. R. Paxton, M. V. Winkle, *Analytical Chemistry* **1953**, 25, 1204.
- [39] J. L. Hovath, *Glas Hem. Drus Beograd* **1974**, 39, 339.
- [40] F. Travers, P. Douzou, *J. Phys. Chem.* **1970**, 74, 2243.
- [41] H. Isnardi, *Z. Phys.* **1922**, 9, 153.
- [42] R. H. Cole, *J. Chem. Phys.* **1941**, 9, 251.
- [43] M. T. Chimenko, N. N. Grizenko, *Zh. Fiz. Khim.* **1980**, 54, 198.
- [44] S. O. Morgan, H. H. Lowry, *J. Phys. Chem.* **1930**, 34, 2385.
- [45] C. Carvajal, K. J. Tolle, J. Smid, M. Szwarc, *J. Am. Chem. Soc.* **1965**, 87, 5548.
- [46] J. Wyman JR, *J Am Chem Soc* **1933**, 55, 4116.
- [47] J. Canosa, A. Rodriguez, J. Tojo, *Fluid Phase Equilibria* **1999**, 156, 55.

- [48] S. V. Rosokha, J. K. Kochi, *J Am Chem Soc* **2007**, *129*, 828.
- [49] A. Szabo, N. S. Oslund, *MODERN QUANTUM CHEMISTRY: Introduction to Advanced Electronic Structure Theory*, MACMILLAN PUBLISHING CO., INC., New York, **1982**.
- [50] C. J. Cramer, *Essentials of Computational Chemistry: Theories and Models*, Second ed., John Wiley & Sons, Ltd, West Sussex, **2004**.
- [51] F. Jensen, *Introduction to Computational Chemistry*, John Wiley & Son Ltd, West Sussex, **2007**.
- [52] P. Hohenberg, W. Kohn, *Phys. Rev.* **1964**, *136*, B864.
- [53] W. Kohn, L. J. Sham, *Phys. Rev.* **1965**, *140*, A1133.
- [54] A. D. Becke, *J. Chem. Phys.* **1993**, *98*, 5648.
- [55] P. J. Stephens, F. J. Devlin, C. F. Chabalowski, M. J. Frisch, *J. Phys. Chem.* **1994**, *98*, 11623.
- [56] S. Grimme, *J Chem Phys* **2006**, *124*, 034108.
- [57] E. K. U. Gross, W. Kohn, *Advan. Quantum Chem.* **1990**, *21*, 255.
- [58] E. Runge, E. K. U. Gross, *Phys. Rev. Letters* **1984**, *52*, 997.
- [59] R. Bauernschmitt, R. Ahlrichs, *Chem. Phys. Lett* **1996**, *256*, 454.
- [60] S. Hirata, M. Head-Gordon, *Chem. Phys. Lett* **1999**, *314*, 291.
- [61] S. Grimme, *J Comput Chem* **2004**, *25*, 1463.
- [62] S. Grimme, *J Comput Chem* **2006**, *27*, 1787.
- [63] K. B. Lipkowitz, D. B. Boyd, *Reviews in Computational Chemistry, Vol. 13*, Wiley-VCH, John Wiley and Sons, Inc., New York, **1999**.
- [64] S. F. Boys, F. Bernardi, *Mol. Phys.* **1970**, *19*, 553.
- [65] K. Hirao, *Chem. Phys. Lett* **1992**, *190*, 374.
- [66] K. Hirao, *Int. J. Quantum. Chem.* **1992**, *26*, 517.
- [67] K. Hirao, *Chem. Phys. Lett* **1993**, *201*, 59.
- [68] A. Klamt, G. Schuurmann, *J. CHEM. SOC.* **1993**, *PERKIN TRANS. 2*, 799.
- [69] J. L. De Boer, A. Vos, *Acta Cryst.* **1968**, *B24*, 542.
- [70] J. L. De Boer, A. Vos, *Acta Cryst.* **1972**, *B28*, 835.
- [71] I. Garcia-Yoldi, J. S. Miller, J. J. Novoa, *Theor. Chem. Acc.* **2009**, *123*, 137.
- [72] I. Garcia-Yoldi, J. S. Miller, J. J. Novoa, *J Phys Chem A* **2009**, *113*, 7124.
- [73] J. Huang, S. Kingsbury, M. Kertesz, *Phys. Chem. Chem. Phys.* **2008**, *10*, 2625.
- [74] A. D. Becke, *J. Chem. Phys.* **1992**, *98*, 1372.
- [75] J. T. H. Dunning *J. Chem. Phys.* **1989**, *90*, 1007.

- [76] T. Petrenko, F. Neese, *J Chem Phys* **2007**, *127*, 164319.
- [77] F. Neese, version 2.7, revision 00 ed., Lehrstuhl für Theoretische Chemie, Wegelerstr. 12, D-53115 Bonn, Germany., **June 2009**.
- [78] *XYZViewer*, version 0.97, <http://www.physto.se/~sven/>.
- [79] P. Flükiger, H. P. Lüthi, S. Portmann, J. Weber, *MOLEKEL 4.1 Swiss Center for Scientific Computing, Manno (Switzerland)*, 2000.
- [80] J. C. Sancho-Garcia, A. J. Perez-Jimenez, *J. Chem. Phys.* **2009**, *131*, 084108.
- [81] M. Itoh, *Bull. Chem. Soc. Jpn.* **1972**, *45*, 1947.
- [82] J. Tanaka, N. Sakabe, *Acta Cryst.* **1968**, *B24*, 1345.
- [83] A. Bondi, *J. Phys. Chem.* **1964**, *68*, 441.
- [84] W. Dannhauser, A. F. Flueckinger, *J. Phys. Chem.* **1964**, *68*, 1814.
- [85] L. Jannelli, A. Lopez, L. Silvestri, *J. Chem. Eng. Data* **1983**, *28*, 166.
- [86] J. M. Lukashov, *Izv. Vyssh. Uchebn. Zaved. Energ.* **1976**, *20*, 89.